Studies On Nonadiabatic Dynamics Within System-Bath Framework

A Thesis submitted for the Degree of Doctor of Philosophy

by

Prachi Pandey





School of Chemistry
University of Hyderabad
Hyderabad - 500 046, INDIA

December 2022





Statement

I hereby declare that the matter embodied in the thesis entitled, "Studies On Nona-diabatic Dynamics Within System-Bath Framework" is the result of investigations carried out by me in the School of Chemistry, University of Hyderabad, India under the supervision of Prof. M. Durga Prasad.

In keeping with the general practice of reporting scientific investigations, acknowledgements have been made wherever the work described is based on the finding of other investigators.

30.12.2022

Date

Hyderabad 500046

Signature of the candidate



Declaration of Authorship

I, Prachi Pandey(Regs.no. 16CHPH21), hereby declare that this thesis entitled "Studies On Nonadiabatic Dynamics Within System-Bath Framework" submitted by me under the guidance and supervision of Prof. M. Durga Prasad, is a bonafide research work which is also free from plagiarism. I also declare that it has not been submitted previously in part or in full to this university or any other university or institution for the award of any degree or diploma. I hereby agree that my thesis can be deposited in Shodhganga/INFLIBNET.

A report on plagiarism statistics from the University Librarian is enclosed.

30.12.2022

Date

Hyderabad 500046

Signature of the candidate

Faculty Incharge
School of Chemistry
University of Hyderabad

Hyderabad - 500046

Supervisor

Prof. M. Durga Prasad

Certificate

School of Chemistry University of Hyderabad Hyderabad-500 046 India





Prof. M. Durga Prasad Phone: 040-2313-4855(O) email:

mdpsc@uohyd.ac.in

It is certified that the work contained in this thesis, entitled, "Studies On Nonadiabatic Dynamics Within System-Bath Framework" by Prachi Pandey (Reg.No. 16CHPH21), has been carried out under my supervision and is not submitted elsewhere for a degree.

This thesis is free from plagiarism and has not been submitted previously in part or in full to this or any other University or Institution for award of any degree or diploma.

Following manuscripts, based on parts of this thesis, are under review and under preparation:

1. **Prachi Pandey**, M. Durga Prasad*,

Criteria for the classification of system and bath variables in nonadiabatic dynamics: Application to pyrazine, J. Phys. Chem. A (revised manuscript under review)

2. **Prachi Pandey**, M. Durga Prasad*,

An MRTDCCM approach for nonadiabatic dynamics in system-bath formalism (manuscript under preparation)

3. **Prachi Pandey**, M. Durga Prasad*,

An MRTDCCM and thermofield dynamics approach for the nonadiabatic systems at zero and finite temperatures: Example of a dimer (manuscript under preparation)

Part of this thesis has been presented in the following conferences:

- 1. **Poster:** Chemfest, 16th Annual In-House Symposium, 22-23 February, 2019, at School of Chemistry, University of Hyderabad, Hyderabad (National).
- 2. **Poster:** 17th conference on Spectroscopy and Dynamics of Molecules and Clusters(SDMC-2020), 20-23 February, 2020, at Kumbhalgarh, Rajasthan, organised by BITS Pilani,

Pilani Campus and IIT Jodhpur (National).

- 3. Poster: DAE symposium on Current Trends in Theoretical Chemistry (CTTC-2020), 23-25 September, 2021, via online, organised by Chemistry Division, BARC, Mumbai (National).
- 4. Poster: 17th Theoretical Chemistry Symposium (TCS), 11-14 December, 2021, via online, jointly organised by IISER-Kolkata, IACS-Kolkata, University of Kalvani and S.N Bose National Centre For Basic Sciences, Kolkata (International).
- 5. Oral Presentation: Chemfest, 19-20 March, 2021, organised by School of Chemistry, University of Hyderabad (National).

Further, the student has passed the following courses towards fulfilment of coursework requirement for Ph.D.

Course code	Name	Credits	Pass/Fail
1. CY-801	Research Proposal	3	Pass
2. CY-805	Instrumental Methods A	3	Pass
3. CY-453	Molecular Spectroscopy	3	Pass
4. CY-457	Physical Chemistry Lab	3	Pass
5. CY-503	Chemical Dynamics	3	Pass
6. CY-504	Chemical Binding	3	Pass

Hyderabad 500046

Advisor: Prof. M. Durga Prasad

Faculty Incharge School of Chemistry University of Hyderabad Hyderabad - 500046

Dean

School of Chemistry ity of Hyderabad Hyderabad-500 046

University of Hyderabad

Acknowledgements

"So many of our dreams at first seem impossible, then they seem improbable, and then, when we summon the will, they soon become inevitable."

Any dreamer who finally transform their goals into reality have people in their lives to thank. People who stood beside them and motivated them throughout their journey. I am a dreamer and I have been blessed to have allies in my life who made this journey possible.

First and foremost, I give all my love and gratitude to my parents. My father Mr. S. K. Pandey and my mother Mrs. Pratibha Pandey have showered me with their love, support and confidence right from my childhood. They recognised and encouraged my inclination towards academics and any hobbies that I showed interest in. They brought me till here and my whole life is a way to make them proud of me in any way I can. I thank my dear brother Pratyush Pandey with all my heart for being a constant guardian and a loving elder brother to me. I thank my dear sister-in-law Mrs. Sarita Pandey and my nephew Kartik, the apple of my eyes, for being an essential part of this journey. I could not have gotten a more loving family than I have and for that I am eternally grateful to the Almighty.

I truly believe that a student is as good as the teacher who mentors him. I have been very lucky that I was guided by wonderful teachers who encouraged my curiosity and imaginations. However, words fall short if I have to acknowledge the contribution of my PhD supervisor, Prof. M. Durga Prasad. I joined this lab as a girl who was interested in yet intimidated by Quantum Chemistry. He graciously took me under his supervision. It would not be an exaggeration to say that he is the best and the most patient teacher that has taught me till date. His expansive knowledge and command on the matter is a testament of his long academic life. He encouraged and helped me to broaden my academic understanding. I truly enjoyed all the sessions that we sat together to discuss work. But, appreciating his role in over six years of my life will be incomplete without noting what a wonderful human being he is. He was always patient to listen to my woes and was always approachable if I had a personal crisis. Of all the ways I could choose my supervisor, I am ever so thankful that I have the fortune to be called his student. All my future academic endeavours will be towards extending the knowledge that I gained from him.

I would like to thank my DRC members, Prof. S. Mahapatra and Dr. D. Barik for their valuable guidance in my PhD journey. I also thank present and former deans and

faculty members of SoC. I appreciate the help that I got from the non-teaching staff of SoC, especially Abraham sir.

This over six years of life was a journey in my life that came with its fair share of lows as well as highs. And, this acknowledgement will not be complete if I do not thanks my beloved friends. Some of them are my extended family and have a very strong place in my heart. I thank my long-time friends, Panchi, Kunzes, Sagarika, Aditya and Lijo for always being there for me. They knew me before I joined the PhD and their support poured constantly through my research especially through the tough-times of Covid Pandemic. They were never physically present around me yet they were just a call or a message away to cheer me up. I thank Divya, Purbasha, Rajiv, Tushar, Arunima,Sameera and Sonam for being my dear friends. To my surprise I made good friends in PhD. We were all united by the same struggles that this life brings and Chai. I thank my dearest friends Mamina, Rameshori, Jayakrushna and Pritam for sharing this PhD experience with me. More than that, we shared all our happiness and worries over cups of chai that I can not possibly count.

Joining MDP-lab gave me seniors who became more like my elder siblings. They guided me academically and also cared for me personally. My heart fills up thanking my seniors: Subrata Da, Lalitha Di and Tapta da. I am so fortunate to have gotten to be your junior. My heartiest thanks also go to dear Lopa, Late Sridhar anna and dear Narasimha anna.

I extend my thanks to Archana, Arun, Daradi, Soutrick, Hafijur, Ajay Singh Rawat, Oindrila, Susmita, Sebanti, Feba, Abin, Sugata and Sameer for being a part of this phase of my life. I would like to thank Priyanka, Shwetang, Bijoy Bakal, Geetumoni Bakal and dear Dhiyara for making my stay in Hyderabad so wonderful.

I acknowledge the help that I got from Prof. G. A. Worth. I am grateful to him for promptly answering my academic queries and providing me data whenever I asked him.

And finally I thank Almighty and myself for making the dream come true. This life is enriching but it comes with its fair share of struggles and tough times. There were times when it was just me against the hurdles on my way. But, I have been always been a reader and lover of movies. And, I would remember some profound story of overcoming obstacles with perseverance and grit. Those late-nights working in the lab, cranking up Eminem's rap on not giving up and endless hours on Spotify are the core personal memories now. All I could say about my experience is that research life demands grit and perseverance. But at the end, if one can be resilient those small

victories wash away all the hardships that we faced. Life of research can be summarized by a quote by Edwin Markham, "For all your days prepare, and meet them ever alike. When you are the anvil, bear—when you are the hammer, strike."

Prachi, December 2022, Hyderabad.

Contents

St	atemo	ent en	i
De	eclara	ation of Authorship	ii
C	ertific	ate	iii
A	cknov	vledgements	vi
Al	bbrev	iations	xi
1	Intr	oduction	1
	1.1 1.2 1.3 1.4	Brief discussion on nonadiabatic dynamics 1.1.1 Born-Oppenheimer approximation 1.1.2 Breakdown of BOA 1.1.3 Conical Intersection and its role in NAD 1.1.4 Representation of PES and Vibronic Hamiltonian Literature review of theoretical methods for NAD Dynamics of a NAS Goal of the present work and overview of the thesis	1 1 3 4 5 8 12 16
2	Clas 2.1 2.2 2.3 2.4	Introduction	19 19 19 24 29
3	3.1 3.2 3.3	Introduction	30 30 31 35 35 45
	3.4	Conclusions	52

<u>Contents</u> x

4	Nu	merical Studies using MRTDCCM for bath subspace	5 4
	4.1	Introduction	54
	4.2	Hilbert spaces and Wave operator	55
	4.3	MRTDCCM ansatz	57
	4.4	Wave function for MRTDCCM	57
	4.5	Results and Discussion	60
		4.5.1 Application on Butatriene cation	60
		4.5.2 Application on pyrazine	65
	4.6	Conclusions	67
5	Dyı	namics of Dimers spectra	68
	5.1	Introduction	68
	5.2	The Hamiltonian	70
	5.3	Symmetry considerations	71
	5.4	Symmetry adapted linear combinations	74
	5.5	Dynamics	76
		5.5.1 Possible representations	76
		5.5.1.1 Symmetrised vibrational representation	76
		5.5.1.2 Symmetrised electronic representation	77
		5.5.1.3 Global symmetrised representation	78
		5.5.2 Ansatz	79
	5.6	Extension to finite temperatures	80
	5.7	Conclusion	83
6	Con	nclusions	85
A			90
Bi	bliog	raphy	94

Abbreviations

ACF Autocorrelation function

ADT Adiabatic to diabatic transformation BOA Born-Oppenheimer approximation

BH Born-Haung
BS Bath-subspace
CA Crude adiabatic
CBS Complete basis set
CC Coupled cluster

CF Configuration function
CIs Conical intersections
CS Configuration space
DOF Degrees of freedom
ES Electronic state
FC Franck-Condon
FG Frozen Gaussian

FGWP Frozen Gaussian wave packet

FT Fourier transform

FWHM Full width at the half maximum

G-MCTDH Gaussian based MCTDH

GS Ground state

GWP Gaussian wave packet

HS Hilbert space

HO Harmonic oscillator

Irrep Irreducible representation

KE Kinetic energy

LVC Linear vibronic coupling

LS Lower surface

MCTDH Multi-configuration time-dependent Hartree MRCI Multi-reference configuration Interaction

NAD Nonadiabatic dynamics NAS Nonadiabatic system PE Potential energy

PESs Potential energy surfaces

PI Path-integral

QM Quantum mechanical

Abbreviations xii

QS Quantum state

QVC Quadratic vibronic coupling

SALC Symmetry adapted linear combination

SP Single-particle

SPF Single-particle function

SS System-subspace TD Time-dependent

TDM Thermal density matrix

TDSE Time-dependent Schrödinger equation

TDWP Time-dependent wave packet

TG Thawed Gaussian
US Upper surface
VC Vibronic coupling

VIEs Vertical ionization energies VEEs Vertical excitation energies

WP Wave packet

Once upon a time,
a little girl dared to dream big.
She dedicates this to her parents,
loved-ones and mentors who helped her reach here.
That little girl is forever grateful!

SYNOPSIS

The thesis entitled 'Studies on Nonadiabatic Dynamics within System-Bath Framework' consists of six chapters. My thesis is divided into an introduction chapter, four working chapters and a chapter enclosing the concluding remarks. All working chapters are divided into (1) Introduction (2) Methods (3) Results and Discussions (4) Conclusions.

Chapter 1: Introduction

Chapter 1 begins with a brief revision of Born-Oppenheimer(BO) approximation. The effects of non-BO approximation and their consequences are highlighted. Various methods to compute these are briefly mentioned. The work of Schneider et. al (Ref: J. Chem. Phys., 92:1045–1061,1990) analyzed the dynamics of a nonadiabatic system (NAS). The spectra of a NAS are often complex and dissipative. Schneider et. al computationally showed that the reduced density matrices of the active vibrational modes develop large amount of statistical entropies monotonically. They have not elaborated the mechanisms of this. However, they did associate the dephasing of the wave packet(WP) with the statistical entropy of these modes. This work is the inspiration for my work presented in this thesis. The goals of the present thesis are presented along with the structure of the thesis in this chapter.

Chapter 2: Classification of system and bath DOF

In this chapter, I elaborate the mechanisms associated with the WP dephasing. These are different for the coupling and tuning modes. The differences are explained in this chapter. We concluded that the dephasing occurs in a discrete manner each time the WP crosses the conical intersection(CI). The number of zeroth order vibrational states required to describe the coupling modes increases during the curve-crossing(CC). Hence, the statistical entropies of these modes increase. The tuning modes, on the other hand, move seamlessly onto the second surface transferring a small amount of their WPs to the other surface that depends on the transfer of the electronic state(ES) populations. Thus, the two types of modes display a different structure in their WPs. Both, however, happen at the time of CC. A sequence of such discrete events determine the WP dephasing in the long time limit.

CC happens based on the tuning mode dynamics. The tuning modes carry the WP into the neighbourhood of the CI. Thus, one should understand which tuning mode carries the WP towards the CI. To determine this, we carried out an algorithm in a qualitative manner based on the classical dynamics of these tuning modes. It turns out that there are two ways by which tuning modes carry the WP across the CI. We term them as **direct crossing** involving a single tuning mode and a **mutually-assisted crossing** involving two tuning modes simultaneously. We developed methods to identify these two types of CC phenomena.

Applications of these criteria are presented in next chapters.

Chapter 3: Numerical studies using Generalized TDSCF for bath DOF

In this chapter I test the validity of the criteria introduced and outlined in Chapter 2. Before discussing the numerical results, I present the timedependent self-consistent field (TDSCF) method used for the description of the bath DOF. This is discussed as part of the computational methodology. Computational methodology encloses discussions on system subspace (SS) configuration functions, TDSCF ansatz and Gaussian WP for the bath subspace (BS). In addition, working equations are derived in this section. Next, I use two models for the purpose of testing the criteria for the classification of system and bath variables. These results are presented as part of Results and Discussions. First is the 24-mode pyrazine molecule. It has a CI between S_2 and S_1 ESs. It has only one coupling mode and five totally symmetric tuning modes. I present a thorough analysis for choosing the system DOF in this case. Auto-correlation functions (ACFs), spectra and electronic populations are presented for the case study of the comparison of two model systems in pyrazine. These results elaborate and emphasize the importance of choice of system DOF. TDSCF results are also compared with numerically exact results of MCTDH. Second testing case is a 3-mode spin-boson model. The vibronic Hamiltonian in this case has only tuning modes and no coupling mode. In this case, I compare the exact 3-mode SS with three 2-mode SSs in which one mode is dropped in each case. These results emphasize the importance of the influence of inclusion of a single mode in the SS. Finally I summarize the conclusions of the chapter.

Chapter 4: Numerical studies using MRTDCCM for bath subspace

My aim in this chapter is to test an alternate approach for describing the bath degrees of freedom(DOF). For this purpose, I use the multi-reference time-dependent coupled cluster method (MRTDCCM) for treating the bath DOF. As part of the methodology, I present the bifurcation of total Hilbert space(HS) done in MRTDCCM into SS and BS. In this approach, system DOF are treated exactly in terms of numerically converged harmonic oscillator(HO) basis functions. The BS is described by an exponential ansatz of the excitations operators. These excitation operators can be expanded as a power series and the series can be conveniently truncated at a lower order of expansion. The total WF in MRTDCCM is written in terms of bath waveoperator acting on the system HS. I analyse the bath wave-operator and present the working equations for the system and bath excitations. Next, as part of the results and discussion I present ACFs and spectra for the nonadiabatic dynamics(NAD) in 18-mode butatriene cation. This system has a CI between electronic ground state and first excited state. Results are presented for three cases of MRTDCCM calculations. First case is calculated only for SS (MS-only), second for SS plus one boson bath excitations(MS+S1) and third for SS, one boson and two boson bath excitations (MS+S1+S2). A (2-mode + ES)- SS is chosen for but at riene cation according to the criteria. I also compare the results with the numerically exact results of MCTDH. I tried using the MRTDCCM for bath modes in a 3+21 model of pyrazine. But, unfortunately the calculations break down at (MS+S1+S2) level of calculations. I summarize the chapter with concluding remarks.

Chapter 5: Dynamics of Dimers spectra

An interesting model system for NAD is the case of a simple dimer. We consider only homogeneous dimers. When the two monomers in a dimer interact, the ES of the two monomers mix and split into two eigenstates. If each of the monomers have their own vibrations, these vibrations are also affected by the mixing of the ESs. Consequently, the overall system becomes a NAS. The analysis can be extended to larger oligomers as well. My analysis in this chapter is limited to a simple dimer. The simplest symmetry analysis of the dimer Hamiltonian indicates that its symmetry can be represented by a four element symmetry point group, $\{E, P_e, P_v, P_{ev}\}$. It can be shown that this group is isomorphic to the C_{2h} point group. Using the character table of C_{2h} the symmetry adapted linear combination of the dimer system are worked

out in a basis defined by the zeroth order basis. Since, the main problem is of either two-state interaction of the ESs or of a displaced HO problem, these are the two limits in which this Hamiltonian is analytically soluble. The MRTDCCM gives solutions to the displaced HO. In addition, the two ES problem can be simply diagonalized. Hence, we decided to attempt solving this problem by MRTDCCM.

One advantage of this choice is that it is also extendable to finite temperature by using thermofield dynamics. Such an extension requires doubling the vibrational DOF, but no other change in the overall ansatz. A program has been written for this purpose but I have not fully debugged it so far. Hence, this work is currently going on and hopefully the results will be ready soon.

Chapter 6: Conclusions

In this chapter I summarize the overall thesis. I highlight the main features of the criteria presented in Chapter 2. Gist from the results presented in Chapter 3 and Chapter 4 are discussed. The important features of these results are highlighted. The methodology developed for the dimers in Chapter 5 are discussed in short. In addition, I discuss the future scope of the work presented in this thesis. Once I obtain the results of the on-going calculations from Chapter 5, my aim in future is to extend this theory to oligomers.

List of publications:

- Manuscript for the work done in Chapter 2 and Chapter 3 is communicated with Journal of Physical Chemistry(A).
- Manuscript for the work done in Chapter 4 is under preparation.
- Chapter 5 is under development and manuscript will be prepared as soon as the results are ready.

Chapter 1

Introduction

1.1 Brief discussion on nonadiabatic dynamics

1.1.1 Born-Oppenheimer approximation

The first step in studying the time-evolution of a molecular system is to solve the timedependent Schrödinger equation,

$$i\hbar\frac{\partial\psi}{\partial t} = H\psi. \tag{1.1}$$

Here, *H* on the RHS of Eq.1.1 is the total molecular Hamiltonian. It encapsulates terms for the nuclear kinetic energy, the electronic KE, the electronic repulsion, the electronic nuclear attraction and the nuclear-nuclear repulsion,

$$H = T_N + T_e + V_{ee} + V_{eN} + V_{NN}. \tag{1.2}$$

The eigenstates, ψ , of H are,

$$\psi(r,Q) = \sum_{i} \phi_i(r;Q) X_i(Q). \tag{1.3}$$

In Eq.1.3, ϕ_i is a member of the set of the electronic wave functions which depend on the electronic coordinates, r. They are also parametrically dependent on the nuclear coordinates, Q. For every nuclear configuration, there exists a different set of electronic WFs. $\{X_i\}$ is the set of nuclear WFs, defined for each i^{th} electronic state. It is dependent

on the coordinates of a given nuclear DOF. In its exact form, Eq.1.3 is called Born-Huang expansion and the set of electronic WFs, $\phi_i(r; Q)$, forms a complete orthonormal basis set for the electronic DOF.

Many chemical studies are restricted to a well-separated single electronic surface, for example the ground electronic surface. In such cases, an approximation can be invoked to Eq.1.3 which separates the electronic and nuclear WFs. This is a well-known approximation named Born-Oppenheimer approximation [1–3]. BOA is based on the assumption that since the electronic masses are much smaller than the nuclear masses, the electrons move much faster than the nuclei. Thus, the electrons can be assumed to be moving in a fixed-nuclei field in BOA. With this, the molecular WF, ψ , becomes product separable in the electronic and nuclear space. So under BOA, Eq.1.3 can be rewritten as,

$$\psi(r,Q) = \phi_i(r;Q)X_i(Q). \tag{1.4}$$

As a result, the molecular Hamiltonian can be written as a sum of the electronic Hamiltonian, H_e , and nuclear Hamiltonian, H_N . The eigenvalues of H_e are generated by solving the electronic SE,

$$H_e\phi_i(r;Q) = \epsilon_i(Q)\phi_i(r;Q). \tag{1.5}$$

Here, i is a given ES and H_e is the electronic Hamiltonian given by,

$$H_e = T_e + V_{ee} + V_{eN} + V_{NN}. (1.6)$$

 ϵ_i , dependent on the nuclear geometry, acts as the potential energy surface for the nuclear WFs. Hence, the nuclear Hamiltonian becomes,

$$H_N = T_N + \epsilon_i(Q), \tag{1.7}$$

and, the nuclear SE is written as,

$$H_N X_i(Q) = \varepsilon_i(Q) X_i(Q).$$
 (1.8)

Eq.1.8 is commonly known as adiabatic approximation.

1.1.2 Breakdown of BOA

While BOA works successfully for the dynamics happening on a well-separated single electronic surface, it is rendered completely obsolete in the case of near-degenerate ESs[2]. In these degenerate regions, the coupled terms resulting from Eq.1.3 become quite strong and they can no longer be ignored. The break down of BOA is quite common in the polyatomic molecules where there are more number of near-degenerate ESs and higher number of nuclear DOF [1, 2]. Under such conditions, approximate ansatz in Eq.1.4 no longer holds and ansatz in Eq.1.3 must be used in the total SE,

$$[T_N + \epsilon_i(Q)]X_i(Q) = EX_i(Q). \tag{1.9}$$

Upon multiplying with ϕ_j^* from the left and integrating over the electronic space, the coupled equations of motion from SE are obtained,

$$[T_N + \epsilon_j(Q)]X_j(Q) - \sum_i \Lambda_{ji}X_i(Q) = EX_j(Q). \tag{1.10}$$

 Λ_{ji} are the nonadiabatic coupling elements (or, derivative couplings) defined as,

$$\Lambda_{ii} = \delta_{ii} T_N - \langle \phi_i(Q) | T_N | \phi_i(Q) \rangle. \tag{1.11}$$

Nonadiabatic coupling terms describe the interaction between the electronic and nuclear DOF in the region of energetically degenerate ESs. Such coupled interactions are called the vibronic couplings. It should be noted that EOM in Eq.1.10 hold for both the complex and real matrices for the electronic energies. We can rewrite Eq.1.10 as,

$$HX_i(Q) = EX_i(Q), \tag{1.12}$$

where, H is given by,

$$H = T_N + \epsilon_j(Q) - \sum_i \Lambda_{ji}. \tag{1.13}$$

Dynamics in which the vibronic effects become too essential to ignore are called

nonadiabatic dynamics. Various photochemical processes, especially those which involve radiationless energy transfers, charge transfer reactions, and electronic quenching, are some examples where nonadiabatic effects are at the core of the dynamics [4–15].

1.1.3 Conical Intersection and its role in NAD

One prime example where NAD become vital is the case of a CI between two ESs[1–3, 16]. The CI is the region of continuous points of electronic degeneracies in the multidimensional coordinate space of nuclear DOF in polyatomic systems. In the neighbourhood of a CI, the derivative couplings Λ_{ji} (Eq.1.11) exhibit rapid growth due to the decreasing electronic energy gap. Thus, a wave packet that starts from a single electronic surface can spread over another surface with no loss in its energy. For this reason, CIs are alternatively called photochemical funnels since they act as the doorways for the ultrafast radiationless interstate crossing, which occurs at femtosecond-timescale.

From the non-crossing rule, the subspace of a CI (between the ESs of same symmetry) is $(N^{int} - 2)$ -dimensional where N^{int} is the total internal degrees of freedom [17]. Hence, for same-symmetry case the CI subspace in linear polyatomic systems will be $(3N^{int} - 7)$ -dimensional while in non-linear polyatomic systems, it will be $(3N^{int} - 8)$ -dimensional. On the other hand, the subspace of the CI is $(N^{int} - 1)$ -dimensional if the intersecting ESs belong to two different irreducible representations. CIs are ubiquitous in polyatomic molecules and there are ample examples available in the literature on the dynamical studies in the vicinity of CIs [1].

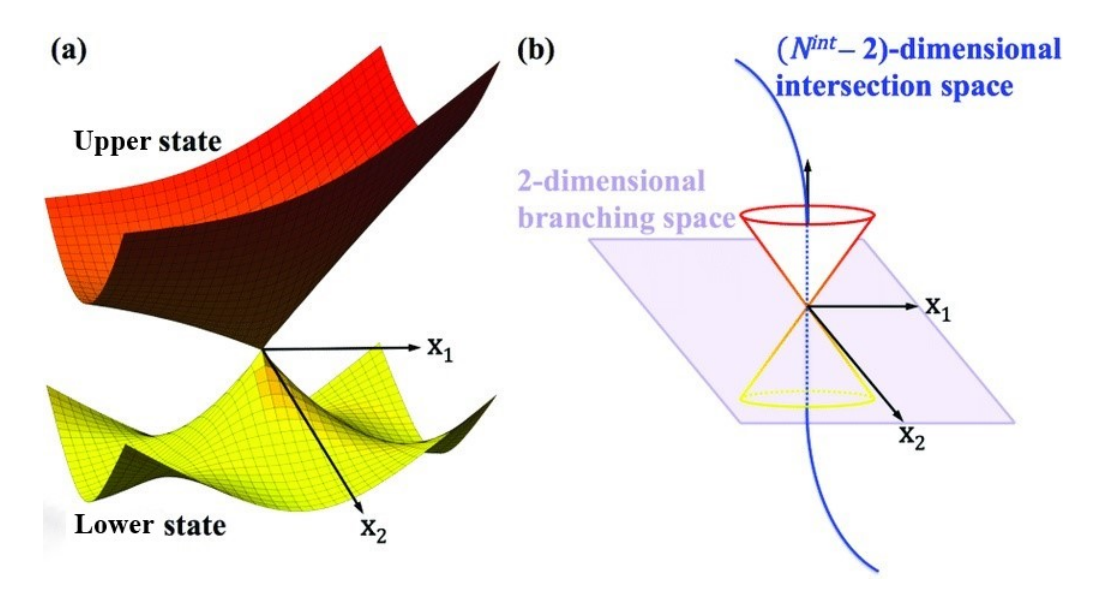


Figure 1.1: Pictorial representation of a CI in $(N^{int} - 2)$ -dimensional space [18])

1.1.4 Representation of PES and Vibronic Hamiltonian

There are two major ways to represent electronic PESs, adiabatic and diabatic. The Hamiltonian in Eq.1.13 is adiabatic Hamiltonian. This representation is valid for cases where ESs are well apart and the derivative couplings in Eq.1.13 can be safely ignored. However, in the vicinity of a CI, the adiabatic electronic surfaces become highly anharmonic. Nonadiabatic couplings gain large and divergent values and so their determination becomes cumbersome. This can be avoided by opting an alternate representation for a small set of strongly coupled ESs. A unitary transformation, U, can be carried out on the adiabatic electronic WFs at each point in space. This provides a new basis for ESs called the diabatic basis [1-3].

$$\varphi = U(Q)\phi. \tag{1.14}$$

The subset of quasi-degenerate ESs used in the above transformation is decoupled from all other ESs in the system. The electronic WFs in the diabatic representation change slowly and smoothly as the functions of the nuclear coordinates. After carrying out the unitary transformation, the first-order derivative couplings disappear and the off-diagonal terms appear. In addition, a diagonal nuclear KE matrix is obtained. Thus, in

diabatic picture the SE (in matrix notation) is written as,

$$[T_N + P]\tilde{X} = i\hbar \frac{\partial \tilde{X}}{\partial t}.$$
 (1.15)

 \tilde{X} and P are the matrix of nuclear functions and the matrix of electronic potential energies in diabatic basis, respectively. The terms that describe the coupling between the ESs are included within P.

In addition, the diabatic potential elements can be expanded as a Taylor series around a fixed nuclear geometry at Q'. For example, the expansion can happen around the point of intersection of two ESs. At Q'_0 , the energies of the two basis are identical. Hence, the adiabatic PES can be generated as the eigenvalues of the diabatic potentials by using the following transformation.

$$\epsilon = UPU^{\dagger}. \tag{1.16}$$

In the case of a two-state system, the transformation in the Eq.1.16 yields two types of coupling terms at the first and second-order expansion of P. First are the diagonal coupling terms, a_{ii}^i , where i=1,2 are the two ESs. The second are the off-diagonal linear coupling terms, c_{ij} where $i\neq j$. The former set of couplings control the energy-gap between the two ESs while the latter couples the two states. The vibrational modes of the first type are called the tuning modes. The modes responsible for the off-diagonal interstate coupling are called the coupling modes. If two intersecting ESs are of different symmetries, the diagonal couplings will be non-zero for the modes that fall in the totally symmetric IRep, A_g . On the other hand, depending on the point group of the concerned molecule, non-zero linear off-diagonal couplings will be caused by the modes belonging to a nontotally symmetric IRep. Thus in diabatic picture, the vibronic Hamiltonian upto second-order can be written as follows [19],

$$H = \sum_{i} \frac{\omega_{i}}{2} \left(-\frac{d^{2}}{dQ_{i}^{2}} + Q_{i}^{2} \right) \mathbf{1} + \begin{pmatrix} \frac{\Delta}{2} & 0 \\ 0 & \frac{\Delta}{2} \end{pmatrix} + \sum_{i \in T_{1}} \begin{pmatrix} a_{i} & 0 \\ 0 & b_{i} \end{pmatrix} Q_{i} + \sum_{(i,j) \in T_{2}} \begin{pmatrix} a_{i,j} & 0 \\ 0 & b_{i,j} \end{pmatrix} Q_{i} Q_{j} + \sum_{i \in C_{1}} \begin{pmatrix} 0 & c_{i} \\ c_{i} & 0 \end{pmatrix} Q_{i} + \sum_{(i,j) \in C_{2}} \begin{pmatrix} 0 & c_{i,j} \\ c_{i,j} & 0 \end{pmatrix} Q_{i} Q_{j}.$$

$$(1.17)$$

This Hamiltonian represents the quadratic VC model. At its linear level, the QVC model becomes the linear VC model. T_1 and T_2 are the groups of tuning modes at linear and bilinear levels, respectively. Similarly, C_1 and C_2 are the groups of coupling modes at linear and bilinear levels, respectively. It should be noted that the normal modes in the above Hamiltonian are defined after removing system's translational and rotational modes. Second, the rotation-vibration coupling terms are dropped. As a consequence, the angular momentum and its z-component are constants of motion. The Hamiltonian is manifestly hermitian within the normal coordinate set. So, its overall energy is also a conserved quantity throughout the time-propagation.

There are no zeroth-order CI in the diabatic representation. Instead, one has the surface of curve-crossing. For two ESs of different symmetries, SCC is also a $(3N^{int}-7)$ -dimensional hyper-surface in the $(3N^{int}-6)$ -dimensional normal mode space. The SCC satisfies the equation,

$$\epsilon_1(Q) = \epsilon_2(Q). \tag{1.18}$$

For the QVC model, the SCC is defined by the equation,

$$\sum_{i} (a_i - b_i) Q_i + \sum_{i,j} (a_{i,j} - b_{i,j}) Q_i Q_j = -\Delta.$$
 (1.19)

Though the CI and the SCC are not identical, they follow each other very closely. Consequently, the two terms can be used interchangeably for all practical purposes. Here onward SCC is used in general.

1.2 Literature review of theoretical methods for NAD

Perturbative approaches do not work well in simulating NAD because of the strongly coupled nuclear DOF in nonadiabatic systems. This motivated the development of numerical methods to study NAD. The main objective of such numerical methods is to calculate the spectra for the ESs involved in the NAD. In time-independent picture, the spectral density for transition from initial state, ψ_i to a final state, ψ_f is given by,

$$P(E) = \frac{2\pi}{\hbar} \sum_{f} |\langle \psi_i | \mu | \psi_f \rangle|^2 \delta(E - E_f + E_i). \tag{1.20}$$

 μ is the electronic dipole transition operator and E is the energy absorbed by the system. In the TD picture, the spectra are obtained by carrying out the Fourier transform of the autocorrelation function, C(t).

$$P(\omega) = \int dt e^{i\omega t} C(t), \qquad (1.21)$$

$$C(t) = \langle \mu \psi_{0,n}(0) | \mu \psi_{0,n}(t) \rangle$$
. (1.22)

Here, $|\psi_{0,n}(0)\rangle$ is the initial ES(before the transition) and $|\psi_{0,n}(t)\rangle$ is the final ES(after the transition).

Earliest numerical studies started with the task of finding the eigenvalues of the vibronic Hamiltonian and the spectrum using Eq.1.20. To do so, ψ_f was expanded in the direct product basis of diabatic ESs, $|\phi_i\rangle$ and suitable harmonic oscillator WFs, $|\nu_k\rangle$.

$$\psi_f = \sum_{i,\nu_1,\nu_2,...,\nu_k} c_{i,\nu_1,\nu_2,...,\nu_f}^{(f)} |\phi_i\rangle |\nu_1\rangle |\nu_2\rangle ... |\nu_k\rangle.$$
 (1.23)

For each k^{th} mode, $\{|n_I\rangle\}$ is the set of basis functions chosen. The size of the vibronic Hamiltonian matrix increases exponentially with the number of basis functions for each vibrational mode. So even for 6-7 vibrational modes, each with basis functions less than 30, the numerical solution of Hamiltonian matrix becomes impossibly tedious. To address this issue, the primitive numerical calculations on NAD considered systems with reduced dimensionality. In most cases two ESs and a few vibrational modes (upto 3 modes) were taken into account . Further, the Hamiltonian matrix was diagonalized in the basis of the unperturbed HO eigenfunctions of the vibrational modes considered.

This technique made the vibronic Hamiltonian matrix sparse. In sparse matrices most of the elements are zero and so, they are much easier to solve [2, 20–23].

The basis set expansion method, as discussed above, can handle only a few number of vibrational modes. It faces the issue of exponential rise in the cost of computations with increasing number of basis functions for the vibrational DOF. Even though it is numerically exact, for larger systems computations become impossibly tedious. For a better description of the NAD it is always desirable to include as many vibrational modes as possible. TD quantum-mechanical approaches in the semi-classical limit offered a good alternative to include more number of vibrational modes in the numerical calculations. These approximate approaches were originally designed to study the dynamics of collision reactions. [24, 25] Heller's work offered a trajectory based method in which a quantum WP was propagated in time. Heller later generalized the EOM of his TD WP method for a wider class of problems such as CCs.[26] This was a variational approach based on Dirac-Frenkel-Mclachlan variational principle.[27, 28] In a way, this method introduced a semi-classical approximation to the TD Hartree theory. It is assumed that initially the WFs of particles are localized and product-separable. EOM for each particle evolve in a self-consistent and are described by its own effective one-particle Hamiltonian. This effective Hamiltonian for each particle includes a meanfield potential exerted by rest of the particles. In this way, the TD self-consistent-field method introduced a trajectory based approach to tackle the QM problems in which some DOF are much more correlated than others. TDSCF was applied in the context of NAD for a two-state, three-mode problem.[29]

Domcke and co-workers proposed a path-integral based approach to treat the multimode VC problem [30–32]. In the general PI approach the total time-interval for the calculation of correlation functions is sliced into intervals of equal lengths. Next, a complete basis of electronic WFs is inserted between each of the slices and the terms are summed up. The total number of terms obtained represents as many electronic paths. For each of these electronic paths a propagator of the TD Hamiltonian can be expressed in the vibrational subspace. The vibrational propagators of the Hamiltonian become separable for each of the electronic trajectories. In this way, the full TD propagator is factorized into a product of single-mode propagator for each electronic path. Thus, the exponential scaling in the full propagator calculations is brought down to a linear scaling in the factorized vibrational propagator calculations for each of the electronic paths. Domcke and co-workers developed the concept of classes of approximately equivalent paths as an additional approximation to the PI approach. For individual classes, the

average value of the vibrational propagators is calculated and then it is multiplied with the combined weight of the class. Thus instead of taking the sum over all the electronic paths, the mean-weighted contribution of each class (of equivalent paths) to the PI is taken. This approximation to the PI approach helps in taking a larger number of slices of the total computational time-interval.

Also various semi-classical methods have been developed over the years with the main goal of describing larger systems[33–38]. These methods were primarily inspired from the early work of Miller[39]. In addition, a variety of mixed quantum-classical approaches have also been developed[40–45].

The numerical calculations on NAD became much more exact with the advent of system-bath based methods. In SB approaches the total molecular system is divided into two subspaces which are coupled to each other. First is the system subspace which includes the DOF which are at the core of the reaction dynamics. Hence, these DOF need a numerically exact treatment using a suitable basis set. Second is the bath subspace which includes the DOF which do not significantly influence the overall dynamics. Such DOF can be approximately described by using a less accurate but computationally more affordable approaches. SB formulations enable the inclusion of all the vibrational DOF in the numerical calculations. It gives a considerable improvement in the simulated results while keeping the computational costs at bay. In this way the exponential bottleneck problem is managed by this approach.

SB formulations have garnered a lot of attraction over the years. Numerical strategies under the SB approach essentially focus on building a TD multiconfiguration treatment for the SS. In this line, MCTDSCF was perhaps the first successful theoretical method[46]. In MCTDSCF two configurations are taken for system WFs. Every system configurations has its own harmonic bath WF. Each of these bath WFs interact with its associated system WF in an averaged way.

The problem with MCTDSCF method is that it requires a priori introduction of projection operators to build the MC space. To this end, the multiconfiguration TD Hartree method introduced much more simpler formulation which does not depend on the projection operators[19, 47–52]. It became the benchmark method for the theoretical calculations. MCTDH method uses a variationally optimized TD single-particle basis to construct the basis of the N-particle Hilbert space. The general TD MC ansatz

for f number of DOF is given as,

$$\Psi(Q_1, Q_2, ..., Q_f, t) = \sum_{i_1=1}^{N_1} ... \sum_{i_f=1}^{N_f} A_{i_1, i_2, ..., i_f} \phi_{i_1}^{(1)}(Q_1, t) \phi_{i_2}^{(2)}(Q_2, t) ... \phi_{i_f}^{(f)}(Q_f, t)$$
(1.24)

 ϕ_f is the SPFs described for f^{th} DOF. For each DOF, the configuration space is made up by N_f number of functions. These SPFs form an orthonormal set with each other and also with their derivatives in time. An effective one-body Hamiltonian operator is defined to upgrade the SP basis. This Hamiltonian consists of two parts. First is the non-interacting part and is written as the sum of all the SP operators in the Hamiltonian. The second is the correlated SP potential. The effective SP potential is generated by averaging the many-body interactions present in the system over the current WF. The resulting SP Hamiltonian is similar to the Fock operator, commonly used in the electronic structure theory particularly for the multi-determinantal many-electron WF. The influence of all effective one-body interactions are absorbed into the definition of the Fock-like operator. This improves the quality of the basis at any given time and thus, the dynamic basis used in MCTDH is expected to be better than a static basis.

MCTDH approach converges very fast even for high-dimensional problems. Having said that, this improvement comes at the cost of doing an additional calculation for constructing the Fock-like operator and the dynamic basis. The ansatz used in Eq.1.24 is very similar to the one used in the exact basis set expansion method (Eq.1.23). So, MCTDH method is also prone to the exponential rise in the computational costs on increasing the number of DOF. Recently, a variant of MCTDH has been suggested in the framework of SB separation of vibrational DOF [53–55]. This variation generalizes the EOM from MCTDH to incorporate the nonorthogonality of the parametrized bath WFs. The Gaussian-based MCTDH is a particularly successful hybrid approach. It can either be applied as a full Gaussian-based method [55] or as a SB-based approach [54]. In the latter version the system DOF are treated by the numerically exact MCTDH method. The bath DOF, however, are treated by TD frozen Gaussian WPs which follow Heller's GWP equation in the fixed width limit. Essentially, the overall product of SPFs in Eq.1.24 is partitioned into two products.

$$\prod_{i=1}^{f} \phi_{i_f}^{(f)}(Q_f, t) = \prod_{k=1}^{s} \phi_{i_k}^{k}(Q_k, t) \prod_{k=s+1}^{b} \phi_{i_k}^{k}(Q_k, t)$$
 (1.25)

First is the product of SPFs for all system modes, s and other is the product of Gaussians for all the bath modes, b. It follows that f = s + b. Each single particle configuration space interacts with the average of the Gaussian CS for each bath mode. Moreover, these Gaussians are coupled to each other and on each ESa different set of CS for each type of vibrational modes can be defined. This complex yet numerically exact hybrid method decreases the exponential scaling issue faced by MCTDH.

1.3 Dynamics of a NAS

In this section, the dynamics of a NAS is summarised in the light of the computational results of the studies done by Schneider and co-workers [56]. That work was concerned with the dynamics of a 2-state 3-mode model. It showed that the expectation values of position and momenta of the totally symmetric normal modes undergo damped oscillations. For the positions of the tuning mode WPs expectation values become small and finite in the long-time limit (Figure 5a of Ref. 24). As for the expectation values of the momenta, they become zero in the long-time limit (Figure 5b of Ref. 24).

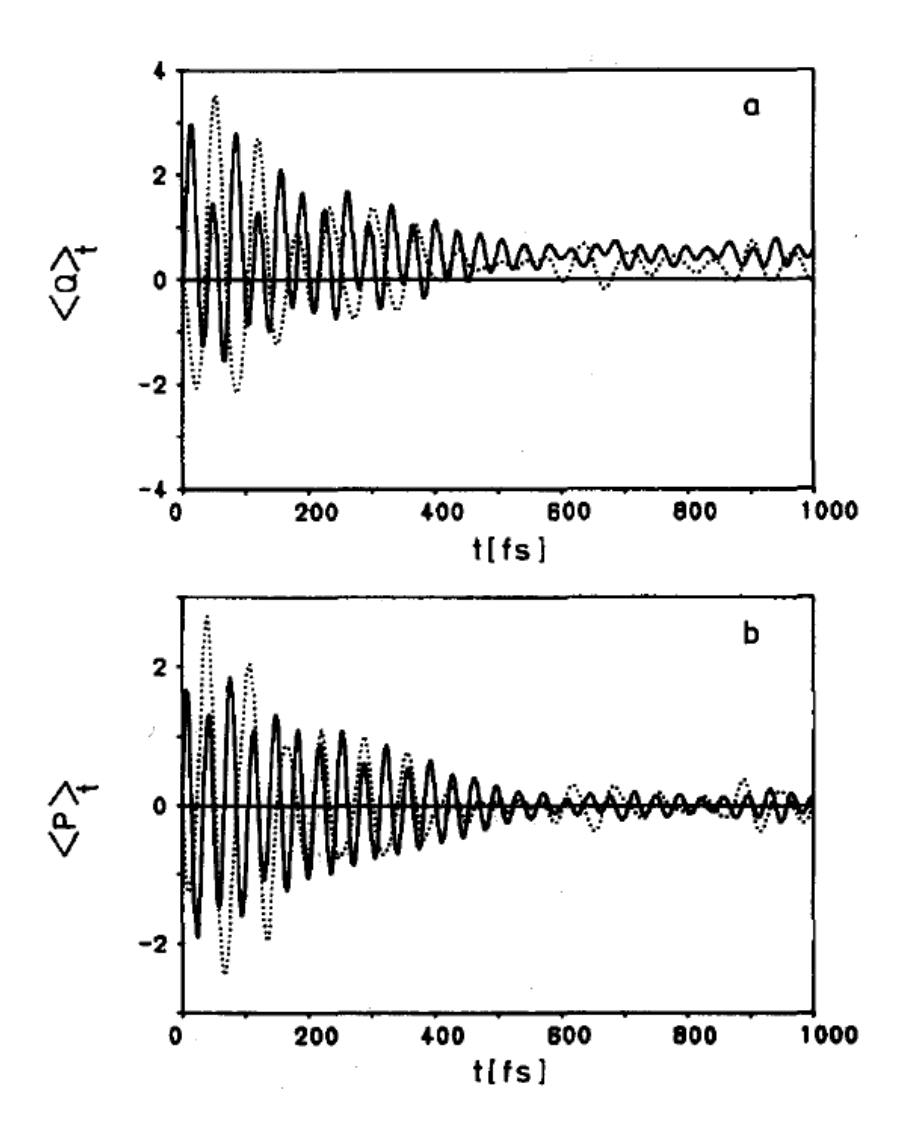


Figure 1.2: Time-evolution of the (a) position expectation values and (b) momentum expectation values for the tuning modes WPs starting from the initial ES(Fig. 5 from Ref. [56], reprinted with permission, Copyright 1990, AIP Publishing)

The authors also observed that the statistical entropies associated with the reduced density matrices of individual modes increased more or less monotonically throughout the time-evolution (Figure 13b of Ref. 24).

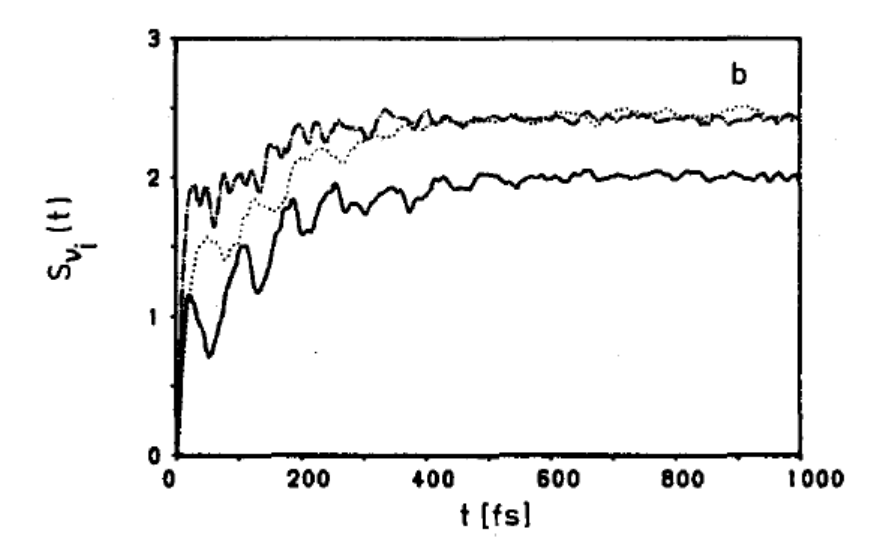


Figure 1.3: Time-evolution of the entropies of the vibrational modes considered in the model system for the WP starting from initial ES(Fig. 13b from Ref. [56], reprinted with permission, Copyright 1990, AIP Publishing)

The statistical entropies can be associated with the degree of dephasing. The monotonic increase of the entropies, thus, is a sign of increasing dephasing. The increasing statistical entropy implies an increase in the required number of single-particle basis functions for that DOF. This properly describes its dynamics in the environment it moves in.

In addition the reduced probability distribution for tuning and coupling modes were discussed. For the tuning modes, in the beginning of time the WP remains localized on the initial surface. Gradually as the population on the initial surface starts to decay the WP along the tuning modes broadens and splits (Fig. 1.4).

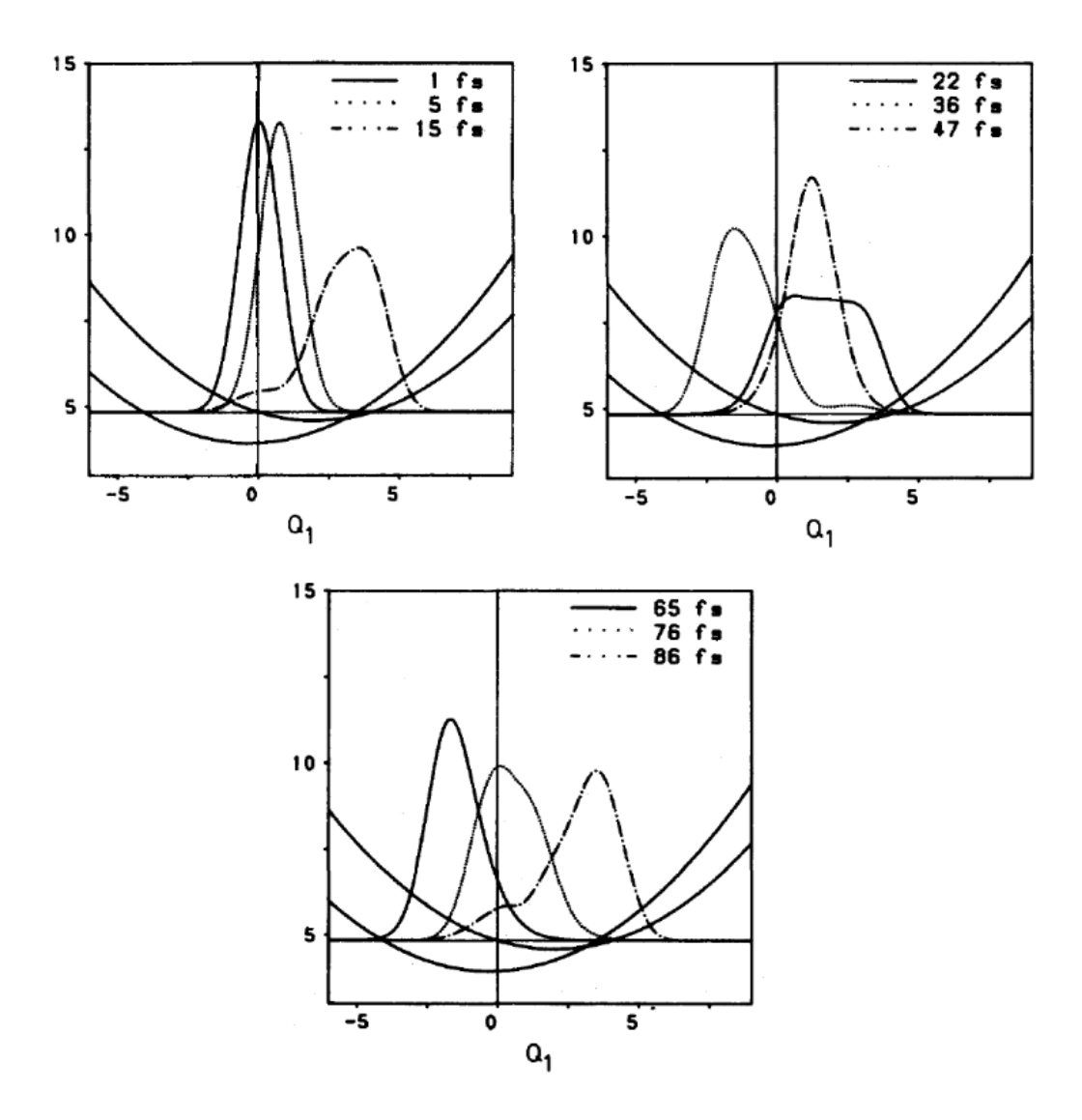


Figure 1.4: Reduced probability distribution of tuning mode WP. An overall broadening and dephasing of the WP (Fig. 9 from Ref. [56], reprinted with permission, Copyright 1990, AIP Publishing)

On the other hand, the coupling mode WP loses its Gaussian-like structure completely by the end of time-propagation. The coupling mode WP is highly subjected to the anharmonicity of the CI region. The WP that started on the upper surface eventually extends onto the lower surface. A complex interference pattern occurs due to the irreversible splittings of the WP along the coupling mode (Fig. 1.5).

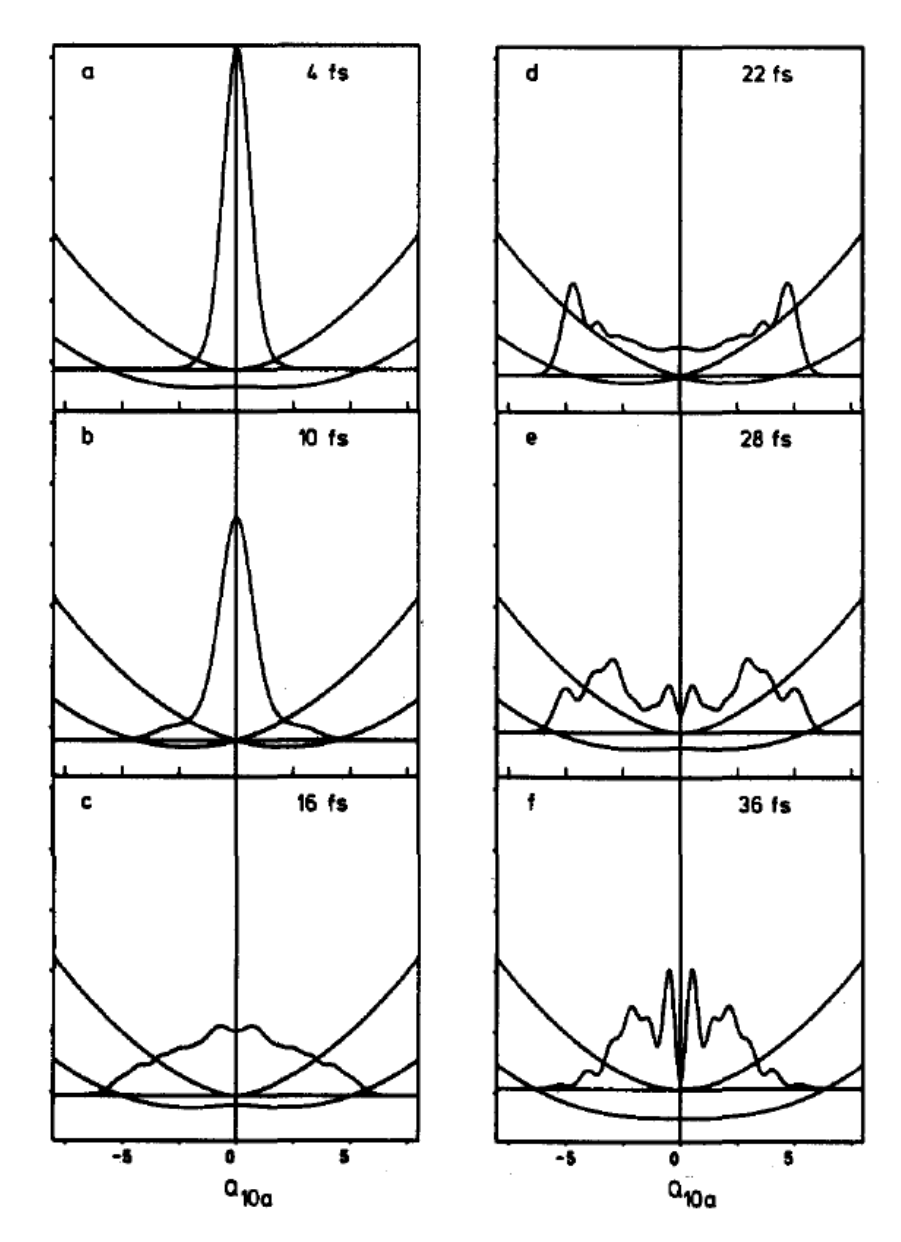


Figure 1.5: Reduced probability distribution of coupling mode WP. A complete loss in the WP structure happens (Fig. 10 from Ref. [56], reprinted with permission, Copyright 1990, AIP Publishing)

1.4 Goal of the present work and overview of the thesis

My own work is described in Chapters 2-5. The SB approaches (as discussed in the Sec. 1.2) have been implemented to varying degree of success, yet no concrete guidelines for the systematic classification of the modes into system and bath DOF have been proposed and tested till date. There have been some efforts in this direction but those were focused around optimizing the BS[57–59, 59, 60, 60–62]. Continuing on the theme of effective-mode approach, Santoro and co-workers[63–65] extended the approach in a hierarchical

manner to construct a sequence of sets of bath modes which in turn extends the period of quantum dynamics from short-time to long-time.

The goal of my thesis work is threefold. The first goal is to put forward a set of criteria that clearly outlines the guidelines for choosing the system modes out of the total vibrational modes. The second goal of my work is to develop two different theoretical approximations for the bath DOF in the SB framework. One of these methods is the generalized TDSCF approach as described in Chapter 3 and the second is the multireference time-dependent coupled cluster method, discussed in detail in Chapter 4. Finally, my third goal in this thesis is to use MRTDCCM for studying the Hamiltonian of a simple dimer and to extend this approach to finite temperature studies in the dimers by using the thermofield method.

The discussions on WP CC presented in Sec. 1.3 lay the foundations for the criteria for classifying the system and bath variables which is the first goal of my work. Essentially the choice of system and bath modes should be made on the extent of WP dephasing along the coordinate of the concerned mode. Extending from the work of Schneider and co-workers [56], the mathematical equations for WP CCs are formulated in Chapter 2. CCs along the coupling and tuning modes are explicitly presented. Repeated CC along a particular mode leads to the rise in its statistical entropy. The importance of this observation is highlighted through these mathematical equations. The proposed set of the criteria is outlined in detail in Chapter 2. Different mechanisms of CC along the tuning modes are defined and discussed at length for general case.

In Chapter 3 the first numerical application of these criteria on realistic systems are presented. The system DOF are treated exactly using a numerically converged HO basis set. For the description of bath modes, a generalized TDSCF approximation has been used [26, 29]. This is the first part of the second goal of my work. We use a GWP to describe the bath DOF. It should be noted that we use the harmonic potential and in that case, GWP method becomes exact. TDSCF ansatz and the working equations are presented in this chapter. The first application is on the benchmark 24-mode pyrazine system which has a CI between S_2 and S_1 ESs. Pyrazine has one non-totally symmetric coupling mode and five totally symmetric tuning mode. Vibronic Hamiltonian for the QVC model is used in this case. To support the proposed criteria, a comparative study between two model cases are carried out. First is 3 + 21-model which has 3 system modes and 21 bath modes. This is compared against a 4 + 20-model which has 4 system modes and 20 bath modes. The results are presented in terms of ACFs, spectra and

electronic population density. In addition, these results are contrasted against the numerically accurate results of MCTDH and G-MCTDH methods. The second case study for the support of these criteria is 3-mode spin-boson model. In spin-boson model the ESs are coupled by a constant. Hence, there is no coupling mode in this model and the discussions on CC for tuning modes alone are valid in spin-boson model. ACF and spectra for this model are presented. The effects of dropping one mode out of the SS on the NAD is discussed using these results.

Chapter 4 serves as the next part of the second goal of this work. It includes the development of MRTDCCM for describing the BS. MRTDCCM uses a time-evolution operator which is expressed as an exponential of a cluster operator. The terms in this cluster operator can be expanded as a Taylor series. MRTDCCM is an attractive approach for the bath dynamics because the lower order truncations include higher-order terms because of its exponential feature. It is a size-consistent approach and highly accurate even for lower order truncations. The ansatz and working equations are presented in detail in this chapter. The 18-mode butatriene cation is used as the first testing case of this approach within the SB framework. A (2+16)-mode model of the butatriene cation is used to test the hybrid approach. The system DOF in this case are determined by the criteria defined in the earlier chapter. ACF and spectra are presented for the study.

We next study the applicability of MRTDCCM to the analysis of the dynamics of a simplified Hamiltonian of a dimer. This and its extension to the finite temperature is the final goal of the work presented in this thesis. The model consists of two ESs and two vibrational modes which are distributed over the two monomers. Consequently, it is a nonadiabatic problem. The interest here is on the applicability of MRTDCCM rather than the NAD, which has been studied widely earlier. We present the equations of the spectra, both at 0 K and at finite temperature. We highlight how MRTDCCM allows a common formulation in both the conditions. This formalism is presented in Chapter 5. The computations for this system are not complete, so no numerical results are presented.

Finally, the overall thesis is concluded in Chapter 6. It includes a brief review of the proposed criteria which makes the primary goal of this work. The results obtained using the two approaches, TDSCF and MRTDCCM, for the description of bath modes are summarised. In addition, the future scope of this work is briefly noted. Lastly the applicability MRTDCCM is explored in the context of the dimer Hamiltonian.

Chapter 2

Classification of system and bath DOF

2.1 Introduction

In this chapter, we present the WP CC along the tuning and coupling modes. These equations are written using the discussions on the CC and WP dephasing presented in Sec. 1.3. We show analytically that the extent of WP fragmentation increases on repeated CC. WP dephases extensively along the mode for which repeated CC happens the most. Using these arguments a detailed set of criteria for separating out the vibrational modes into system and bath DOF is put forward. A greater emphasis is put into choosing the system DOF. Coupling modes and tuning modes are handled separately in the proposed criteria.

2.2 WP dynamics along vibrational modes

The dynamics along the coupling modes initiate the significant changes in the WP. These observations on the coupling mode dynamics are specifically meant for the LVC/QVC models. Since, the initial nuclear WP is a Gaussian and the driving potentials are harmonic, the WP starts moving towards the classical turning points along the totally symmetric tuning modes. Depending on the potential, they may encounter the SCC. As the centroid of the vibrational WP approaches the SCC, the effective ES energy-gap becomes small. We assume that the WP is initially located on a upper excited electronic surface. The coupling mode WF on the initial surface, $|v_c\rangle$, mixes strongly with an appropriate vibrational state on the other electronic surface because of the small energy

gap. The corresponding coupling mode state is determined by the nature of the coupling. At linear level, the change in quantum number is from $|v_c\rangle$ to $|(v_c \pm 1)\rangle$ on the other surface. For the bilinear couplings, the quantum number changes to $|(v_c \pm 2)\rangle$ or $|v_c\rangle$. If the coupling is a constant (such as in the spin-boson systems discussed later), there is no coupling mode. Instead, the electronic WP bifurcates smoothly to move on both the surfaces. The norm of WP transferred to the other surface would depend on its residence time in this quasi-degenerate region and the strength of the coupling operator. Thus, limiting to coupling mode and electronic DOF, before and after crossing the SCC, the WP would have the following structure,

$$\psi(0) = |e_2\rangle |v_c\rangle, \tag{2.1}$$

and

$$\psi(\delta_{1}) \approx c_{2} |e_{2}\rangle |v_{c}\rangle + c_{1} |e_{1}\rangle |v_{c} \pm 1\rangle + c_{1}' |e_{1}\rangle |v_{c}\rangle + c_{1}'' |e_{1}\rangle |v_{c} \pm 2\rangle,$$
(2.2)

after an elapsed time-interval, (δ_1), encompassing t=0 and the time needed to cross the SCC. The two fragments of the WPs, one on each electronic surface, go up to their respective turning points along the tuning modes and return to the SCC. After the second CC, the mixing between the appropriate coupling mode quantum states on the two surfaces occurs again. Each component of the coupling mode WP transfers part of it onto the other surface and to its own allowed vibrational states. Symbolically, the final WP after second crossing across the SCC (incorporating only coupling mode and electronic DOF) can be represented as,

$$\psi(\delta_1 + \delta_2) \approx c_2 \left[c_{22} |e_2\rangle |v_c\rangle + c_{21} |e_1\rangle |v_c \pm 1\rangle \right] + (2.3)$$

$$c_1 \left[c_{12} |e_2\rangle |v_c, v_c \pm 2\rangle + c_{11} |e_1\rangle |v_c \pm 1\rangle \right].$$

The coefficients for the fragments from the first and second CC will multiply each other for the individual surfaces. c_2 is the coefficient of the coupling quantum state, $|v_c\rangle$ on the initial US after δ_1 . Similarly, c_1 is the linear coefficient of the coupling mode state, $|v_c \pm 1\rangle$ on the LS at the end of the first crossing. The influence of bilinear or

quadratic terms are ignored in writing Eq. 2.3. c_{22} is the coefficient of the coupling state of the WP fragment that remained in $|v_c\rangle$ on the initial surface at the end of δ_2 . A part of the WP from the US jumps to the LS after the second crossing and it corresponds to c_{21} coefficient of the $|v_c \pm 1\rangle$ state on LS. Similar arguments hold for WP crossing of the fragment on the LS. c_{11} corresponds to the WP fragment on the LS that remains in its initial quantum state, $|v_c \pm 1\rangle$ at the end of the second CC. c_{12} is the coefficient for the part of the WP that jumps from the LS to $|v_c \pm 2\rangle$ or $|v_c\rangle$ state on US. A cartoon representation of this can be seen in Fig.2.1.

It should be noticed that the number of coupling mode states that are populated just after the second crossing of SCC is already more than 3 even at LVC level. These re-crossings of SCC and hence further fragmentation of WP will continue for each of the components for several vibrational periods. Each of those fragments has its own weight. Each of these transitions through the SCC will change the population profile of the coupling mode states. The highest occupied quantum number of the coupling mode on each surface would generally increase after each CC event is completed. It is obvious that all coupling mode WFs dephase extensively during the repeated passages through the SCC. The nature of the WP is no longer like any single HO eigenfunction. It loses its coherence over time and the statistical entropy associated with it increases more or less monotonically (Fig. 1.3). From this, it is clear that the multiple re-crossings of the WP across SCC are at the origin of the coupling mode dephasing. The reduced probability distribution looks significantly distorted compared to its original coherent shape along the coordinate of the coupling mode (Fig. 1.5).

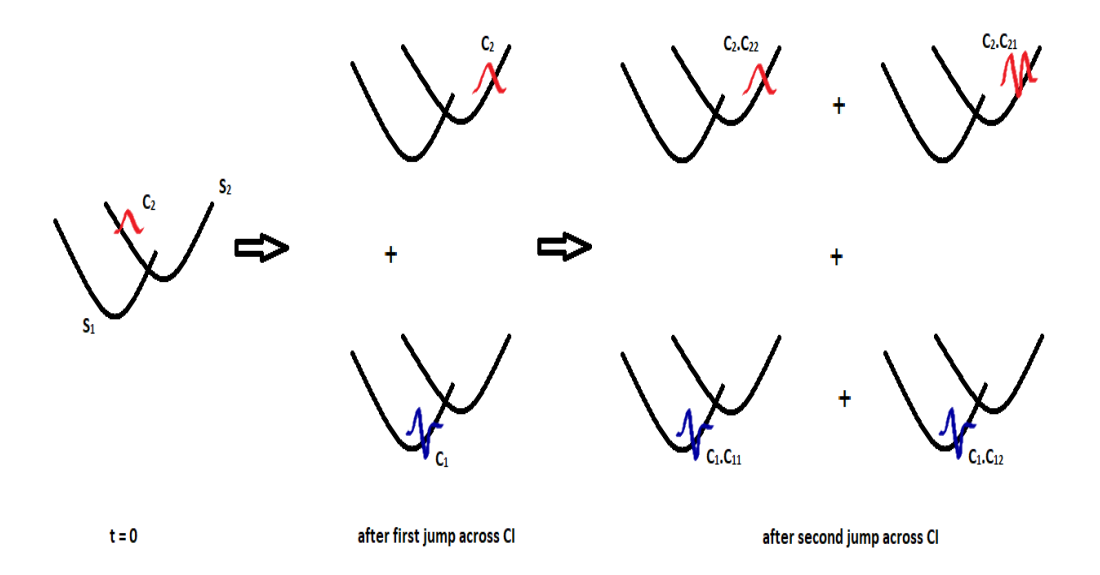


Figure 2.1: WP dynamics for CC along the tuning modes and coupling modes(at linear level)

Next, the dynamics of the WP along the direction of the tuning modes is discussed. Crossing the SCC does not affect the tuning mode WF directly. The degeneracy of the ESs is lifted after each SCC crossing is over. Each of the WP fragments propagates on one surface. After the first SCC crossing stops, the two chunks of the overall WP differ from each other in terms of the ESs and the quantum number of the coupling mode associated with them. The WFs of the tuning mode now evolve differently under the influence of their new (surface dependent) vibrational Hamiltonians. As a result, their trajectories would be different. Continuing along the coordinates of the tuning modes these two fragments go up to their respective (electronic surface dependent) turning points and return back to the SCC. Incorporating the dynamics of the tuning modes, Eqs. 2.1 and 2.2 (for only linear level) can be rewritten as

$$\psi(0) = |e_2\rangle |v_c\rangle |\chi_t(0)\rangle, \qquad (2.4)$$

and

$$\psi(\delta_1) = c_2 |e_2\rangle |v_c\rangle |\chi_t^o\rangle + c_1 |e_1\rangle |v_c \pm 1\rangle |\chi_t^o\rangle. \tag{2.5}$$

Here the evolution along the tuning mode is governed by its Hamiltonian on the US, h_2 , as given below

$$\chi_t^o = e^{-ih_2\delta_1} |\chi_t(0)\rangle, \qquad (2.6)$$

is defined until the end of the first crossing. Similarly, at the end of δ_2 , Eq. 2.3 can be rewritten for the overall dynamics including the tuning mode dynamics.

$$\psi(\delta_{1} + \delta_{2}) = c_{2} \left[c_{22} |e_{2}\rangle |v_{c}\rangle |\chi_{t}^{1}\rangle + c_{21} |e_{1}\rangle |v_{c} \pm 1\rangle |\chi_{t}^{2}\rangle \right] + c_{1} \left[c_{12} |e_{2}\rangle |v_{c}, v_{c} \pm 2\rangle |\chi_{t}^{1}\rangle + c_{11} |e_{1}\rangle |v_{c} \pm 1\rangle |\chi_{t}^{2}\rangle \right].$$
(2.7)

Here,

$$\chi_t^1 = e^{-ih_2(\delta_2 + \delta_1)} |\chi_t(0)\rangle,$$
 (2.8)

and,

$$\chi_t^2 = e^{-ih_1\delta_2} e^{-ih_2\delta_1} |\chi_t(0)\rangle.$$
 (2.9)

 h_1 and h_2 are harmonic Hamiltonians with different local minima and force constants. Hence, the two WPs are displaced Gaussians with different widths, centroids, momentum expectation values and phase factors. The trajectories on the two surfaces are different. As a result, the WPs of the tuning modes are a superposition of relatively displaced Gaussians after the second and subsequent re-crossings. These parts of the WP are not orthogonal but linearly independent. Consequently, the overall reduced density matrix has several non-zero eigenvalues. The overall reduced probability distribution along the position of the tuning modes appears like a sequence of Gaussians chasing each other (Fig. 1.4). This type of fragmentation will continue on each surface as long as the WPs on two surfaces have a time-lag in reaching the SCC. This in turn increases the dephasing of the overall WP. It should be noted that the tuning modes on each surface would develop a secondary Gaussian such as χ_t^2 , roughly in the same

time interval as the coupling mode transition. Thus, it appears as a coupled two-body excitation. This is one of the origins of the concerted many-body dynamics mediated through a SCC. It is because of such many-body interaction that a full configuration interaction(FCI)-like method is necessary for DOF which go through the SCC.

2.3 Criteria for classifying system and bath variables

Based on these discussions, we now present the criteria for dividing the vibrational modes into the system and bath variables in the system-bath formulation. Vibrational modes that undergo extensive dephasing are the most affected in the overall system dynamics. These must be included in the system DOF. The rest of the vibrational modes that neither touch the SCC nor are strongly affected by the CC can be treated as bath modes. As a consequence, only the coupling and tuning modes would qualify for the consideration of the system modes, though not all of them need to be incorporated into the system DOF. Thus, the first of the criteria is that *all the spectator modes that neither couple the two ESs nor tune the ES energies can be relegated to the bath modes*.

Next, the WFs associated with coupling modes are influenced strongly when the WP motion along the tuning modes carries the system WP through the SCC. This leads to the redistribution of the coupling mode WFs between the ESs. WPs of all the coupling modes are affected when the overall WP crosses the SCC irrespective of the magnitude of the coupling constants they have. So, the second part of the criteria is that *all the coupling modes must be included in the system DOF*.

The dephasing of the WP in the direction of the tuning modes depends on its crossing the SCC for the concerned mode. It is possible that the motion of the WP along some tuning modes may not take it across the SCC. Such modes have a comparatively insignificant influence on the overall dynamics and can be classified as bath modes.

We address the question of the WP crossing the SCC in a hierarchical manner. In the absence of vibronic coupling, the WP follows its classical trajectory. It begins in the FC zone and goes up to its classical turning point along each tuning mode and returns to the FC zone from there. We now specialize to the case of a single tuning mode. In this case, the WP can cross the SCC only if the point of SCC along the concerned tuning mode, (Q_k^{SCC}) , lies between the FC zone and its classical turning point (Q_k^T) . Thus, the necessary criterion for extensive dephasing of a tuning mode WP is that its classical turning point must lie beyond its point of SCC. The qualitative condition for the WP to

cross the SCC becomes

$$0 \le Q_k^{SCC} \le Q_k^T, (Q_k^{SCC} > 0, Q_k^{T_2} > 0)$$
 (2.10a)

$$0 \ge Q_k^{SCC} \ge Q_k^T, (Q_k^{SCC} < 0, Q_k^{T_2} < 0)$$
 (2.10b)

In one dimension the SCC point (in the linear approximation to Eq. 1.19) is given by,

$$Q_k^{SCC} = \frac{-\Delta}{b_k - a_k}. (2.11)$$

Similarly, the turning point on the US is

$$Q_k^{T(2)} = \frac{-2b_k}{\omega_k}. (2.12)$$

The argument can be extended to all the tuning modes in a straightforward manner. We call this type of crossing a *direct crossing*.

Going beyond one dimension, it is not necessary for the WP to cross the SCC along a single tuning mode alone. It could cross, for example, in a plane defined by two tuning modes but not in the direction of either of the tuning modes. In this case, our attention is expanded to a two-dimensional plane formed by two tuning modes, Q_1 and Q_2 . The SCC in this plane (at linear approximation to Eq. 1.19) is given by the straight line

$$(b_1 - a_1) Q_1 + (b_2 - a_2) Q_2 = -\Delta (2.13)$$

Classically, the energetically allowed trajectories in this two-dimensional space fall within the ellipsoid defined by the initial energy of the WP. We expect that this holds for the quantum WP as well, at least during the initial phase of its evolution. The WP is likely to be exposed to the SCC during its sojourn through the plane of two tuning modes if the line of SCC (Eq. 2.13) has a part within the energetically allowed region. On the other hand, if they do not have any common region, the WP is unlikely to touch and cross the SCC in this plane. This type of crossing where the WP flows

through the SCC in both directions can be called a *mutually assisted crossing*. It affects the WPs of both the tuning modes simultaneously. This leads to a correlated two-body modification in the WP. The presence of such connected two-body correlations over a period of time is another reason why a FCI type of WF becomes necessary to describe the dynamics of the system DOF. Some typical examples of the varying extent of SCC line (blue dashed) inside the energetically allowed region (red solid line) are presented in following figures. To simplify the analysis, we have approximate the ellipsoid by a rectangular region in these figures. The four vertices of this rectangular box (red line in figures) in the two-mode plane are the origin, $(T_1, 0)$, $(0, T_2)$ and (T_1, T_2) . Here, T_1 and T_2 are the classical turning points of the two modes, respectively.

In Fig. 2.2, a large segment of the SCC falls in the energetically allowed region. Thus, in this case the journey of the WP through the SCC is significant. WP undergoes considerable repeated CC. As a result, extensive dephasing of the WP happens in this case of two-mode vibrational subsystem. Moreover, it could travel in the direction of both the normal modes.

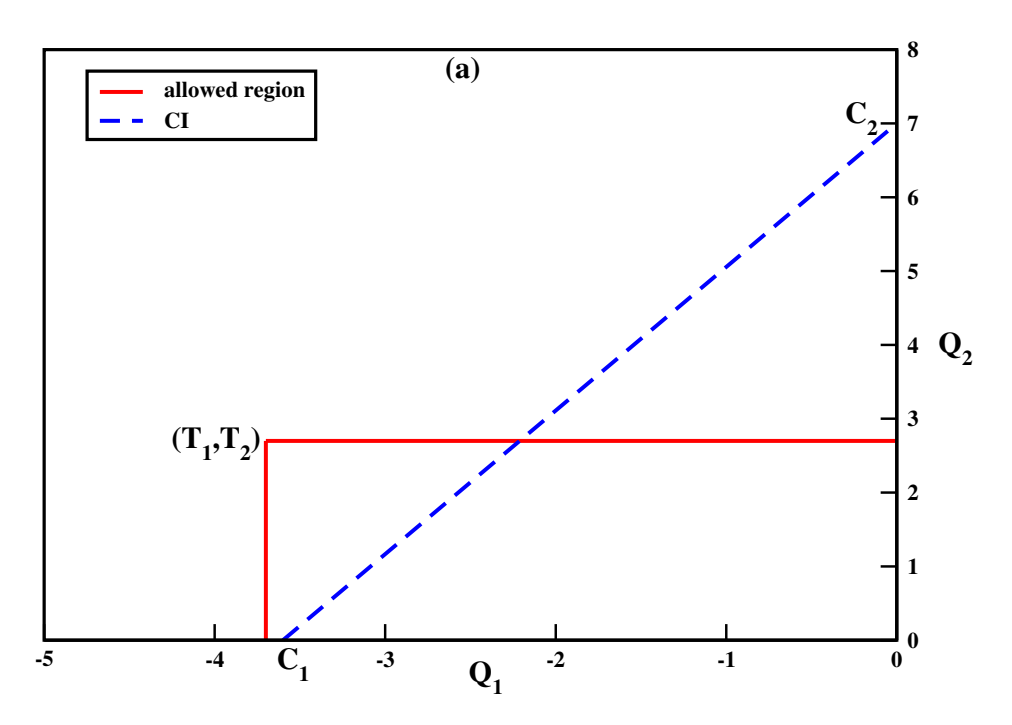


Figure 2.2: Two dimensional CC along two modes for which significant part of CI line falls inside the energetically allowed region.

Fig. 2.3 represents a situation where only a tiny segment of the SCC is present inside the energetically accessible rectangle. Thus, only a very small part of the WP can

pass through the SCC. The extent of WP dephasing for in this plane will be insignificantly small.

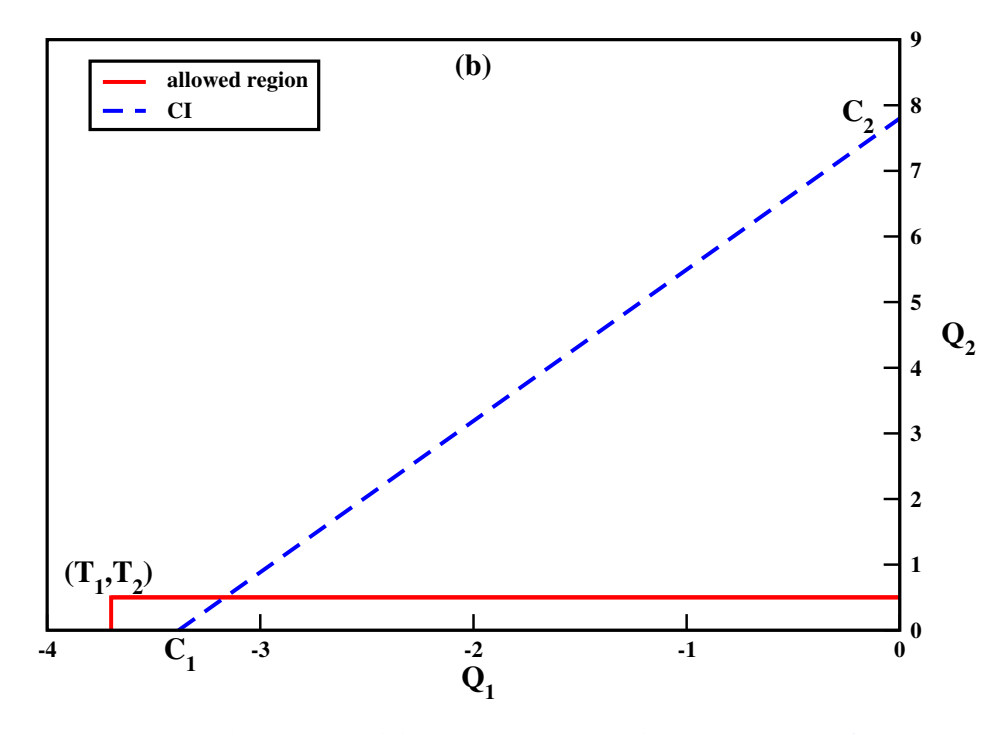


Figure 2.3: Two dimensional CC along two modes for which insignificant part of CI line falls inside the energetically allowed region.

In Fig. 2.4 the SCC in the plane lies completely outside the energetically accessible region. The WP will not cross over the SCC in this plane. And, hence the WP will not dephase in this plane. It is observed that any extent of mutually-assisted crossing happens only in the plane where one of the modes is a direct-crossing mode. If there is no direct-crossing mode involved in the plane, there will be no mutually assisted in that plane. In Fig. 2.4, the WP does not reach SCC along the direction of both the modes. In such a case, the WP in their plane will only be limited within the energetically-accessible box as the line of SCC lies far away from the box. In addition, the direction of SCC point and turning point from the Franck-Condon zone for a concerned mode on a given electronic surface will decide the extent of WP crossing. In general, if for both the modes their SCC point and the turning point lie in opposite direction to each other, then no mutual crossing will happen in that plane.

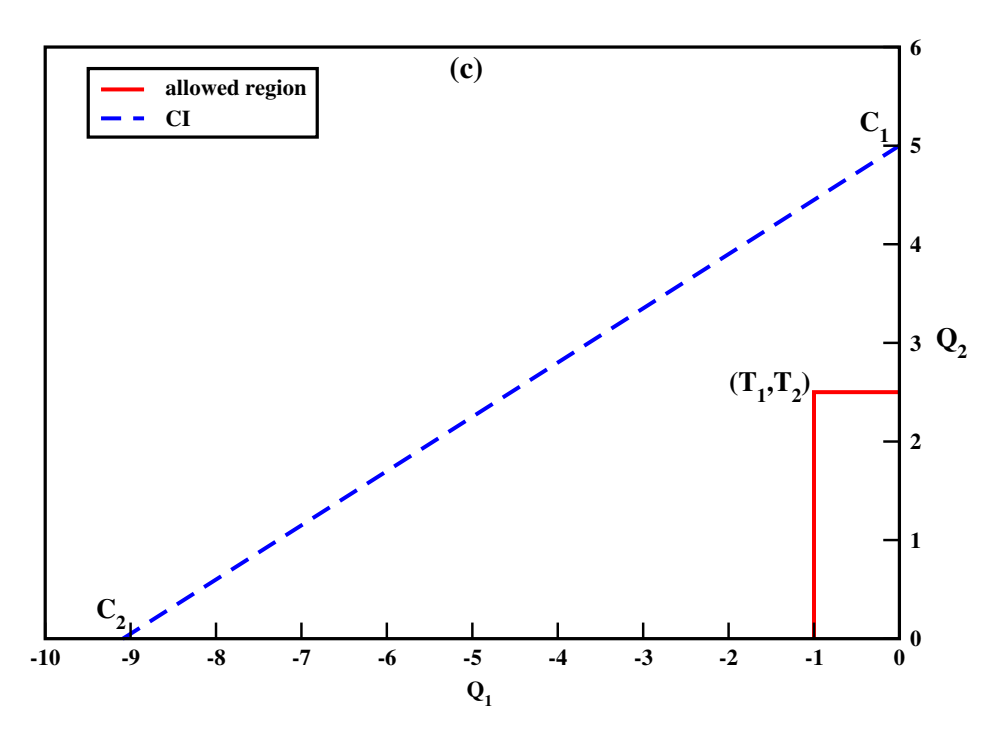


Figure 2.4: Two dimensional CC along two modes for which no part of CI line falls inside the energetically allowed region.

We next turn to possible higher-order mutually assisted, concerted crossing of SCC by the WP of three or more modes. The energetically accessible region in three modes has the shape of a cuboid embedded in the three dimensional space of the concerned normal modes. The two-dimensional segment of the SCC in this three dimensional subspace has to fall in this cuboid, if a concerted three-body crossing is to happen. Obviously, in such a case, a component of this two-body SCC surface would pass through at least two of the six faces of the cuboid defining the energetically accessible region of the three dimensional subspace. However, these modes for which the WP crossing is happening in three or higher dimensions would have been already recognized at two dimensional crossing. In another words, modes along which the WP does not cross at two dimensional level, will not appear in higher order crossings. Therefore, an analysis of two dimensional correlated crossings of the SCC is adequate to cover all possible SCC crossings.

Crux of the third part of the criteria is that the tuning modes along which the WP can directly cross the SCC before it reaches the classical turning point must become a

system DOF. In addition, tuning modes along which the WP encounters mutual assistance from one of the direct crossing modes may be put in the system-subspace provided the extent of mutual assistance is significant.

2.4 Conclusion

In summary the choice for the system DOF depends on the extent of the WP dephasing along a particular mode. Along the coupling mode the WP repeatedly jumps across SCC. The quantum state of coupling mode keeps on getting populated with repeated CC. Thus, WP along all the coupling modes undergoes extensive dephasing. So all the coupling modes must be included in the system subspace. Amongst the totally symmetric tuning modes, only some will lead to extensive WP dephasing. The WP CC can happen in different dimensions along the tuning modes. Along its trajectory, a tuning mode can have the point of CI before its classical trajectory point. Such tuning modes will lead to direct-crossing of the WP and will heavily dephase the WP. These tuning modes must be kept in the system DOF. WP can also dephase through the mutually-assisted mechanism in second or higher dimensions. In the plane of two modes, where one is a direct-crossing mode, the extent of dephasing decides whether the second will be kept in the system subspace or not. For tuning modes which do not lead to WP dephasing in any dimension can safely be kept in the bath. Also, rest of the normal modes in the molecule can be put as bath DOF.

Chapter 3

Numerical studies using Generalized TDSCF for bath DOF

3.1 Introduction

In the previous chapter the EOM for WP CC and the set of criteria for choosing the system DOF were proposed. In order to establish the validity of the criteria they have to be numerically tested on realistic systems. It is clear that the system DOF must be treated exactly since they dominate the NAD. On the other hand, the bath DOF can be described by a suitable approximation. As a starting point, we use a TDSCF ansatz to describe the dynamics of the BS. Generalized TDSCF is a simplistic approach where the overall molecular WF can be written as a product of system WF and bath WF. A GWP representation [26] is used to represent the bath DOF. We present the TDSCF ansatz and the working equations for the system and BSs. We study three model NASs to verify the generality of the criteria that are put forward here. The first is the well tested $S_2 - S_1$ vibronic system of the 24-mode pyrazine. The second is a 18-mode butatriene cation. Last, we use 3-mode spin-boson system as the testing ground. In all cases, we compute the ACF and the associated spectra. We identify the important modes and their influence on ACF and the spectra in each model case.

3.2 Computational Methodology

TDSCF approach has been previously applied on a two-state three-mode NAS[29]. In that study, the subspace of electronic and coupling mode was treated exactly and a suitable number of basis functions was chosen. On the other hand, the tuning modes were treated by EOM generated from TDSCF method. Although, the spectra was satisfactorily reproduced in the short-time limit, the ACF was deprived of dephasing features. This further emphasizes the point that along with the coupling mode certain tuning modes must be treated exactly. This interaction can essentially be described by a multiconfiguration self-consistent field ansatz,

$$\psi \approx \phi(s)\chi(b)e^{i\theta}. \tag{3.1}$$

Here, s and b refer to system and bath variables and ϕ and χ are the respective WFs of the two subspaces. θ is the overall phase factor.

The equations required to propagate the two components are generated via Frenkel-Dirac variational principle[27]. The Hamiltonian defined in Eq. 1.17 is conveniently partitioned as,

$$H = H_s^o + H_b^o + V_{sb}, (3.2)$$

to simplify the equations later. Here, H_s^o is the Hamiltonian involving all the system DOF. It is essentially the full Hamiltonian but limited only to the system variables. H_b^o is similarly defined for the bath modes. V_{sb} represents the interaction between the system and bath variables.

The time-dependent variational principle leads to three equations for the three components of the overall wave packet. The equation for the SS is given by

$$i\dot{\phi}(s) = [H_s^o + U_s(s)]\phi(s), \tag{3.3}$$

where,

$$U_s(s) = \langle \chi(b) | V_{sb} | \chi(b) \rangle_b. \tag{3.4}$$

The subscript *b* implies that partial averaging is to be done on the bath variables alone. The system variables come out as the additional potential for the system DOF after

averaging out the bath variables in the SB interaction terms. Similarly, for the bathsubspace, we find

$$i\dot{\chi} = \left[H_b^o + U_b(b)\right]\chi,\tag{3.5}$$

where,

$$U_b(b) = \langle \phi(s) | V_{sb} | \phi(s) \rangle_s. \tag{3.6}$$

And last, the phase factor corrects for the double-counting of the mutual interaction between the two subspaces

$$\dot{\theta} = -\langle \psi | V_{sb} | \psi \rangle_{sh}. \tag{3.7}$$

We now specify the components $\phi(s)$ and $\chi(b)$ with their respective ansatze. As is well known, the system DOF interact strongly with each other. A set of HO eigenfunctions, $\{f_k^{\alpha}(s_{\alpha})\}$ is defined for each DOF, α . We define a configuration function, F_{i,k_1,k_2,\dots,k_n} as the product of the WFs of all the system modes.

$$F_{i,k_1,k_2,\dots,k_n} = |e_i\rangle \prod_{\alpha=1}^n |f_{k_\alpha}^{\alpha}\rangle.$$
 (3.8)

We describe the system WFs as a superposition of all possible configurations. With this $\phi(s)$ takes the following form

$$\phi = \sum_{I} C_{I} F_{I}. \tag{3.9}$$

Here, F_I are the various configuration states in a large basis set of SP WPs. We experimented with the number of functions for each DOF until the dynamical results converged with respect to the basis (more details are given in Sec. 3.3.1). All configurations that are possible from that set of SP basis sets have been included in the calculations. In this sense, the present calculations are said to be numerically converged FCI. I is the combined index of $(n, k_1, k_2, ..., k_n)$. The working equations for C_I are,

$$i\dot{C}_I = \sum_J H_{IJ}C_J,\tag{3.10}$$

$$H_{IJ} = \langle F_I | H_s^o + U_s | F_J \rangle. \tag{3.11}$$

We next turn to the working equations for the bath DOF. Because we are using a quadratic potential for the vibrational part, the self-consistent field part of the bath mode potential, $U_b(b)$, is also quadratic. Consequently, the generator for the time-propagation of bath WF in Eq. 3.5 is a TD harmonic Hamiltonian. The starting WF (at t=0) is

a multidimensional Gaussian. As a consequence, it remains a Gaussian as long as it evolves under the influence of a harmonic Hamiltonian. In view of this, we posit a GWP ansatz for bath DOF as[24]

$$\chi = exp\left[-\frac{i}{\hbar} \left[\sum_{i,j} (b_i - b_i^o) A_{ij} (b_j - b_j^o) + \sum_i p_i (b_i - b_i^o) + \gamma \right] \right]. \quad (3.12)$$

We note that in the present approximation, the GWP propagation for the bath modes is exact[24]. We drop the subscript b in U_b to simplify the equations from here onward. The working equations for the various parameters in χ are given below.

$$\dot{A}_{ij} = -2.0 \sum_{k} A_{ik} \omega_k A_{kj} - \left[U_{ij} + 0.5 \omega_j \delta_{i,j} \right]. \tag{3.13}$$

$$\dot{b}_i^o = \omega_i p_i. \tag{3.14}$$

$$\dot{p}_{i} = -U_{i} - \omega_{i} b_{i}^{o} - \sum_{i} U_{ij} b_{j}^{o}. \tag{3.15}$$

$$\dot{\gamma} = i \sum_{i} 0.5\omega_{i} A_{ii} + \sum_{i} \left[p_{i}^{2} - b_{i}^{o^{2}} \right] - \sum_{i} \left[U_{i} \right] - \sum_{i,j} U_{ij}. \tag{3.16}$$

$$U_{ij} = \left\langle \phi \left[\left[\sum_{e,e'} |e\rangle V_{i,j}^{e,e'} \langle e'| \right] \right] \phi \right\rangle. \tag{3.17}$$

$$U_{i} = \left\langle \phi \left\| \sum_{e,e'} |e\rangle V_{i}^{e,e'} \langle e'| \right\| \phi \right\rangle + \left\langle \phi \left\| \sum_{e,e',s} |e\rangle V_{i,s}^{e,e'} q_{s} \langle e'| \right\| \phi \right\rangle. \tag{3.18}$$

Our purpose in this exercise is the computation of the electronic spectra. The spectrum of the system is obtained after performing a Fourier transformation of the ACF,

$$X(t) = \langle \psi(0) | \psi(t) \rangle. \tag{3.19}$$

The ACF in the framework of this work can be written as,

$$X(t) = \langle \phi_s(0) | \phi_s(t) \rangle \langle \chi_b(0) | \chi_b(t) \rangle e^{i\theta}. \tag{3.20}$$

The function was multiplied by the window function, $cos(\pi t/2T)$, to eliminate Gibbs phenomenon and further multiplied by an exponentially decaying function, $exp(-\gamma|t|)$, where the value of decay, γ was set to be 0.03. This accounts for other decay mechanisms and corresponds to damping time of about 22 fs. Thus, the spectrum is given by,

$$P(\omega) = \int e^{i\omega t} X(t) cos(\pi t/2T) exp(-\gamma |t|) dt.$$
 (3.21)

Gaussian WFs have been used for describing the bath dynamics earlier also, as discussed in Sec. 1.2 [54]. The authors in this work have used the following ansatz for SB dynamics (in our notation)

$$\psi = \sum_{I} C_{I} F_{I} \prod_{\alpha} g_{I}^{\alpha}. \tag{3.22}$$

In G-MCTDH, for each bath mode there are as many Gaussians as there are system CFs since every bath mode is described by a separate Gaussian in each system CF. In contrast, in this work we use one Gaussian for each bath mode, independent of the CF of the SS. These are driven by the average potential felt by that bath mode from the complete system configurations. Within the framework of our approximation, the bath modes undergo harmonic dynamics and hence, the EOM for Gaussians become quite simple in our approach. This is not the case in the work of Burghardt *et al.* because of the more sophisticated ansatz used for the overall system. The complicated equations used in G-MCTDH are probably far more accurate in describing SB interactions. We have used thawed Gaussian in the framework of our calculations. TG yield the exact solution for the generator of the HO problem and causes no problems with harmonic potentials. This would not have been possible in the G-MCTDH approach, which use frozen Gaussian because equations for various Gaussians are coupled. As a consequence, TG approximation is not an exact solution in the case of G-MCTDH. Since, TG approximation

is known to be susceptible to instabilities during numerical solutions, the authors have presumably opted to limit themselves to FG approximation.

3.3 Results and Discussion

3.3.1 Applications to Pyrazine

Our first example is the SCC between S_2 and S_1 ESs of pyrazine. Pyrazine has 24 vibrational modes[19]. Of these, v_{10a} is the sole coupling mode for the given pair of ESs in this molecule. There are 5 tuning modes, $(v_1, v_2, v_{6a}, v_{8a}, v_{9a})$ in pyrazine. These belong to the totally-symmetric representation. The rest of the DOF belong to various Irreps but act neither as coupling nor as tuning modes. These are the spectator modes as defined in Chapter 2.

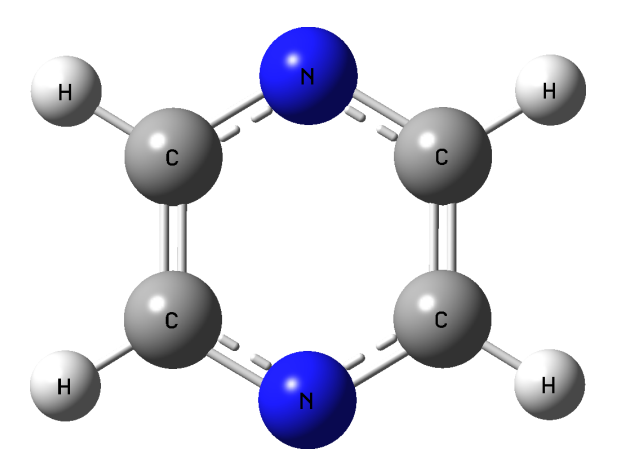


Figure 3.1: Pyrazine molecule

An initial population of S_2 ES is considered. We have taken the PES from Ref. [19] and calculated the SCC and turning points on S_2 using Eqs. 2.11 and 2.12. We summarise the data in Table 3.1.

mode	Q_T^1	Q_T^2	Q^{SCC}
v_{6a}	2.655	-3.667	-3.622
ν_1	0.800	2.719	7.009
v_{9a}	-1.904	-0.492	7.855
v_2	-0.130	-0.086	99.53
v_{8a}	0.454	-0.171	-13.80

Table 3.1: Turning points and SCC points along tuning modes in pyrazine between S_1 and S_2 surfaces. Direct crossing, assisted crossing and (practically) noncrossing modes are given in red, green and blue, respectively.

As can be seen from the table, only mode v_{6a} can go through a direct crossing. For this reason, v_{6a} is the most important totally symmetric mode in the dynamics of pyrazine. So, along with the coupling mode, v_{10a} , v_{6a} must also be kept in the SS. As we shall see later, it also influences the other modes in the CC. Next, we look at possible mutually assisted crossings. Fig. 3.2 represents (v_{6a} , v_1) plane. Along the trajectory of v_1 the WP does not directly cross the SCC. However, in (v_{6a} , v_1) plane, a moderately large segment of the SCC line is enclosed within the energetically accessible region. As a consequence, mode v_1 also becomes active in the multisurface CC dynamics. However, this is always together with mode v_{6a} .

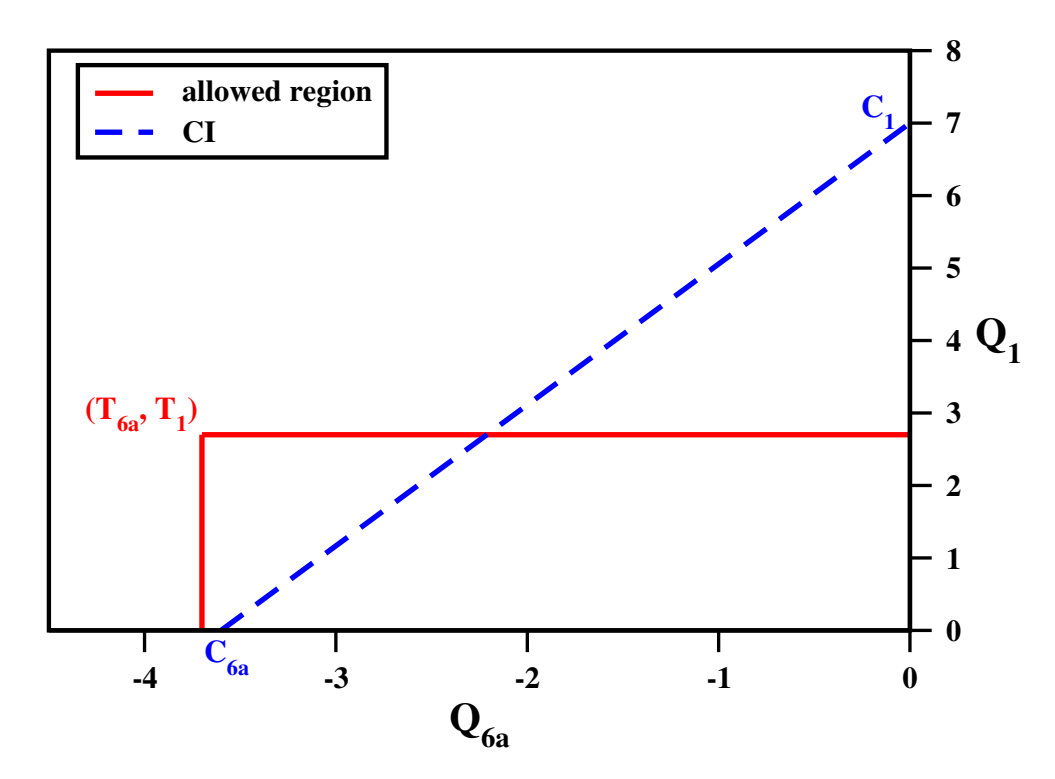


Figure 3.2: Two dimensional CC in (ν_{6a}, ν_1) plane.

The corresponding ACF for the dynamics of the above SS is presented in Fig. 3.3.

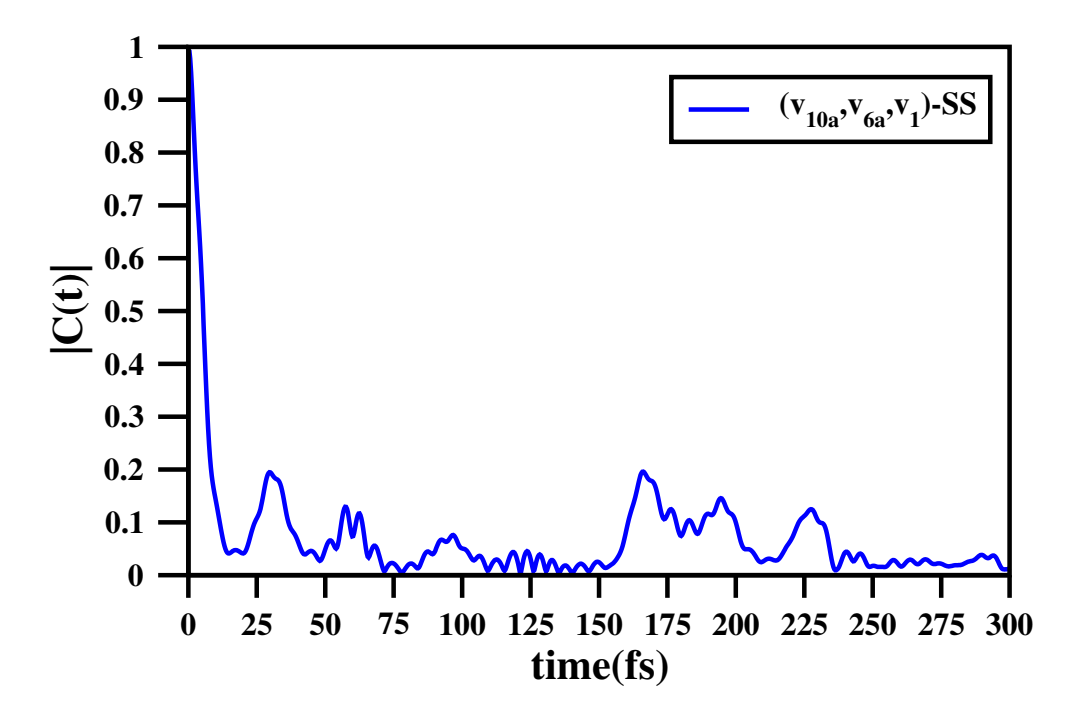


Figure 3.3: ACF for the SS dynamics in (v_{6a}, v_1) plane.

Fig. 3.4 is a representation of the (ν_{6a}, ν_{9a}) plane. In this case, a very small segment of the SCC lines falls inside the energetically allowed region. This segment of the SCC

line is so small that although CC is possible in principle in this plane, it is unlikely to affect the vibronic dynamics to any noticeable extent. The corresponding ACF for the dynamics in (v_{6a}, v_{9a}) plane is presented in Fig. 3.5.

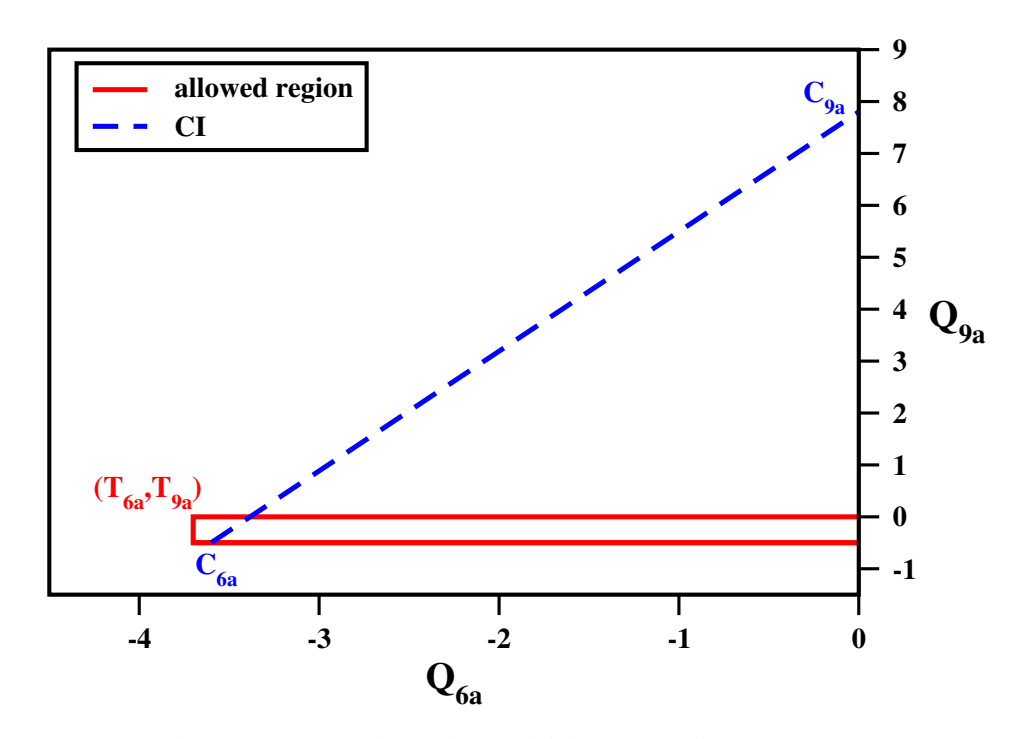


Figure 3.4: Two dimensional CC in (v_{6a}, v_{9a}) plane.

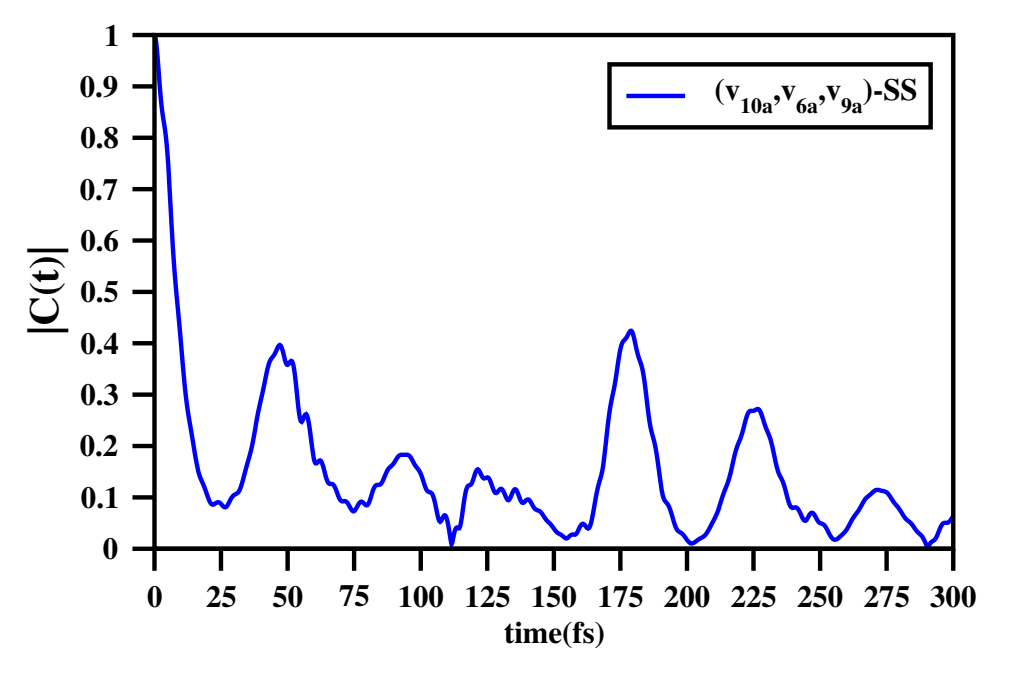


Figure 3.5: ACF for the SS dynamics in (v_{6a}, v_{9a}) plane.

Unlike in Fig. 3.3, the ACF in Fig. 3.5 is much more resolved. This implies that WP dynamics in (ν_{6a}, ν_{9a}) plane is not as much dephased as in the (ν_{6a}, ν_{1}) plane.

Thus, the CCs in two different planes (Figs. 3.2 and 3.4, respectively) are in harmony with their respective ACFs. This gives support to the argument presented in our criteria that the extent of mutually assisted CC decides the degree of WP dephasing along the involved modes.

For modes v_{8a} and v_2 the turning points on the upper electronic surface is almost at the FC zone. On the other hand, the SCC points are too far away and in the case of v_2 , it is in the opposite direction (Table 3.1). So, in (v_{6a}, v_{8a}) and (v_{6a}, v_2) planes there is practically no CC (Figs. 3.6 and 3.8). As a result, the ACF for their respective SS dynamics will be resolved and will not show signatures of damped oscillations (Figs. 3.7 and 3.9). Hence in these two planes, there will be no WP dephasing.

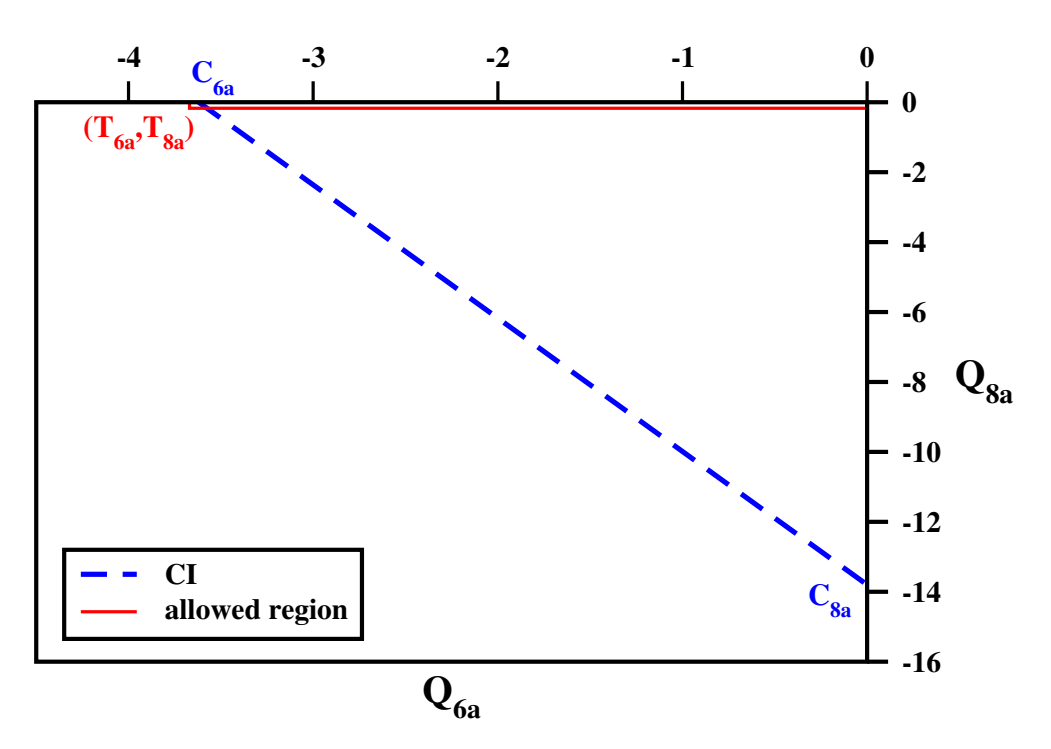


Figure 3.6: Two dimensional CC in (v_{6a}, v_{8a}) plane.

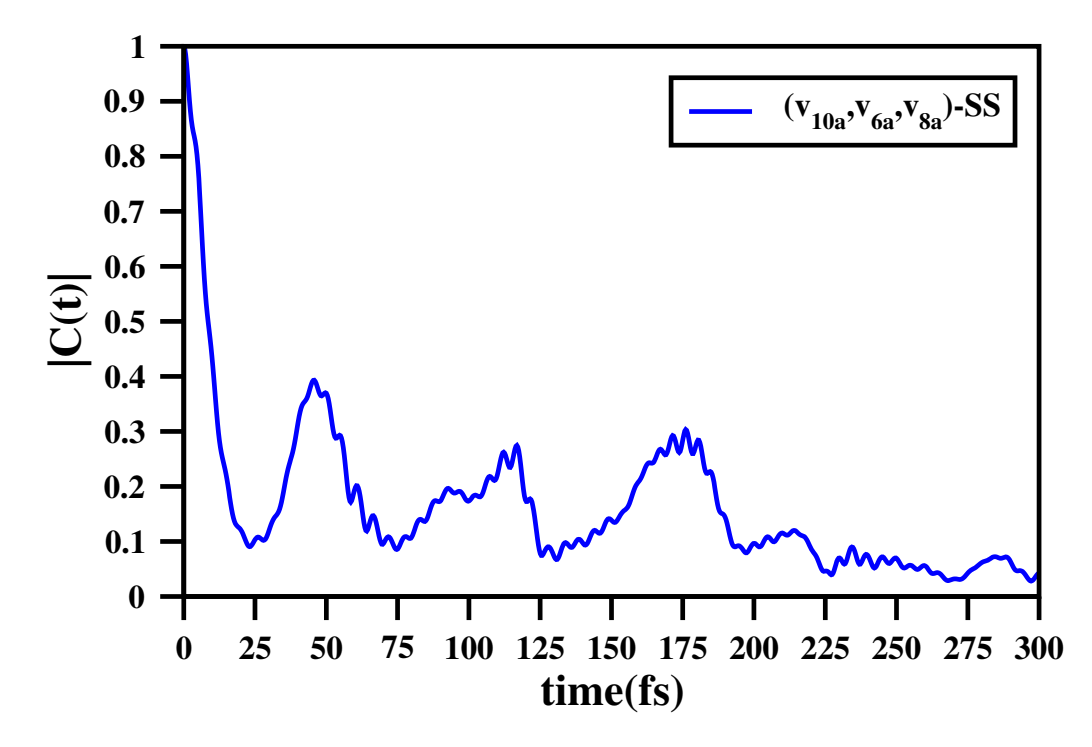


Figure 3.7: ACF for the SS dynamics in (v_{6a}, v_{8a}) plane.

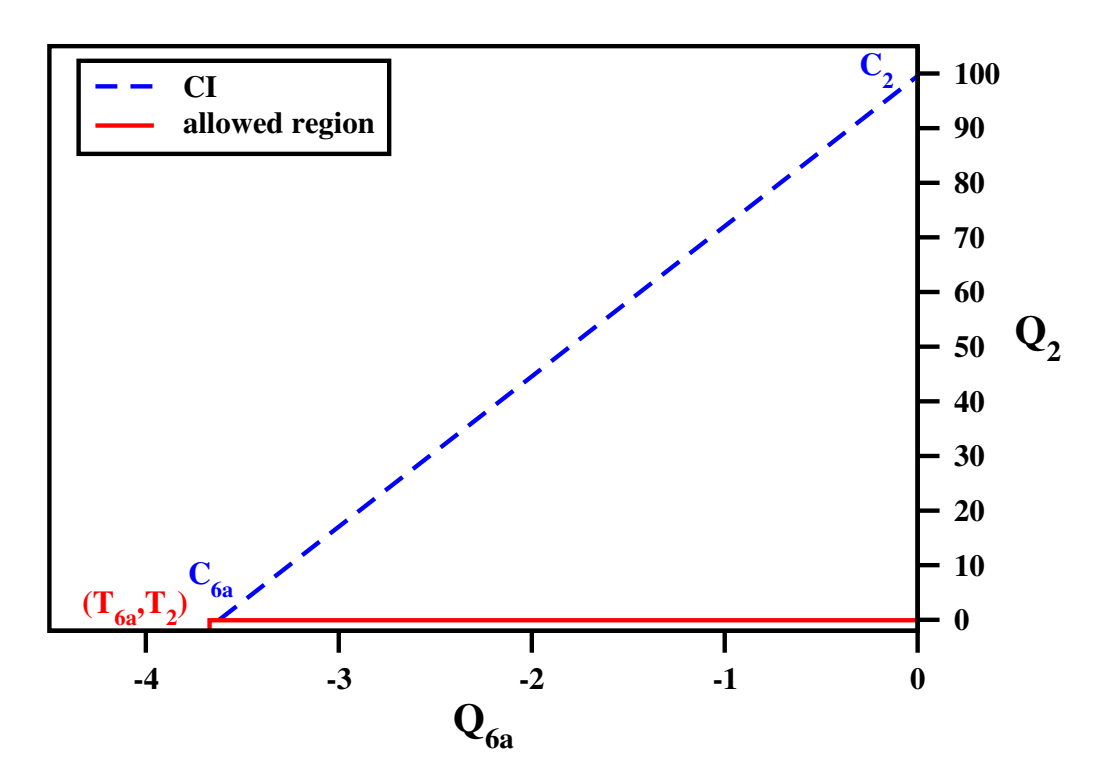


Figure 3.8: Two dimensional CC in (v_{6a}, v_2) plane.

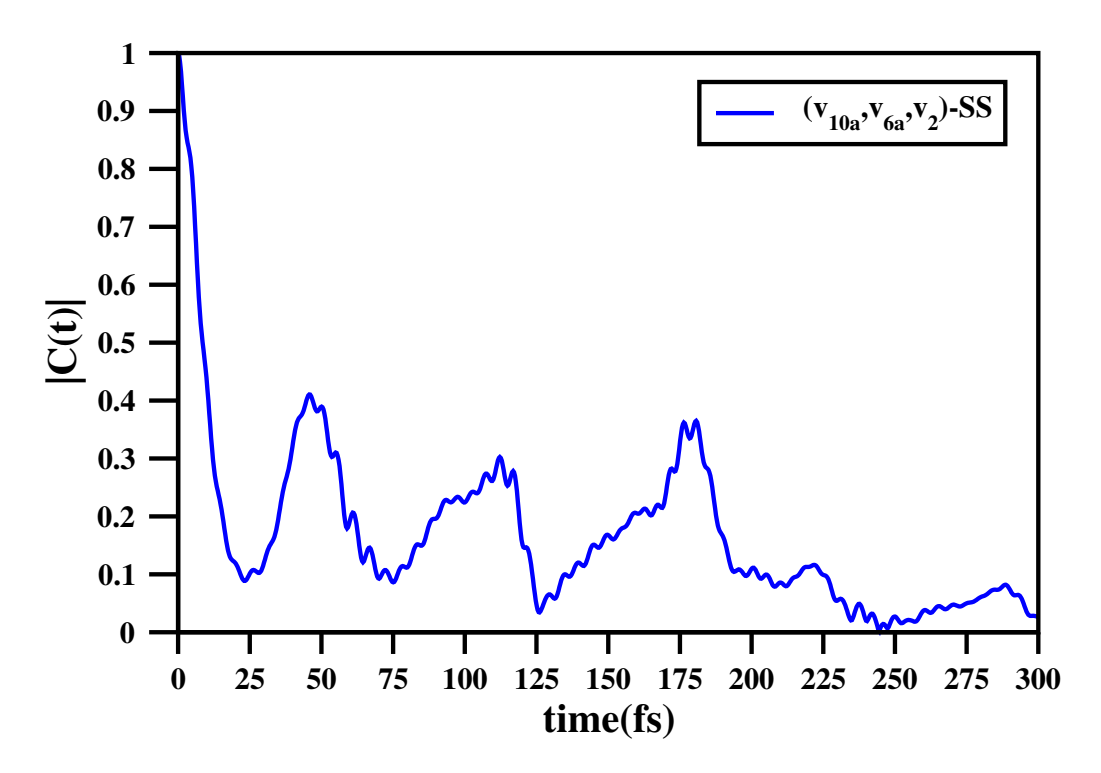


Figure 3.9: ACF for the SS dynamics in (v_{6a}, v_2) plane.

Hence, according to our criteria, the SS in pyrazine must include the only coupling mode, v_{10a} , present in the molecule and the only tuning mode with direct crossing, v_{6a} . In addition to these two modes, mode v_1 which undergoes mutually assisted crossing in the plane with mode v_{6a} should also be included in the system DOF. While it is difficult to set quantitative limitations, mode v_{9a} could be moved to the bath DOF. The effect of this mode on the overall dynamics is expected to be negligible as the WP has access only to a small region to make the transition across the SCC. Modes v_{8a} and v_2 are to be placed in the bath-subspace.

In order to numerically verify the classification of the vibrational modes in pyrazine, we carried out the calculations on two model cases for the system subspace. The remaining number of modes in each case go into the BS which is dealt with a generalized TDSCF ansatz. In the first model, modes (v_1, v_{6a}, v_{10a}) are the system variables. We did some experimentation with the number of basis functions for the numerical convergence in the time-interval for the calculations. Numerical convergence was achieved with 22, 24 and 20 HO eigenfunctions for modes v_1, v_{6a} and v_{10a} , respectively. In a second set of calculations, 4 vibrational modes, $(v_1, v_{6a}, v_{9a}, v_{10a})$ go into the SS. In this case, for mode v_{9a} 5 HO eigenfunctions were sufficient to get the numerically converged results. All possible configurations that could be generated from these sets of single-particle basis sets were included in the calculations(Eq. 3.9) leading to 10560 configurations for the

3-mode SS and 52800 for 4-mode SS. All the equations were numerically integrated by a fourth order Runge-Kutta method for 330 femtoseconds with a step-length of 0.066 fs. The ACF was sampled after every 3.3 fs for 1024 steps. δw after the Fourier transform was 0.012 eV.

For the initial population of S_2 ES, we can rewrite Eq. 3.20 for the three-mode and four-mode system models with coefficients, C, for the system DOF as follows:

$$X(t) = C(2, 0, 0, 0) \langle \chi_b(0) | \chi_b(t) \rangle e^{i\theta},$$
 (3.23)

$$X(t) = C(2, 0, 0, 0, 0) \langle \chi_b(0) | \chi_b(t) \rangle e^{i\theta}.$$
 (3.24)

In Fig. 3.10, we compare the ACF for two model cases, (3 + 1) and (4 + 0). In (3 + 1)-model, the ACF is computed with two ESs and three modes, (v_1, v_{6a}, v_{10a}) , in the system DOF and a single bath degree of freedom, v_{9a} . A second ACF calculation for (4 + 0)-model is made with two ESs and all the four modes, $(v_1, v_{6a}, v_{9a}, v_{10a})$ as system DOF. There are no bath DOF in the second case. As can be seen, the two ACF are nearly identical up to about 150fs. The quality of agreement goes down but only marginally after that.

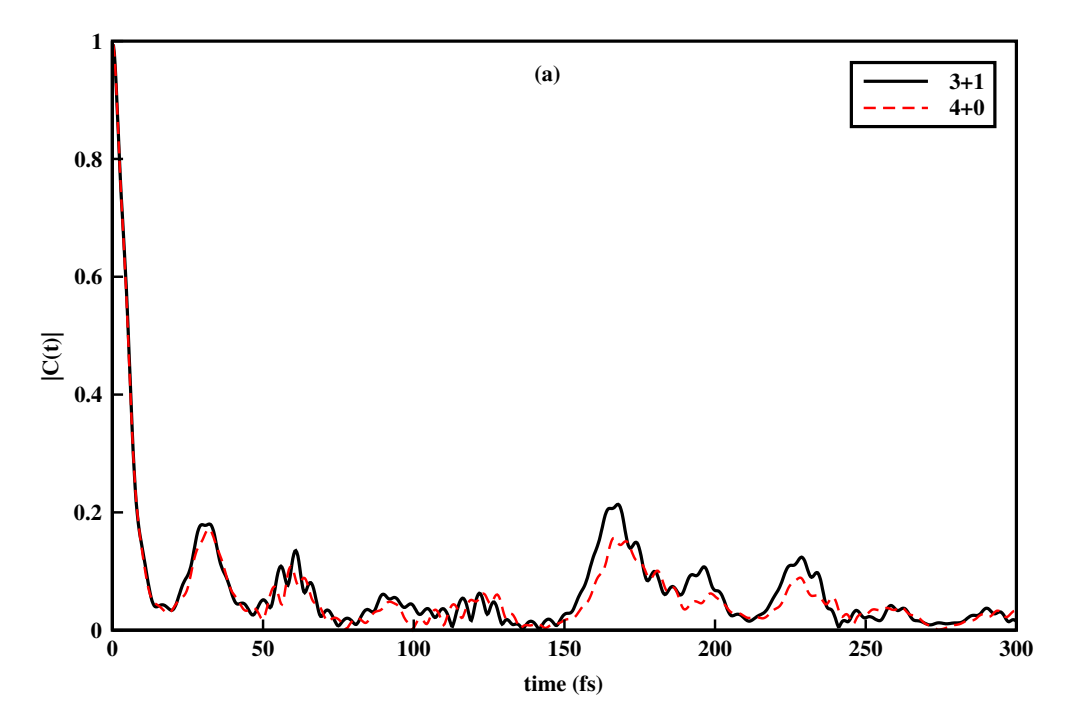


Figure 3.10: Comparison of ACF in pyrazine between 3 + 1 model (black solid) with $(\nu_1, \nu_{6a}, \nu_{10a})$ in system and ν_{9a} in bath and 4 + 0 model (red dashed) with $(\nu_1, \nu_{6a}, \nu_{9a}, \nu_{10a})$ in system and no mode in bath

In Fig. 3.11, we present the ACF for (3 + 21) and (4 + 20) models and compare these results with the numerically exact results of MCTDH (private communications from Prof. G. A. Worth) and the digitized G-MCTDH result (Figure 6(b) of Ref. 41). In both the model cases, it is implicit that the electronic DOF go into the SS. In (3 + 21), $(\nu_1, \nu_{6a}, \nu_{10a})$ are the 3 system-modes and rest 21 vibrational modes go into the bath-subspace. In the second case we have a (4 + 20) model with 4 modes, $(\nu_1, \nu_{6a}, \nu_{9a}, \nu_{10a})$ in the system DOF and 20 modes in the bath DOF. It is quite apparent that (3 + 21) and (4 + 20) calculations are very close to each other even in the long time limit. Thus, incorporating the fourth mode, ν_{9a} in the BS instead of into the system is an acceptable approximation.

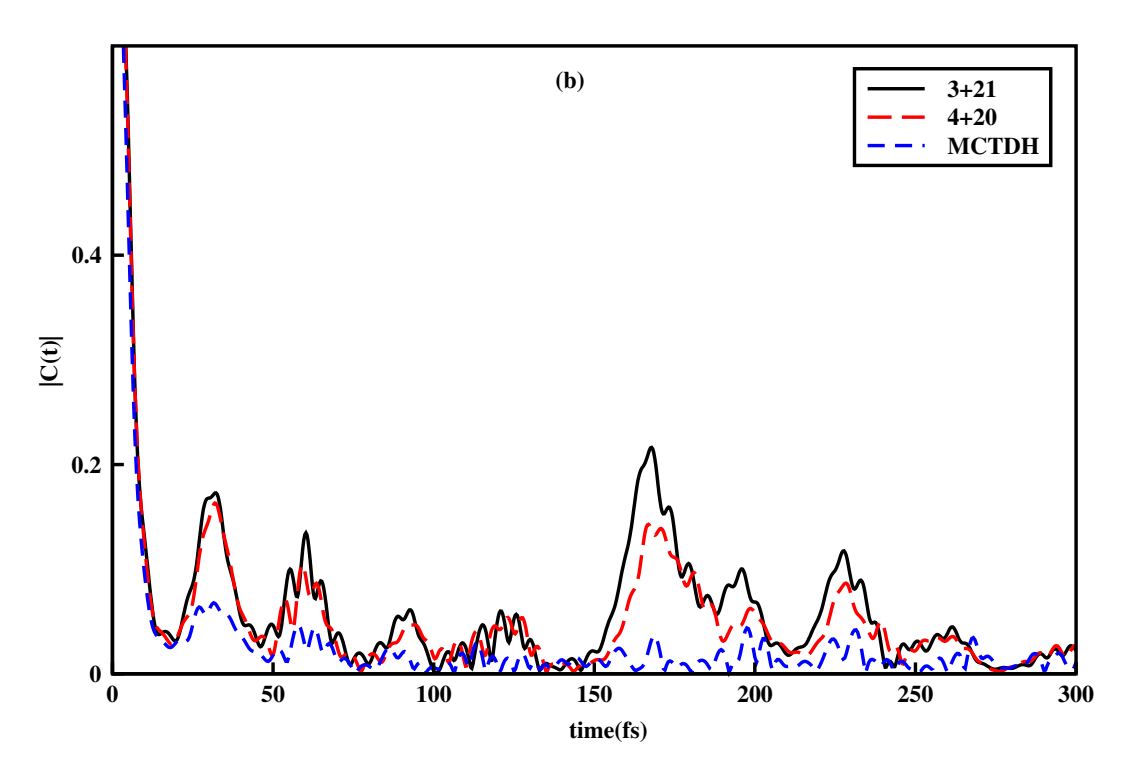


Figure 3.11: Comparison of ACF in pyrazine between(3 + 21) model (black solid), (4 + 20) model (red dashed), exact MCTDH calculation (blue dot-dashed)

In addition, it can be seen that our calculations deviate from that of MCTDH to some extent. Specifically, our results show more pronounced recurrences in the ACF through the full time interval. This is probably due to the inadequacy in the treatment of the system-bath interactions implied by ansatz in Eq. 3.1. So, post SB separation, the ansatz must be improved further. Since, the system part of the WF is described exactly within the limits of the basis set used, one can only improve upon the nature of the bath WF and how it couples with the system WF, something on the lines of the ansatz used in G-MCTDH[54], for example, or some other approach.

We next present, in Fig. 3.12, the spectrum of pyrazine corresponding to the two models, (3 + 21) and (4 + 20). The origin of the energy in the computed spectrum is set to be the mid-point of the two ESs in the FC zone. The two are almost identical. It is well known that the short time dynamics is adequate for predicting the spectra. The near identical spectra indicate that the short time dynamics up to 150 fs is correctly reproduced by the approximations that we have made. In addition, we also compare our results with the digitized MCTDH spectrum as given in Figure 5 of Ref. [19]. As is evident from Fig. 3.12, our results capture all the important features of the spectrum shown by MCTDH approach. We note here that the decay constants used in the two approaches are different. Due to this some of the smaller peaks seen in the MCTDH spectrum are missing in our results.

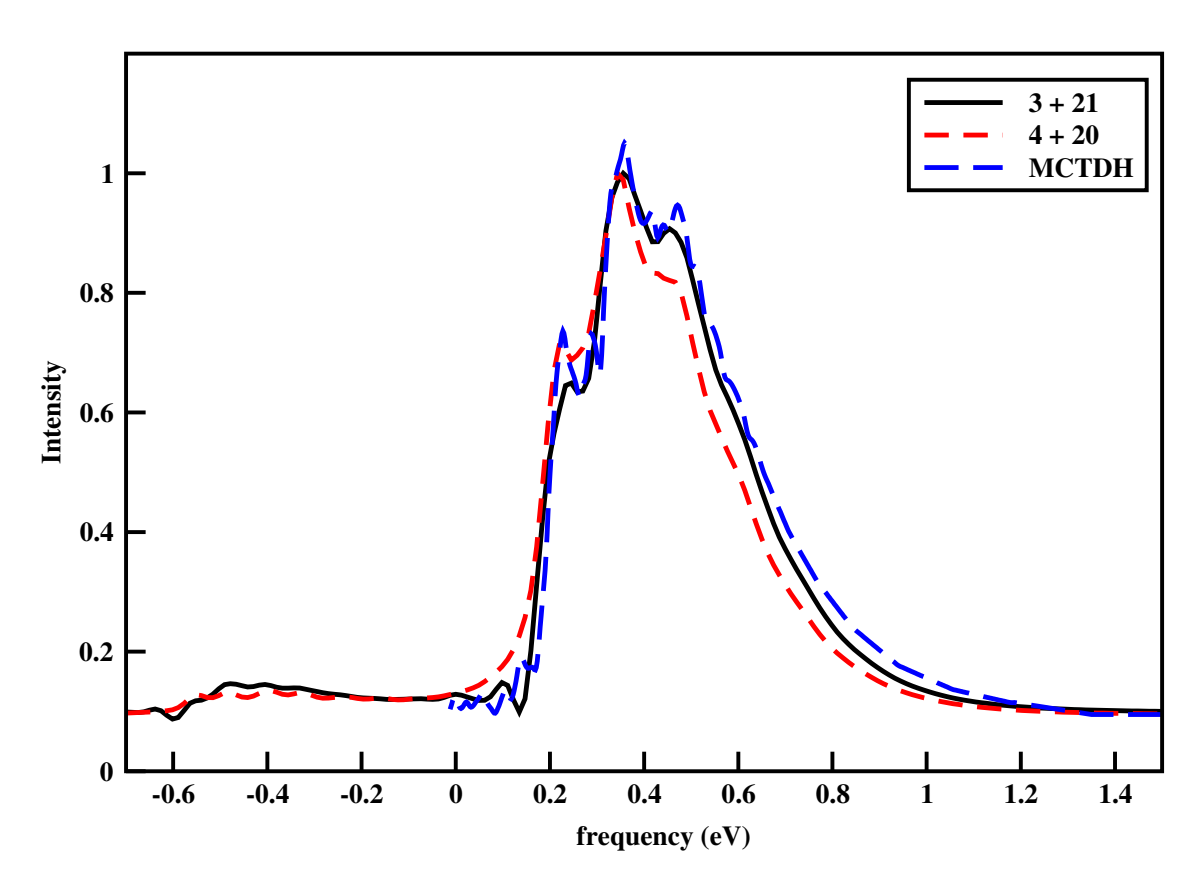


Figure 3.12: Comparison of 24-mode pyrazine spectra for 3 + 21 model (black solid), 4 + 20 model (red dashed) and (digitized) MCTDH (blue dot-dash) from Ref. [19]

Finally, in Fig. 3.13, we present the electronic populations of S_2 and S_1 states in pyrazine for the two the two models. We also compare them with the near exact results of Ref. [54]. As is evident from Fig. 3.12, the results of the 3+21- model and 4+20-model are almost identical. These results however deviate to some extent from

the results of G-MCTDH. Not withstanding that, however, the identity of the two model systems used in this work support our criteria for classifying the normal modes.

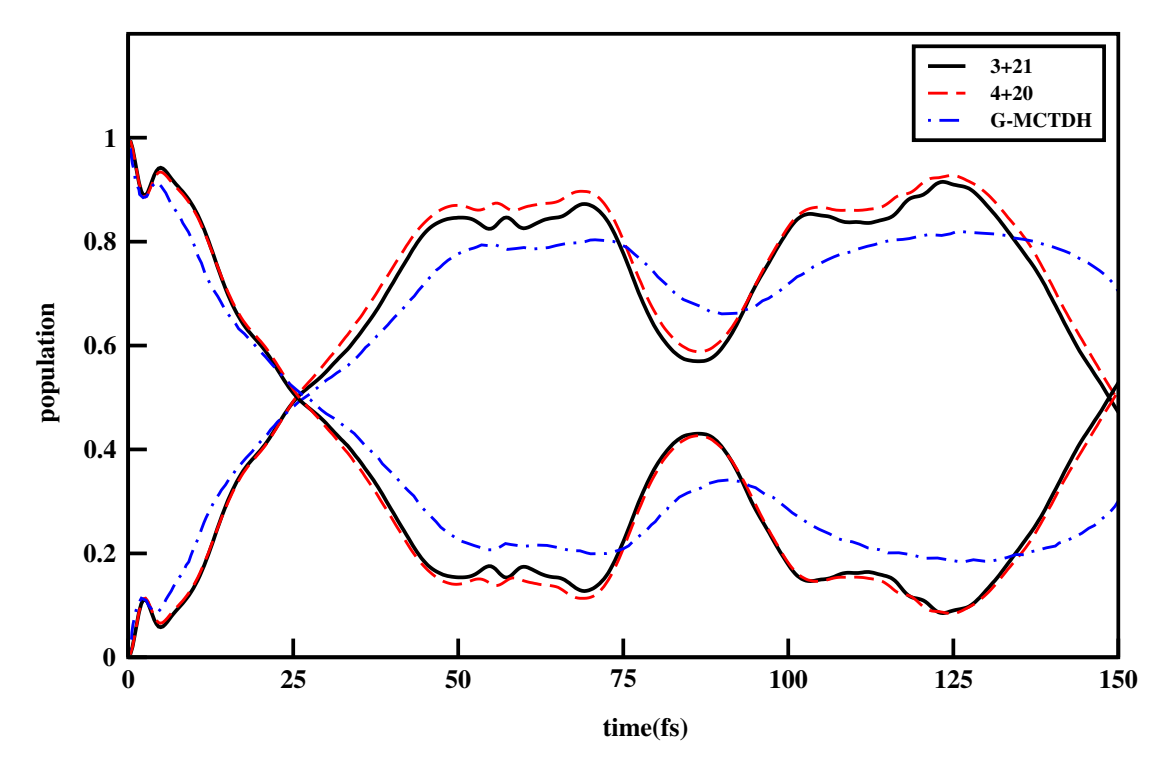


Figure 3.13: Diabatic populations for two surfaces compared for the cases of (a) (3+21) model (black solid line), (b) (4+20) model (red dash trace), (c) 3-mode SS without bath (black two dots-single dash trace), (d) 4-mode SS without bath (red dash-dot trace) and (e) G-MCTDH (blue dot-dash trace), digitized from Ref. [54]

All the analysis, done so far, was for the S_2 surface of pyrazine. It can be repeated for the S_1 surface as well. In such a case, the classical turning points are defined on S_1 surface (Table 3.1). It turns out that none of the classical trajectories starting from the FC zone on S_1 surface cross the SCC either directly or through mutual assistance. The obvious implication is that if the system is excited to the S_1 surface, the resulting spectrum shows very small signature of vibronic coupling. This is supported by the experiments.

3.3.2 3-mode spin-boson model

As a second example of the applicability of our criteria, we consider a 3-mode spin-boson model system. A spin-boson system consists of two ESs and (in our case) three vibrational tuning modes. The two states are coupled through a constant coupling. The

vibronic Hamiltonian in this case is written as,

$$H = \sum_{i} \frac{\omega_i}{2} \left(-\frac{d^2}{dQ_i^2} + Q_i^2 \right) \mathbf{1} + \begin{pmatrix} \frac{\Delta}{2} & J \\ J & \frac{\Delta}{2} \end{pmatrix} + \sum_{i \in T_1} \begin{pmatrix} a_i & 0 \\ 0 & b_i \end{pmatrix} Q_i.$$
 (3.25)

The parameters used in the above Hamiltonian are summarised in the Table 3.2

mode	a_i	b_i	ω
$ u_1$	0.027	-0.362	0.392
ν_2	-0.178	0.50	0.155
ν_3	0.155	0.102	0.180

Table 3.2: Linear diagonal couplings on two states, a_i and b_i and vibrational frequencies for the modes in spin-boson model(All values are in eV). $\Delta = 1.9eV$ and J = 0.402eV.

The arguments for WP dynamics along the tuning modes presented in Sec.2.2 hold true for a spin-boson model too. However, the arguments for the dynamics along the coupling mode do not exist in this case. Because of the presence of tuning modes, the two states intersect and thus have a CI. The dynamics of a spin-boson system are more or less parallel to the LVC model and reflect similar complexity when the CI is active in the dynamically significant region of the co-ordinate space. The advantage of studying a spin-boson system is that it has fewer DOF and thus requires much less computational efforts than a large molecule like pyrazine. The parameters-set that defines the system are summarised in Table 3.3.

mode	\mathcal{Q}_T^1	Q_T^2	Q ^{scc}
$ u_1$	-0.138	2.99	4.88
<i>v</i> ₂	2.30	-4.88	-2.8
ν ₃	-1.72	-1.13	35.8

Table 3.3: Turning points of and SCC points along tuning modes in spin-boson model. Direct crossing, assisted crossing and non-crossing modes are given in red, green and blue, respectively.

We subjected the three tuning modes to the criteria for selecting important modes. It turned out that direct surface crossing happens only along mode v_2 on the US. WP along mode v_1 crosses the surface through assistance from mode v_2 . CC in v_1 - v_2 plane shows a behaviour marked in Fig. 3.2. SCC line in v_2 - v_3 plane just touches the box of allowed trajectories. The CC in this plane is similar to that shown in Fig. 3.8.

In following figures we present the ACF of this system for different cases. Fig. 3.14 depicts the ACF of the full 3-mode system. It shows the marked signatures of damped oscillations. The remaining three panels depict the calculations after dropping one mode from the system. Fig. 3.15 deals with a 2-mode model system with modes (v_2,v_3) . Mode (v_1) is dropped for this calculation. The ACF still shows damped behaviour although the not as much as in Fig. 3.14(a). This implies the loss of mutual assisted crossing in v_1 - v_2 plane by dropping mode v_1 . Fig. 3.16 represents ACF with modes (v_1,v_3) in system by dropping mode v_2 . It is completely devoid of any signature of damped oscillation and is completely resolved. This emphasizes the importance of v_2 as a direct-crossing mode that leads to extensive dephasing. Finally, in Fig. 3.17 SS

consists of (v_1,v_2) . Absence of mode v_3 in this case has very little effect on the damped signatures in ACF.

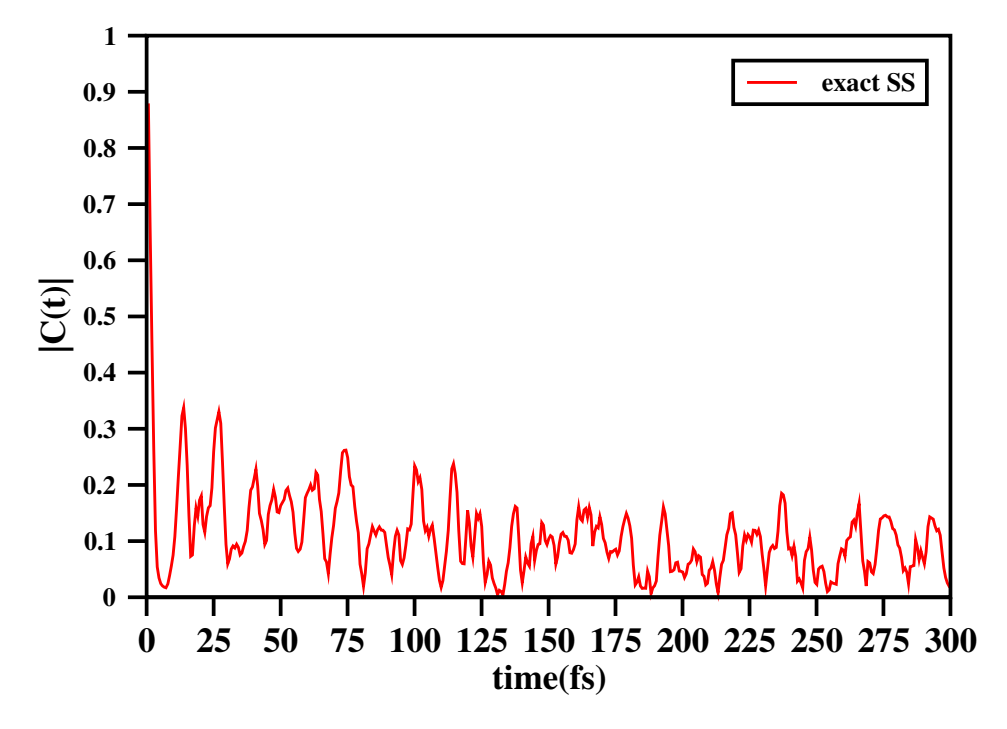


Figure 3.14: ACF in spin-boson model for an exact 3-mode SS with (ν_1, ν_2, ν_3) .

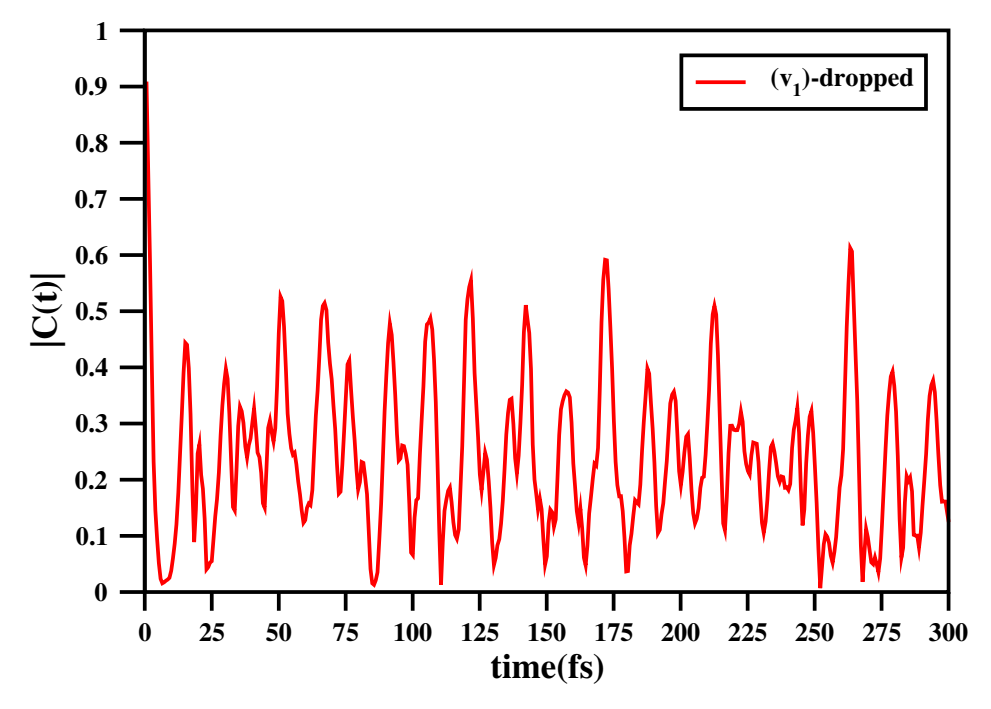


Figure 3.15: ACF in spin-boson model for a 2-mode SS with (ν_2, ν_3) and without ν_1 .

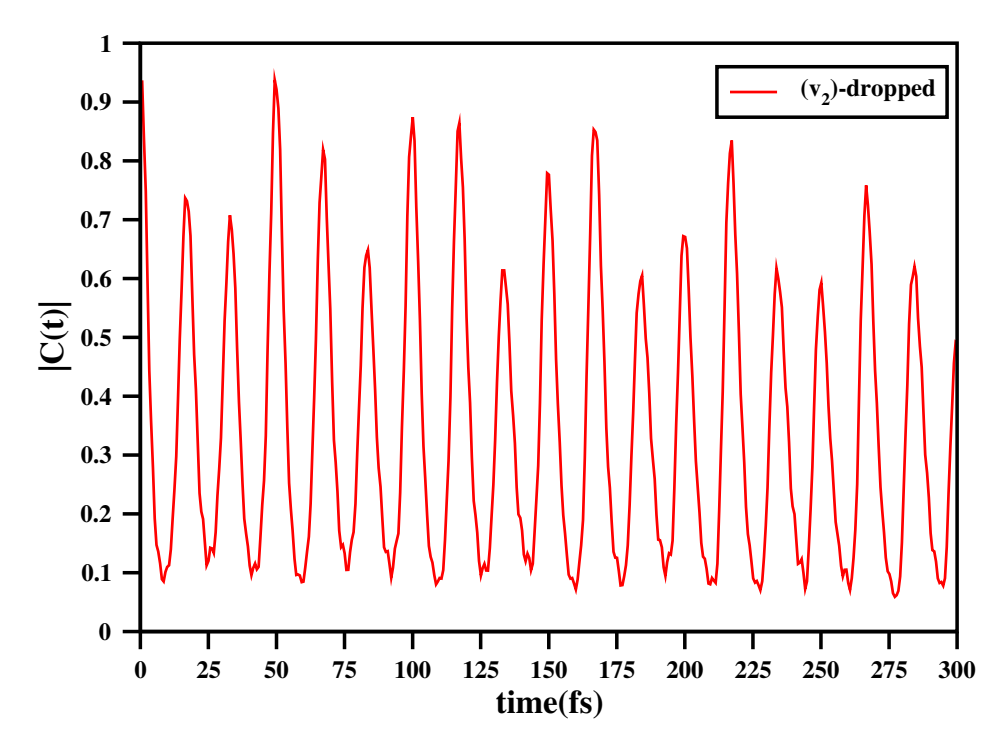


Figure 3.16: ACF in spin-boson model for a 2-mode SS with (ν_1, ν_3) and without ν_2 .

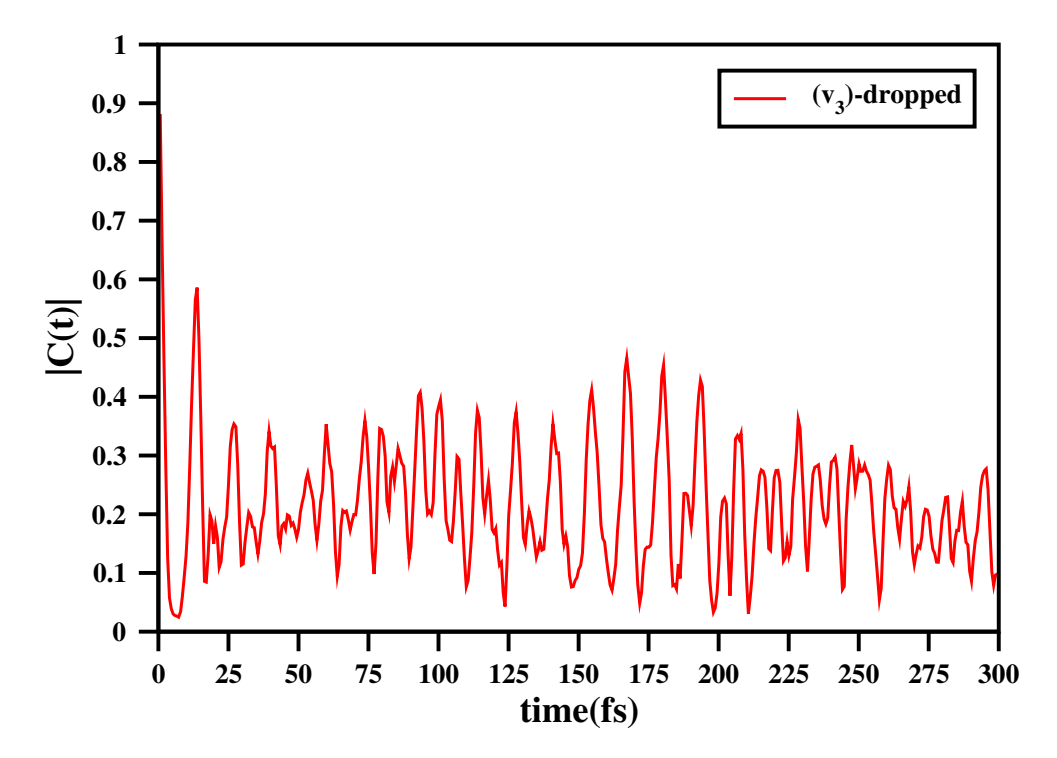


Figure 3.17: ACF in spin-boson model for a 2-mode SS with (v_1, v_2) and without v_3 .

Thus, v_2 is the most influential mode in the 3-mode spin-boson system. Since the other two modes cross only with assistance from v_2 , dropping it renders the other two modes vibronically inactive. Consequently, dropping it resolves the dynamics to a simpler displaced HO dynamics with no nonadiabatic signature. Dropping v_1 or v_3 , on the other hand, still leaves the system as a NAS with noticeable CC. Thus, the ACF of these two systems will show significant degree of decay.

The corresponding spectra of the four ACFs in Figs. 3.14-3.17 are presented in Figs. 3.18-3.21. The significance of direct surface crossing along mode v_2 and its role in assisting crossing along the other two modes are abundantly clear. From these numerical results, we suggest a model with v_1 and v_2 as system modes and mode v_3 in bath.

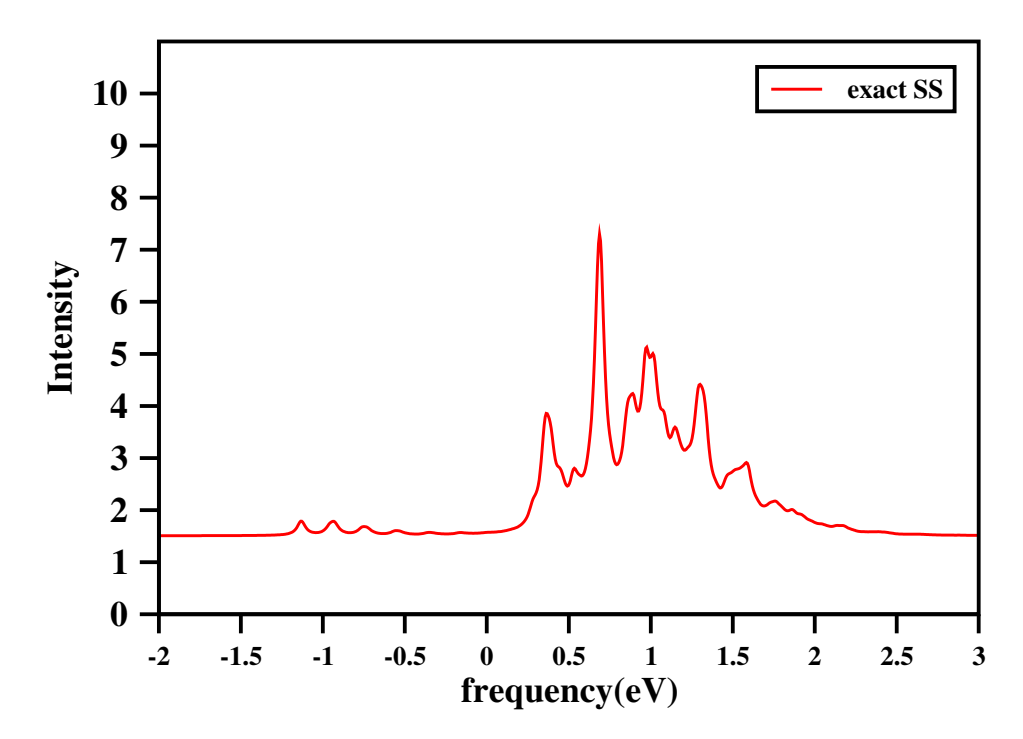


Figure 3.18: Spectrum in spin-boson model for an exact 3-mode SS with (v_1, v_2, v_3) .

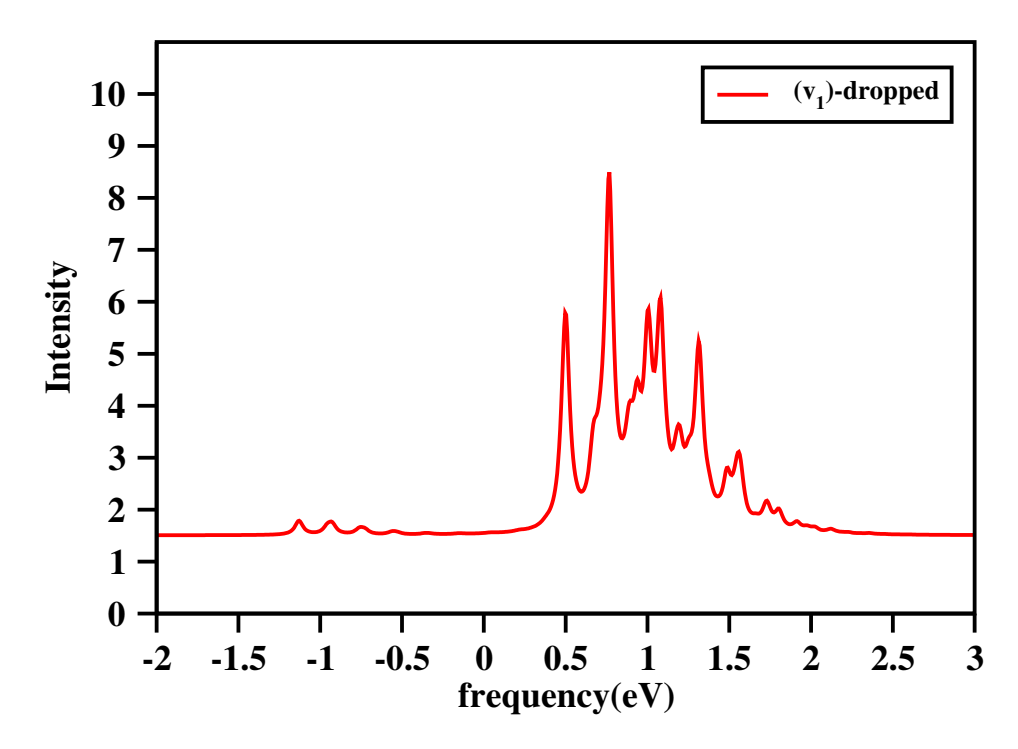


Figure 3.19: Spectrum in spin-boson model for a 2-mode SS with (v_2, v_3) and without v_1 .

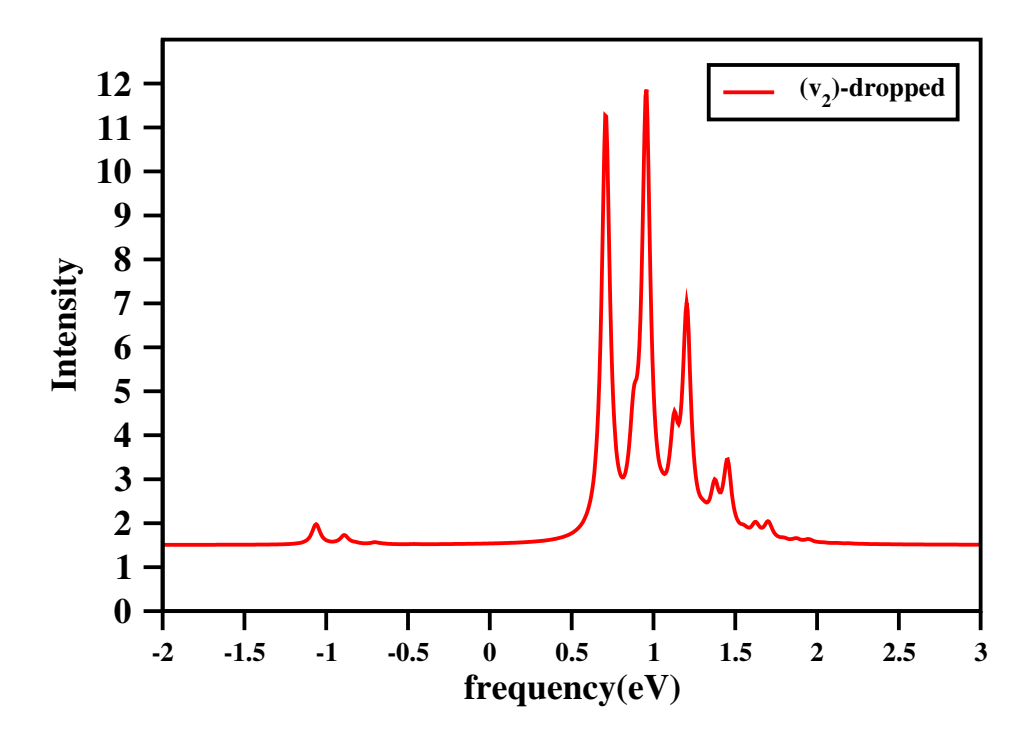


Figure 3.20: Spectrum in spin-boson model for a 2-mode SS with (ν_1, ν_3) and without ν_2 .

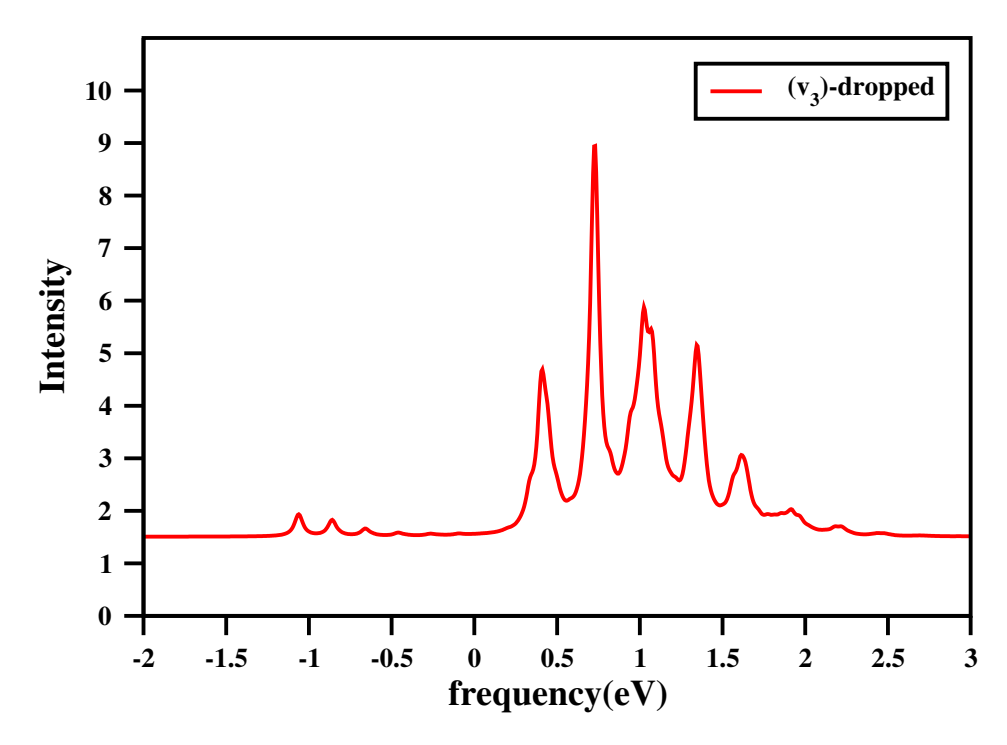


Figure 3.21: Spectrum in spin-boson model for a 2-mode SS with (ν_1, ν_2) and without ν_3 .

3.4 Conclusions

In the light of the set of criteria presented before, we presented in this chapter some numerical calculations to validate the theory. We used an FCI-like approach for the system DOF. Since, our attention is focused on the adequacy of the system dynamics, we have opted to use a simple GWP for the bath DOF.

We applied our set of criteria to the S_1 and S_2 electronic system of pyrazine and a 3-mode spin-boson system. Our analysis for pyrazine showed that only three modes are necessary to define the SS for 24-mode pyrazine. Our ACF calculations made on (3+21) model and (4+20) model (where the most active bath mode is added to the system) are near identical. The spin-boson system needed all the three modes in the system space. These results indicate that we are on the right track.

That some normal modes dominate the overall dynamics of a NAS has been apparent for a while. One specific example which illustrates this is the photo-electron spectrum of allene [66]. In Figure 3 of Ref. 53, the effect of dropping a mode for three different modes was shown. The spectrum of the molecule is almost harmonic when the tuning mode, v_3 , is dropped from the computations. The complexity increases when v_3

is incorporated but a second tuning mode, v_2 , is dropped. These observations indicate the importance of few modes among the several modes in the molecule.

Chapter 4

Numerical Studies using MRTDCCM for bath subspace

4.1 Introduction

In this chapter we develop and test the MRTDCCM formalism[67] for the QM description of the dynamics of the bath DOF. We do this in the context of SB separation of a NAS as discussed in previous chapters. It is already established that the system DOF have to be treated exactly by using an appropriate numerically converged basis set. In the previous chapter, we used a general TDSCF induced GWP approach for the treatment of the bath subspace. We were focused on numerically establishing the validity of the proposed criteria and so, a simplistic TDSCF ansatz was used. Now that the validity of the criteria for choosing the system DOF is established, we want to test a different approximation for the bath subspace. Since, the SS is treated rigorously the only scope to improve the description of NAD is to improve the approximation used for the bath DOF and its coupling to the system DOF. In this context, MRTDCCM seems promising. In this method, the total HS is bifurcated into a model space and a virtual space. In SB formalism, the MS is same as the SS and the VS is identical to the BS. In this work, we keep the electronic DOF and the few important vibrational DOF(chosen by the criteria) in the SS. This SS is treated by a suitable numerically converged (and, in our case) HO basis set. On the other hand, the rest of the vibrational DOF are kept in the BS(or VS). For the bath DOF, we posit an exponential time-evolution operator. The time-evolution operator acts on the MS to cause excitations out of it to the BS. We present the general structure of MRTDCCM, the ansatz used in the method and the working equations. We

test this approach on two molecular systems, butatriene cation and pyrazine. ACF and spectra in each case are presented.

4.2 Hilbert spaces and Wave operator

An N-particle Hilbert space is described as the direct product of the HSs of each of the particles.

$$\mathbb{H} = \mathbb{H}_1 \otimes \mathbb{H}_2 \otimes \mathbb{H}_3 \otimes ... \mathbb{H}_N \tag{4.1}$$

Out of these N-particles, we construct a HS for the system DOF. This system HS or MS is chosen to be made of the electronic DOF and those vibrational modes which dominate the NAD.

$$\mathbb{H}_s = \mathbb{H}_1 \otimes \mathbb{H}_2 \otimes \dots \mathbb{H}_M, (M < N) \tag{4.2}$$

The equations for the SS WF and the related CF is same as in Eqs. 3.9 and 3.8, respectively.

Next, we look at the BS dynamics for which we use TDCCM. The BS in this work is described by the TD exponential wave operator, U, that acts on the SS. TDSE for the total WF is given as (keeping $\hbar = 1$),

$$i\frac{\partial\psi}{\partial t} = H\psi\tag{4.3}$$

We use the same vibronic Hamiltonian as written in Eq. 1.17. The partitioning of the Hamiltonian in the SB framework is same as in Eq. 3.2. A projection operator is defined to project the full HS onto the system HS,

$$\phi(s) = P\psi \tag{4.4}$$

Next, a wave-operator U is defined which takes us back to the full HS from the WFs on the SS.

$$\psi = U\phi(s) \tag{4.5}$$

The two operators are related with each other by the following equations,

$$P\Omega = P, (4.6)$$

and

$$\Omega P = \Omega, \tag{4.7}$$

where, Ω is the wave-operator that takes the projection back to the full WF. In the multireference configuration interaction method, the wave operator is written as the sum of all possible excitations out of the reference SS, taking care that the target final state is not generated more than once. The system part of the WF is same as in Eq. 3.9. Here, F_I are the CFs and C_I are the coefficients. Coupled-cluster theory is inherently a Fock-space theory. To use that formalism, we augment the ansatz of the system to a more general form as the set of the functions, $\{F_{i,k_1,k_2,\dots,k_N}\prod_{\alpha\in BS}|0_k\rangle\}$. This is what we mean by the MS. We define all excitations from this MS to the rest of the HS. Such operators are of two types. First are those which induce excitations within the BS alone (Fig.4.1)(3-4). The second type causes scatterings within the MS (Fig.4.1)(5). Finally, those which cause simultaneous scatterings in the MS and excitations in the BS (Fig.4.1)(1-2). The second category of excitation operators are irrelevant, since by construction all the possible configurations of the MS are already available within the MS.

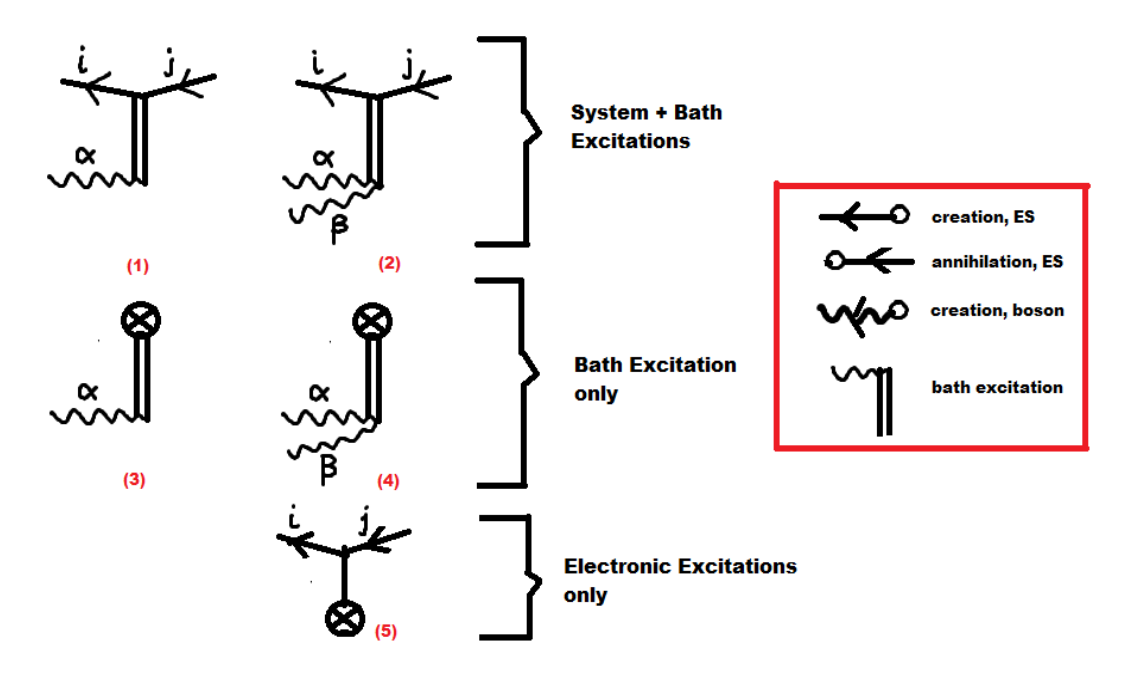


Figure 4.1: All possible excitations in MRCI

4.3 MRTDCCM ansatz

MRTDCCM uses a product of the exponentials to map the reference state WFs to the exact WF.

$$\psi = exp(S_d)exp(S_c). \tag{4.8}$$

The two generators represent the two sets of operators. Here, S_d consists of the individual excitations in both the BS and the SS. On the other hand, S_c consists of the connected excitations from the bath and simultaneous scatterings within the SS. From Liealgebraic decoupling theorems, the equations for S_d are decoupled from the equations of S_c [68, 69]. Second, there are no bath excitation operators in the Hamiltonian. Consequently, the equations of S_d will integrate to give zero throughout the time-evolution. So, the final ansatz of the dynamics becomes,

$$\psi = \exp(S_c) |\phi(s)\rangle. \tag{4.9}$$

Here, $\phi(s)$ is a linear combination of all the configuration states,

$$\psi(s) = \sum_I C_I F_I.$$

This is Eq. 3.9.

4.4 Wave function for MRTDCCM

We now turn to the analysis of the WF in MRTDCCM. We recall that the generalized TDSCF approach had some limitations in describing NAD. We concluded that the generalized TDSCF did not provide either a good ansatz or a proper coupling to the system DOF. We show below that MRTDCCM provides a more complex ansatz for the bath. It is also more tightly coupled to the individual CFs of the SS. The bath part of the MRTDCCM WF is governed by the exponential structure of the wave operators.

$$U = exp\left[\sum_{i,j,\alpha} S^{\alpha}_{ij} c^{\dagger}_{i} c_{j} a^{\dagger}_{\alpha} + \sum_{i,j,\alpha,\beta} S^{\alpha\beta}_{ij} c^{\dagger}_{i} c_{j} a^{\dagger}_{\alpha} a^{\dagger}_{\beta}\right]. \tag{4.10}$$

The generators of this operator form a Lie-algebra. As a consequence, it can be written as a product of multiple exponentials whose generators belong to the same Lie-algebra[70]. Using this, we rewrite Eq.4.10 as,

$$U \approx exp \left[\sum_{i \neq j,\alpha} S^{\alpha}_{ij} c^{\dagger}_{i} c_{j} a^{\dagger}_{\alpha} + \sum_{i \neq j,\alpha,\beta} S^{\alpha\beta}_{ij} c^{\dagger}_{i} c_{j} a^{\dagger}_{\alpha} a^{\dagger}_{\beta} \right]$$

$$exp \left[\sum_{i,j,\alpha} S^{\alpha}_{ij} c^{\dagger}_{i} c_{j} a^{\dagger}_{\alpha} + \sum_{i,j,\alpha,\beta} S^{\alpha\beta}_{ij} c^{\dagger}_{i} c_{j} a^{\dagger}_{\alpha} a^{\dagger}_{\beta} \right].$$

$$(4.11)$$

In these equations, c_i^{\dagger} and c_j are the ES creation and annihilation operators. a_{α}^{\dagger} and a_{β} are the ladder operators of the bath HO. Notice that the second exponential in Eq. 4.11 is diagonal in the ESs. Consequently, it combines the transformations brought about by the wave operator independently on each surface. The transformations it brings about are displacements (from $S_{ii}^{\alpha}a_{\alpha}^{\dagger}$), dilations of the WP (through $S_{ii}^{\alpha\alpha}(a_{\alpha}^{\dagger})^2$) and finally, the coordinate rotations ($S_{ii}^{\alpha\beta}a_{\alpha}^{\dagger}a_{\beta}^{\dagger}$). This is essentially doing a thawed GWP time-evolution on each surface. So, this part of the MRTDCCM ansatz is similar to the full GWP propagation as shown in the previous chapter.

The non-diagonal exponential in Eq.4.11 can be expanded in a power series. This gives to the first-order, the operator, $(S_{ij}^{\alpha}c_i^{\dagger}c_ja_{\alpha}^{\dagger} + S_{ij}^{\alpha\beta}c_i^{\dagger}c_ja_{\alpha}^{\dagger}a_{\beta}^{\dagger})$. This transfers the WP from whichever ES it on to the other ES. It generates two different dynamics on the two ESs. Since, the position and the width parameters of the vibrational WPs are not the same on the two surfaces, it will not add to the coefficient of the GWP already present on that surface. In other words, a non-Gaussian structure develops on that surface. Since, every S_{ij} is accompanied by a S_{ji} (though different in magnitude and phase), an overall WF is developed which is more general than the GWP propagation provided by the generalized TDSCF.

There are two limitations to this generalization. First, the coefficients of the higher orders are parametrized in terms of the basic variables, $S_{ij}\alpha$, ... rather than being independent. Second, the solutions are not variationally determined. This has the disadvantage of losing the state-averaging of the presently occupied states. But, for that as we discussed, the structure of MRTDCCM is more general than that of the TDSCF approach. It is more akin to the G-MCTDH[54] except that in G-MCTDH, the Gaussian expansion coefficients are variationally determined.

Next, we derive the working equations for the BS and the SS (We note that both MS and SS language is used here for addressing the system DOF). We write the operator U generally instead of writing explicitly writing U(t). First, Eq. 4.5 is inserted into the TDSE to get,

$$iU |\dot{\phi}(s)\rangle = \left[HU - i\dot{U}\right] |\phi(s)\rangle.$$
 (4.12)

Premultiply both LHS and RHS by U^{-1} to get,

$$iU^{-1}U|\dot{\phi}(s)\rangle = \left[U^{-1}HU(t) - iU^{-1}\dot{U}(t)\right]|\phi(s)\rangle.$$
 (4.13)

We define an effective Hamiltonian as,

$$\overline{H} = U^{-1}HU - iU^{-1}\dot{U} \tag{4.14}$$

In term of the effective Hamiltonian, Eq. 4.13 can be written as,

$$\left[i\frac{\partial}{\partial t} - \overline{H}\right] |\phi(s)\rangle = 0. \tag{4.15}$$

Thus, the working equations for the MS is given by,

$$P\left[i\frac{\partial}{\partial t} - \overline{H}\right] P |\phi(s)\rangle = 0, \qquad (4.16)$$

and for the BS the working equation is,

$$Q\left[i\frac{\partial}{\partial t} - \overline{H}\right] P |\phi(s)\rangle = 0. \tag{4.17}$$

Q is defined so that Q = 1 - P. Eqs. 4.16 and 4.17 can be expanded using Hausdorff expansion and the terms on the LHS and RHS can be equated to give the terms for the effective MS Hamiltonian and the time-derivatives of the excitation operators. These terms are diagrammatically given in the Appendix. These diagrams were programmed and the numerical integration was carried out by a fourth-order Runge-Kutta integration.

4.5 Results and Discussion

4.5.1 Application on Butatriene cation

In this section, we test the use of MRTDCCM for bath DOF in the SB approach on realistic model. Our first testing ground is the 18-mode butatriene cation.

$$c = c = c$$

Butatriene belongs to the D_{2h} point group and its cation has a CI between the GS and the first excited state. It has only one coupling mode and four tuning modes. We took the electronic energies and the coupling values from the Ref. [71]. According to our criteria (Table 4.1), the SS in butatriene cation should include the coupling mode, v_5 and the only direct crossing mode, v_{14} .

mode	Q_T^0	Q_T^1	Q^{SCC}
ν_8	0.975	1.09	85.71
v_{12}	0.130	-0.113	360
v ₁₄	1.262	-2.654	-1.069
v ₁₅	0.217	-0.173	7.46

Table 4.1: Turning points and SCC points along tuning modes in butatriene cation between GS and first excited ES. Direct crossing mode is given in red

Hence, we use a (2 + 14)-model for testing the theoretical approach using MRT-DCCM for the bath DOF. Our calculations numerically converged for 30 HO functions

for the coupling mode, v_5 and 15 HO functions for the tuning mode, v_{14} . We present the results in terms of ACFs and the spectra. The ACFs are separately presented for the electronic GS, B_{2g} and the first excited state, B_{2u} . We present ACFs for the two cases. First, for each ES we compare the ACFs for three levels of calculations done in MRTD-CCM. These three are MS-only where only SS is considered. The second is (MS+S1) where in addition to MS, one boson excitations are added. Finally, in (MS+S1+S2) we include MS, one boson and two boson excitations (Figs. 4.2 and 4.4). In the next set of calculations, we compare the (MS+S1+S2) calculation to the numerically exact MCTDH results from Ref. [71](Figs. 4.3 and 4.5). The spectra is presented for the total population of ($B_{2u} + B_g$) states. We follow the same set of calculations for MRTDCCM as done for the ACF (Fig. 4.6). We also compare the spectra for the (MS+S1+S2) calculation with the spectra of MCTDH method (Fig. 4.7).

In Fig. 4.2 for B_{2u} state, the ACF is clearly damped. This indicates that the WP is highly dephased for this state. Although the overall shape of the ACFs in Fig. 4.3 look similar for MRTDCCM and MCTDH, there are clear differences in the two results. We believe that this is because of the difference in the size of the converged basis set taken in the two approaches.

In Fig. 4.4 the ACF for the B_{2g} is much less dephased than in the case for B_{2u} state. This is because the two system vibrational modes do not lead to the dephasing of the WP as much as they do on the B_{2u} state. In Fig. 4.5 the matching of the ACFs for the two methods, MRTDCCM and MCTDH, is quite good.

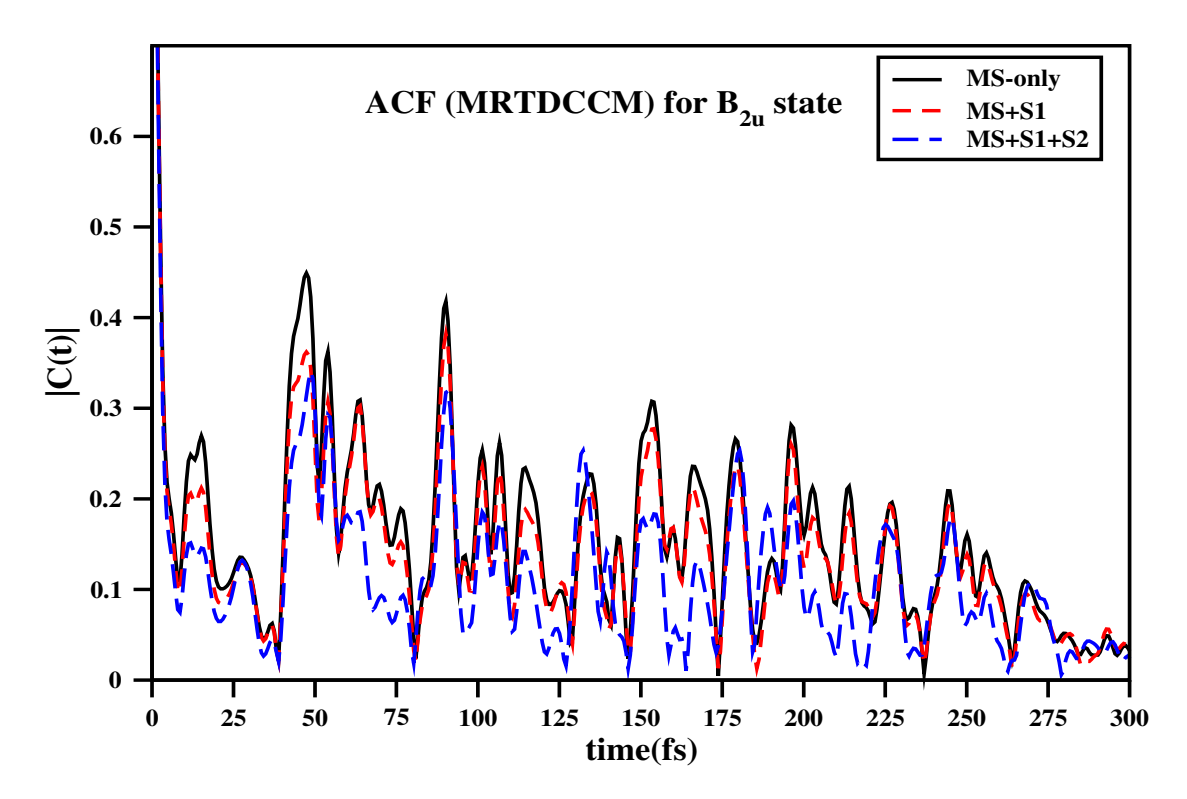


Figure 4.2: Comparison of ACF for B_{2u} state in butatriene cation for three cases: MS only, MS+S1 and MS+S1+S2, using MRTDCCM for bath.

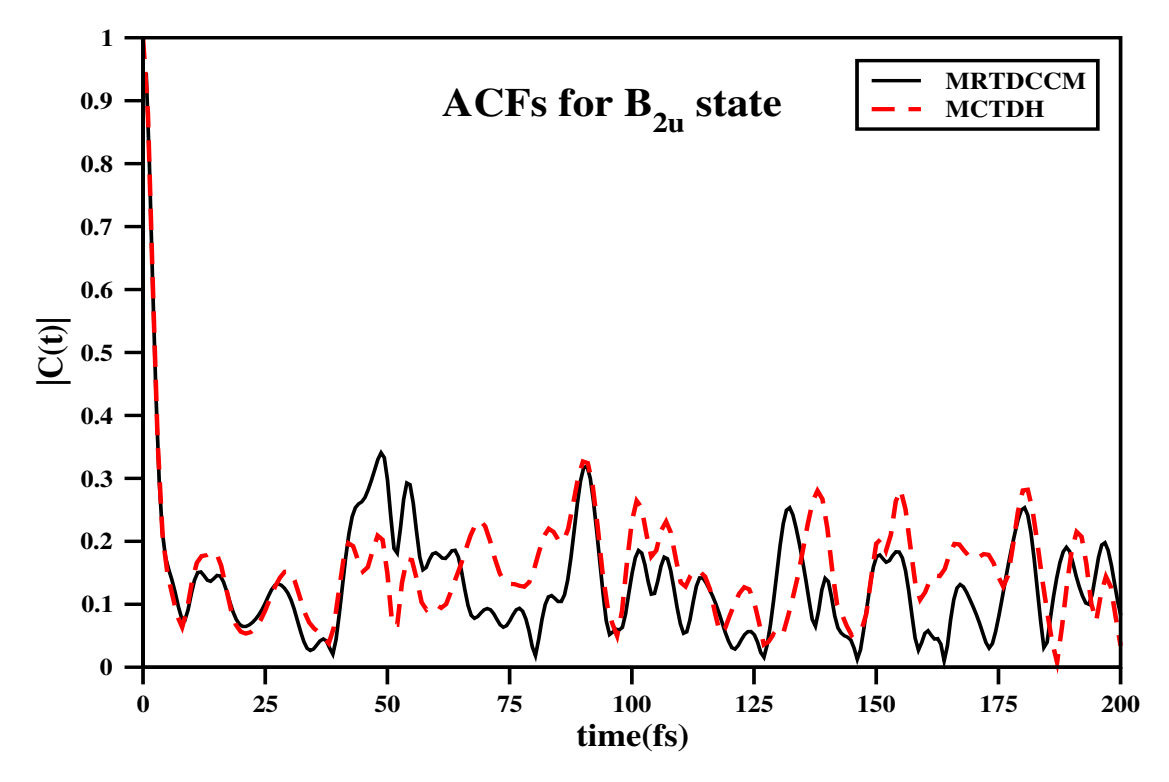


Figure 4.3: Comparison of ACF for B_{2u} state in butatriene cation between MCTDH method and MRTDCCM (MS+S1+S2)

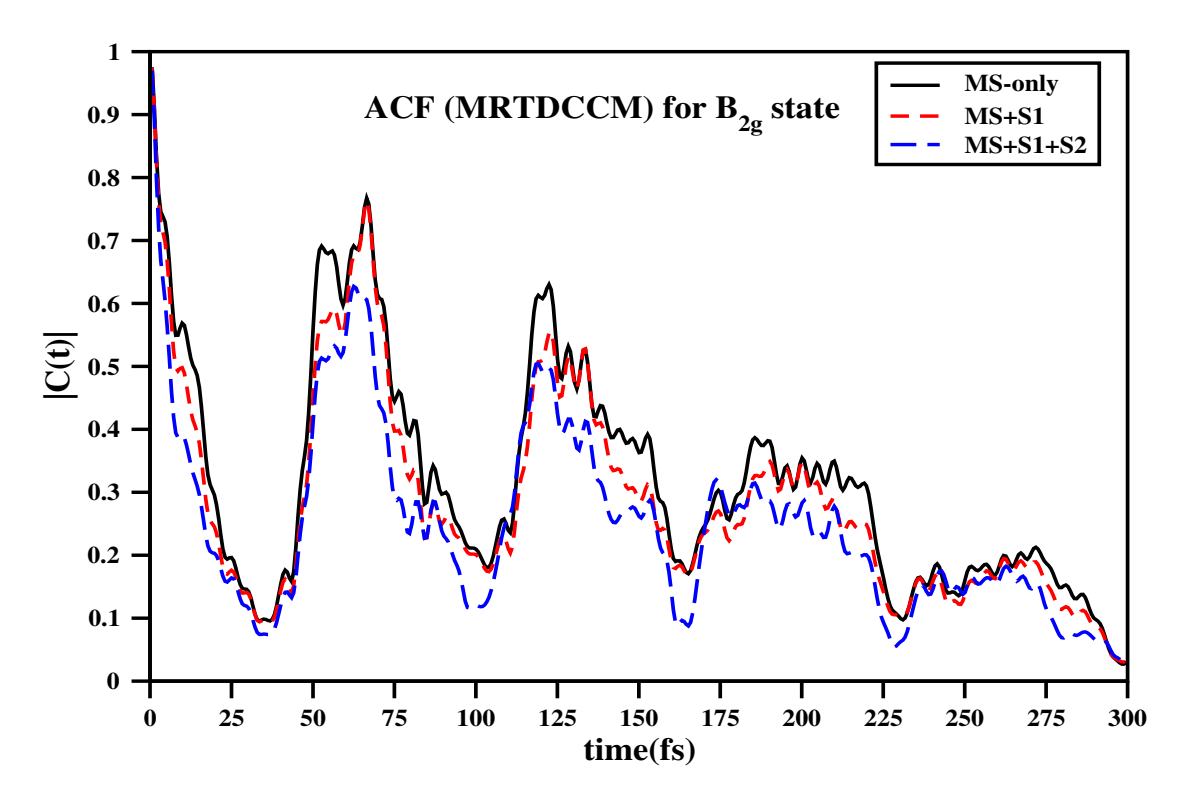


Figure 4.4: Comparison of ACF for B_{2g} state in butatriene cation for three cases: MS only, MS+S1 and MS+S1+S2, using MRTDCCM for bath.

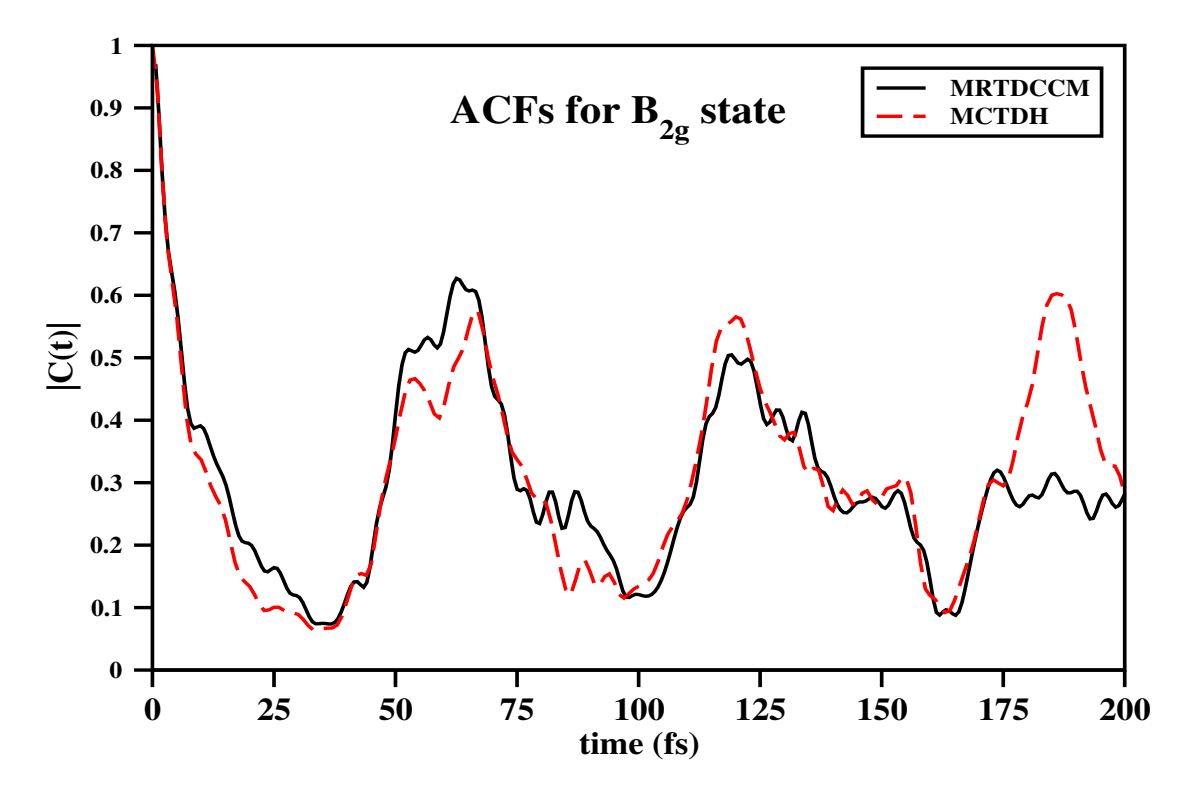


Figure 4.5: Comparison of ACF for B_{2g} state in butatriene cation between MCTDH method and MRTDCCM (MS+S1+S2).

In next two figures, we present the spectra for the overall population of the two ESs, $B_{2u} + B_{2g}$. In Fig. 4.6, the spectra using the MRTDCCM is presented. As can be seen, the famous "mystery" band [20] is well reproduced. This depicts the CI between the two ES. Further, in Fig. 4.7 the spectra from MRTDCCM is matched against the MCTDH spectrum. The matching between the two spectra is very good.

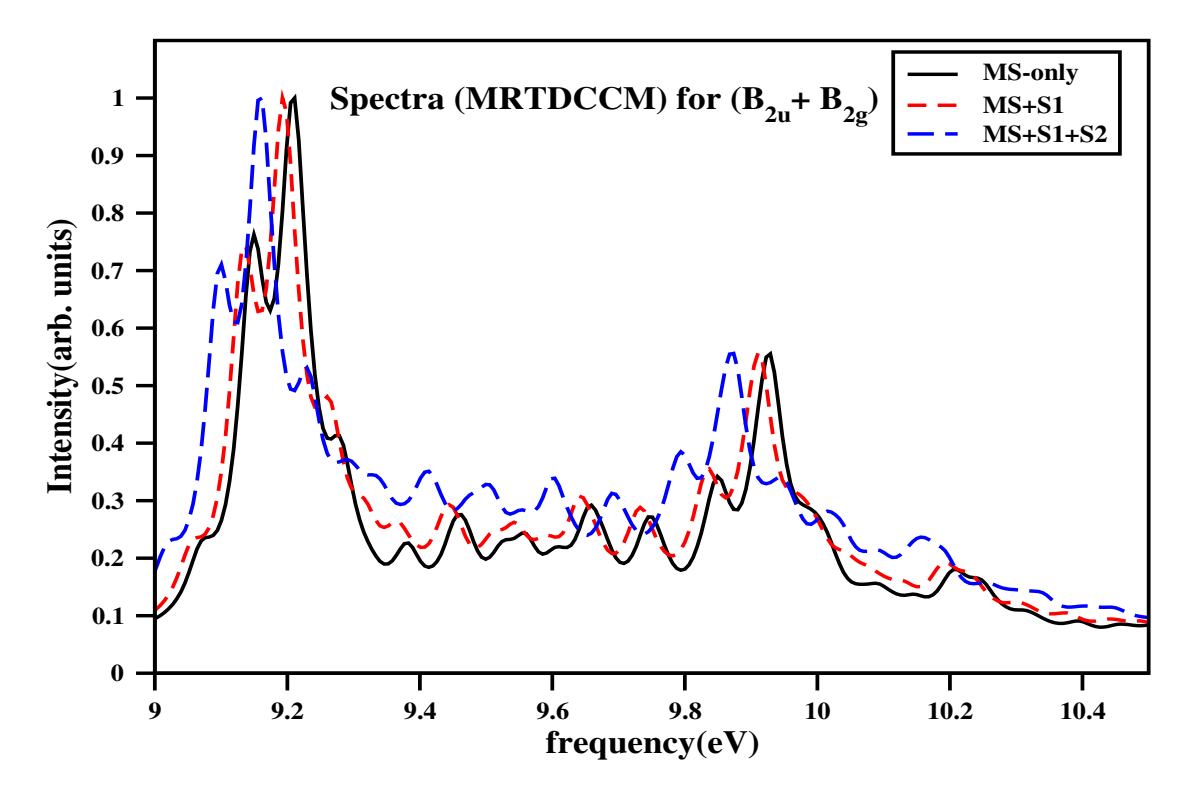


Figure 4.6: Comparison of spectra for $(B_{2u} + B_{2g})$ states in butatriene cation for three cases: MS only, MS+S1 and MS+S1+S2, using MRTDCCM for bath.

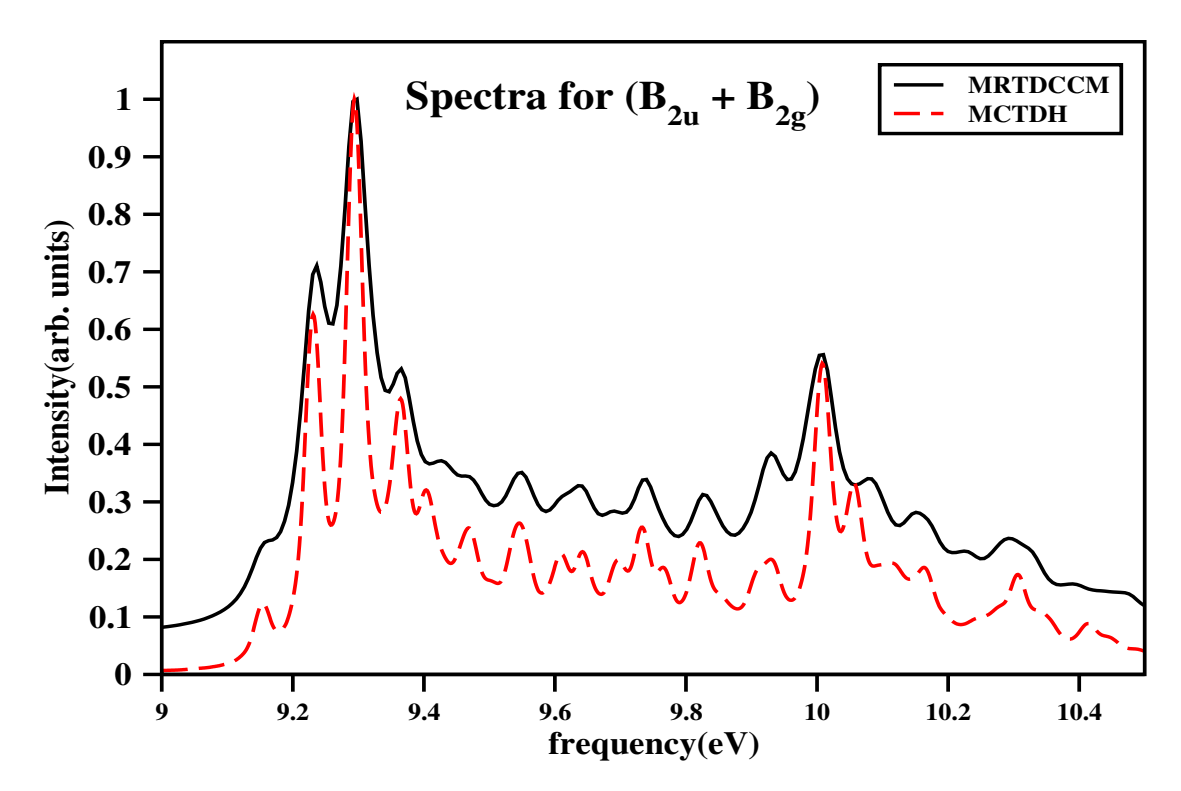


Figure 4.7: Comparison of spectra for $(B_{2u} + B_{2g})$ states in butatriene cation between MCTDH method and MRTDCCM (MS+S1+S2).

4.5.2 Application on pyrazine

Next, we aim to test the MRTDCCM for bath dof in pyrazine molecule. The details of the electronic energies and the couplings are giving in the Chapter 3. We used the (3+21)-model for the testing goal in this section. The numerically converged basis set used in this work is same as used in the previous chapter. We present the ACF (Fig. 4.8) and the spectra (Fig. 4.9) for pyrazine using MRTDCCM. Unfortunately, the calculations could run only upto (MS+S1) level of theory. For (MS+S1+S2) calculations, the calculations terminated with infinities. This is due to rapid divergence of the renormalization diagrams in the method.

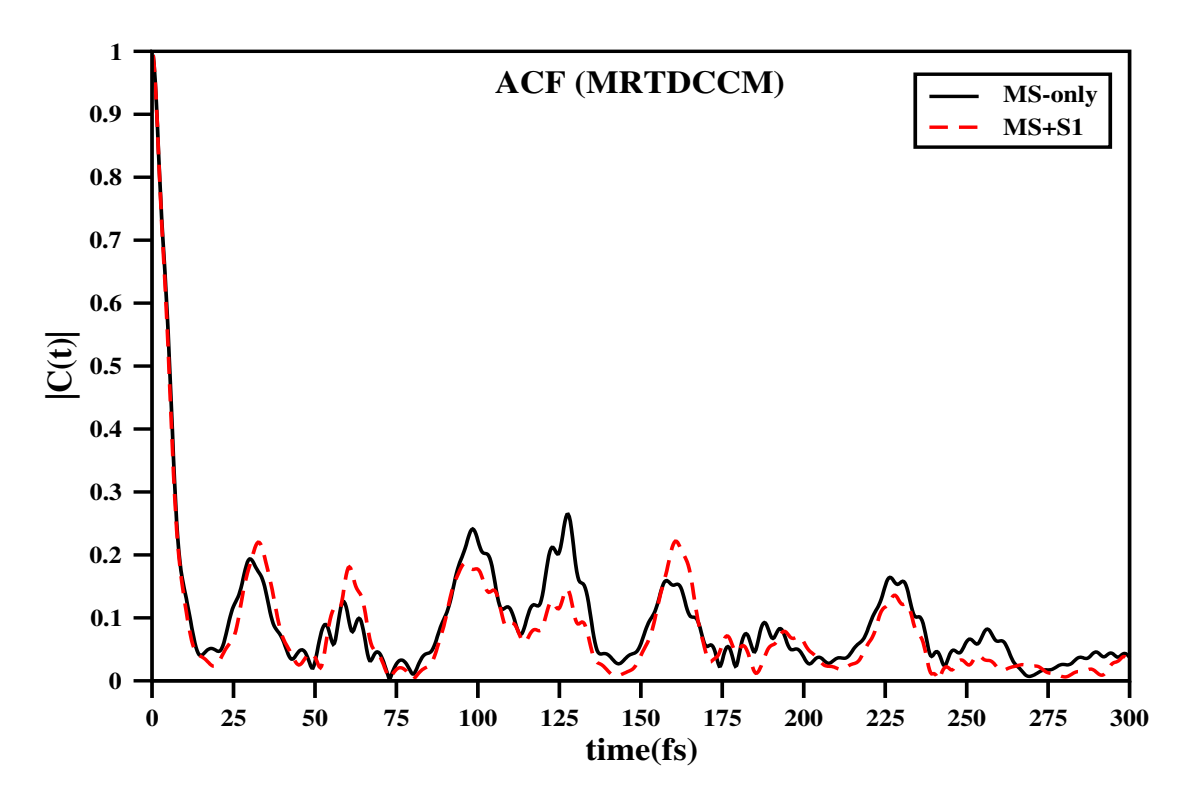


Figure 4.8: ACF for (3+21)-model of pyrazine using MRTDCCM

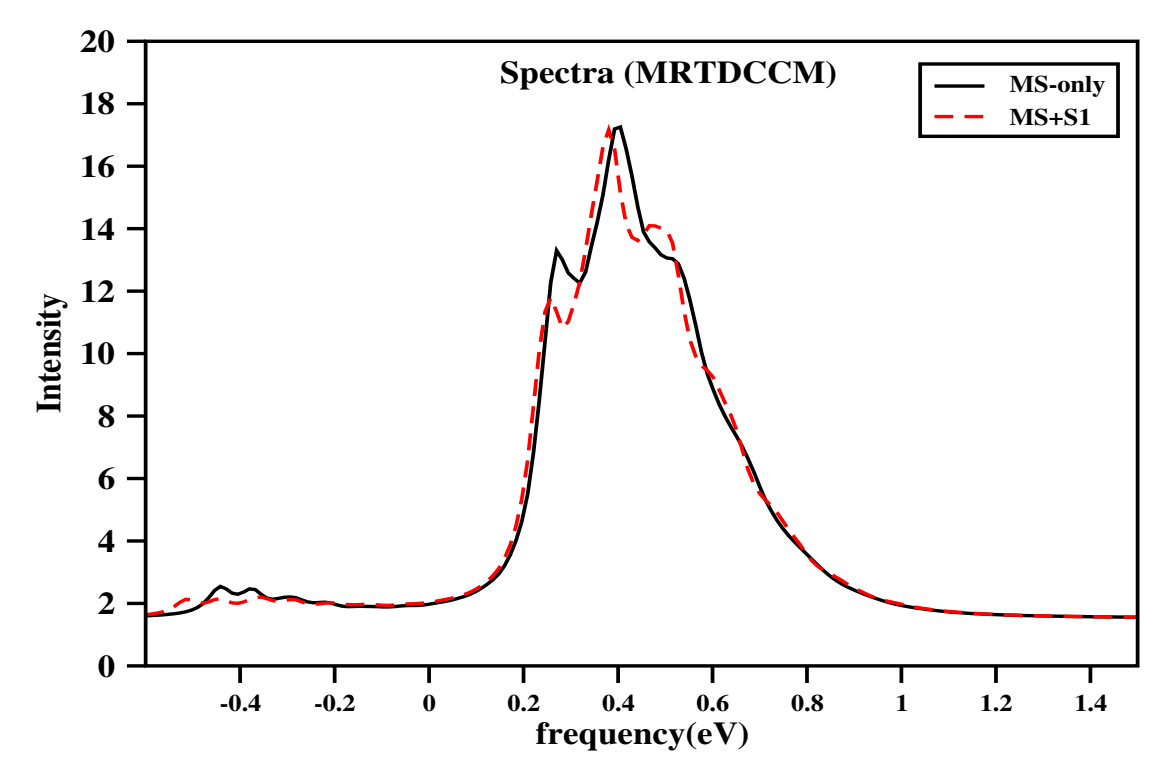


Figure 4.9: Spectra for (3+21)-model of pyrazine using MRTDCCM

4.6 Conclusions

The main aim of this chapter was to test the performance of the MRTDCCM on the bath DOF in SB classification. In this method, the MS is same as the SS and the VS is equivalent to the BS. It uses an exponential time-evolution operator, U(t), for the bath DOF which acts on the MS. This operator is written in terms of the excitation operators, S. We expanded U(t) as a power series in S which given an infinite series for various boson excitations. In this work, we truncated the series to the two boson excitations. These lower level excitations include the effect of higher order excitations as well. Next, the working equations for the SS and the BS were derived. These were expanded using Hausdorff expansion and the similar on the two sides were equated. These MS, effective MS Hamiltonian and S-derivative diagrams were drawn (as given in the Appendix) and programmed.

Next, we tested this approach on the 18-mode butatriene cation. We included the only coupling mode in the SS. In addition, through our analysis of the four tuning modes, we concluded that only mode v_{14} qualifies for the SS. Thus, we used a (2+16)-model for testing purpose. We presented the ACFs for the two ESs separately. On the first excited state, the ACF depicts strong WP dephasing through the damped oscillations. On the other hand, the ACF for the population on the electronic GS is much less damped. The two ACFs using MRTDCCM match satisfactorily with the corresponding MCTDH spectra. The differences arise due to the different sizes of the CFs used for the system DOF. The spectra for MRTDCCM is presented for the total population of the two ESs. The spectra reproduces the "mystery band" very well. Further, the spectra from MRTDCCM and MCTDH method exhibit a fairly good agreement.

We also tested MRTDCCM for the description of the bath DOF in (3+21)-model of pyrazine. Although the method gave good results upto (MS+S1) level of calculations, it failed to converge for (MS+S1+S2) calculations. This illustrates the divergence of certain terms in the coupled-cluster method.

Chapter 5

Dynamics of Dimers spectra

5.1 Introduction

An interesting model system for NAD is the case of molecular aggregates[72–74, 74–78]. The simplest case of this is a dimer[73, 79–83]. A dimer consists of two monomers. We consider only homogeneous dimers. In a homogeneous system the monomers are degenerate. Both of them have their own ESs and associated vibrations. We will call these as local ESs and local vibrations. Given the attractive interaction between the two monomers, the two associate with each other. It is implicitly assumed that the intermonomer interactions are rather weak to the extent that the internal structure of the two monomers is not noticeably affected. That implies that a zeroth order description is very much acceptable to begin with. There are also additional internal DOF in the dimer that were originally part of the relative translational and rotational DOF. We ignore these. We treat the monomers within the dimer as structure-less particles. The interaction strength is assumed to be confined to the ESs alone and it is taken to be independent of any vibrational coordinate.

We now describe the states in detail. We will consider two ESs for each of the monomers. We will call them as α and β . Here, the energy of the α -state is taken to be zero. β is the higher energy state with an energy of ϵ . In terms of these two states, four states can be constructed for the dimer system. These are $|\alpha_1, \alpha_2\rangle$, $|\beta_1, \alpha_2\rangle$, $|\alpha_1, \beta_2\rangle$ and $|\beta_1, \beta_2\rangle$. Only the first three states are relevant for spectroscopic purposes. Within the approximations commonly used, the interaction between the two monomers are confined to second and third states. This defines the simplified overall Hamiltonian for the dimer. The GS is assumed to be unaffected by the inter-monomer interactions. The

highest energy state, $|\beta_1, \beta_2\rangle$ is ignored because it is too high in energy to be accessible. Once the interaction is switched-on the two ESs are coupled through this interaction. This results in NAD. Each monomer has several local vibrations. For simplicity, we assume that only one vibrational mode on each monomer is active. It is assumed that both the local vibrations have the same frequency. It is also assumed that the monomer vibration suffers a displacement in the excited state compared to its GS geometry. The displacement coefficient for both the monomers is taken to be identical. This combined system (interacting ESs and displaced vibrations) forms a vibronic system. Our attempt is to provide a simple description for the dynamics of such a system. We describe the Hamiltonian of such a system in the next section. We then look at the symmetry properties of this simplified Hamiltonian. Next, in Sec. 5.2 it is shown that this symmetry group is isomorphic to the point group C_{2h} . Using the character table of C_{2h} we construct symmetry adapted linear combinations of the local mode basis. We next analyze four possible representations of the system and its Hamiltonian to see which of them would be most convenient for computational purposes.

The dimer problem admits two limiting situations that are analytically soluble. In the absence of vibrations, the problem reduces to (2 X 2) diagonalization of the two ESs as its solution. In the other limit where the electronic coupling is zero the problem reduces to a pair of displaced HO. This is analytically soluble in terms of an exponential similarity transformation of the vibrational part of the Hamiltonian. Given these two limiting conditions, we use MRTDCCM which handles both these limiting conditions. Possible approximations to this ansatz are discussed. We use the systembath formalism. The electronic sub-system is taken as the system. The vibrational part is dealt as the bath part. This is similar to what we did in Chapter 4. The requisite equations for the MRTDCCM are identical to the equations derived in Chapter 4, except for an additional diagram to account for intermonomer interactions. This situation holds in the zeroth order basis. In two other representations the equations are identical. This is described in Sec. 5.5.

The last topic of our discussion is the finite temperature spectra of dimer systems. Thermofield dynamics was developed specifically for describing finite temperature behaviour of many-body systems[78, 83–86]. Specifically for HOs it has a simple representation in ladder operator formalism. Using the permutational symmetry of traces and transferring part of the density matrix to the left, one can write the finite temperature dynamics involving excitations from vacuum alone. A single surface spectroscopy at finite temperatures using thermofield dynamics was developed earlier in our group[85]. It

will now be generalised to multi-surface excitations. The details of the ansatz and working equations will be presented in Sec. 5.5. One of the advantages of the MRTDCCM is that except minor reorganisation of the DOF the ansatz and the working equations remain similar both at zero K and finite temperature. This was one of the motivations for us to choose MRTDCCM to deal with the dimer problem. A program has been written for this purpose but has not been debugged fully so far. As a consequence, I have no result to present in this Chapter.

5.2 The Hamiltonian

We now set out our notation. We define the following,

$$|\phi_1\rangle = |\beta_1\alpha_2\rangle. \tag{5.1}$$

$$|\phi_2\rangle = |\alpha_1\beta_2\rangle. \tag{5.2}$$

and,

$$|\phi_g\rangle = |\alpha_1\alpha_2\rangle. \tag{5.3}$$

In terms of these, the second quantized form of the Hamiltonian of a monomer for the relevant excited states is given by,

$$H_M = |\beta\rangle \epsilon \langle \beta| + \hbar\omega |\beta\rangle a_m^{\dagger} a_m \langle \beta| + V |\beta\rangle (a_m^{\dagger} + a_m) \langle \beta|. \quad (5.4)$$

Here, the first term gives the electronic energy, the second term gives the vibrational energy and the last term is the displacement of the vibrational coordinate. HS of the Hamiltonian will include its electronic GS and one electronic excited state.

A dimer is a case where two monomers interact with each other in such a way that their ESs mix. This mixing causes splitting of ESs into two eigenstates of the dimer Hamiltonian. The dimer Hamiltonian is written as,

$$H_{D} = |\phi_{1}\rangle \epsilon \langle \phi_{1}| + |\phi_{2}\rangle \epsilon \langle \phi_{2}| + |\phi_{1}\rangle J \langle \phi_{2}| + |\phi_{2}\rangle J \langle \phi_{1}| + \hbar\omega |\phi_{1}\rangle a_{1}^{\dagger} a_{1} \langle \phi_{1}| + \hbar\omega |\phi_{2}\rangle a_{2}^{\dagger} a_{2} \langle \phi_{2}| + V |\phi_{1}\rangle (a_{1}^{\dagger} + a_{1}) \langle \phi_{1}| + V |\phi_{2}\rangle (a_{2}^{\dagger} + a_{2}) \langle \phi_{2}|.$$

$$(5.5)$$

In Eq. 5.5, $|\phi_i\rangle$ are the respective WFs for the monomers with i=1,2. The first two terms are the electronic energies of each monomer, respectively. The third and fourth terms represent the electronic couplings between the two monomers. The vibrational energies of monomer 1 and monomer 2 are given by fifth and sixth terms. Finally, the last two terms are the displacements of the vibrational coordinates for the two monomers. The vibrations in the two monomers are influenced by the mixing of the electronic energies.

5.3 Symmetry considerations

The basis for the dimer can be constructed with respect to the two monomers. It is given by,

$$\{|\phi_k\rangle|v_1\rangle|v_2\rangle\}, \forall k, v_1, v_2.$$
 (5.6)

The analysis of the symmetries of the Hamiltonian indicate that it belongs to a group containing four symmetry elements. The first symmetry element is the usual identity operator, E. Next, there are permutations of the ESs, P_e . There will be exchanges amongst the vibrational modes of two monomers and this gives P_v symmetry. In addition, the electronic and vibrational DOF can be simultaneously exchanged forming P_{ev} symmetry. Hence, the symmetry group formed by these elements is $G_D = \{E, P_e, P_v, P_{ev}\}$. Its group multiplication table is,

	E	P _e	P_{v}	P_{ev}
E	E	P_e	P_{v}	P_{ev}
P_e	P_e	E	P_{ev}	P_{ν}
P_{ν}	P_{v}	P_{ev}	Е	P_e
P_{ev}	P_{ev}	P_{ν}	P_e	E

Table 5.1: Group multiplication table of the symmetry group of a dimer

It can be shown that this table is isomorphic to the point group C_{2h} . The symmetry elements in the C_{2h} point group are $\{E, C_2, \sigma_h, i\}$. We label the symmetry elements $\{E, C_2, \sigma_h, i\}$ as $\{A, B, C, D\}$, respectively. Thus, the group multiplication table of C_{2h} can be written in Table5.2. Similarly, we can rewrite Table5.1 where we replace $\{E, P_e, P_v, P_{ev}\}$ by A, B, C, D respectively. In this case, the group multiplication table is identical to Table 5.2. This establishes the mapping of the elements of the two groups as,

$$P_e \rightarrow C_2$$

$$P_v \to \sigma_h$$

$$P_{ev} \rightarrow i$$
.

	E	C_2	σ_h	i
A	A	В	С	D
В	В	A	D	С
C	С	D	A	В
D	D	С	В	A

Table 5.2: Group multiplication table for a C_{2h} point group in terms of A, B, C, D

Thus, the character table for the symmetry group of the dimer is,

	A_g	A_u	B_g	B_U
E	1	1	1	1
P_e	1	1	-1	-1
P_{v}	1	-1	-1	1
P_{ev}	1	-1	1	-1

Table 5.3: Character table for the symmetry group of a dimer.

5.4 Symmetry adapted linear combinations

The next exercise is to write the symmetry adapted basis functions and vibrational coordinates for the dimer. We use here onward, $|k, m, n\rangle$ in place of $|\phi_k\rangle |v_m^1\rangle |v_n^2\rangle$. The states $|k, m, n\rangle$ for k = 1, 2 are degenerate with zeroth order energies,

$$E = \epsilon + (m+n)\omega. \tag{5.7}$$

We form the symmetry adapted basis for it. The projection operators for the SALCs are,

$$P_{A_g} = E + P_e + P_v + P_{ev}, (5.8)$$

$$P_{A_u} = E + P_e - P_v - P_{ev}, (5.9)$$

$$P_{B_g} = E - P_e - P_v + P_{ev}, (5.10)$$

and,

$$P_{A_e} = E - P_e + P_v - P_{ev}. (5.11)$$

Thus, for A_g representation the symmetry adapted and normalised basis are,

$$(E + P_e + P_v + P_{ev})(|1, m, n\rangle) = \frac{1}{2}[|1, m, n\rangle + |2, m, n\rangle + |1, n, m\rangle + |2, n, m\rangle].$$
(5.12)

Similarly the basis functions for A_u , B_g and B_u Irreps are given by following equations (Eqs. 5.13-5.15), respectively.

$$(E + P_e - P_v - P_{ev})(|1, m, n\rangle) = \frac{1}{2}[|1, m, n\rangle + |2, m, n\rangle - |1, n, m\rangle - |2, n, m\rangle].$$
(5.13)

$$(E - P_e - P_v + P_{ev})(|1, m, n\rangle) = \frac{1}{2}[|1, m, n\rangle - |2, m, n\rangle - |1, n, m\rangle + |2, n, m\rangle].$$
(5.14)

$$(E - P_e + P_v - P_{ev})(|1, m, n\rangle) = \frac{1}{2}[|1, m, n\rangle - |2, m, n\rangle + |1, n, m\rangle - |2, n, m\rangle].$$
(5.15)

The exact eigenstates can be found by configuration interaction under each symmetry Irrep separately. The zeroth order states to which excitation happens are, $|\phi_1, n, m\rangle$ and $|\phi_2, n, m\rangle$ via dipole operators, d_1 and d_2 . Hence, the doorway state for the TD picture of the spectra is given by,

$$\psi(0) = d_1 |\phi_1 00\rangle + d_2 |\phi_2 00\rangle \tag{5.16}$$

This belongs to the totally symmetric representation, A_g and continues to belong to the A_g representation throughout its time evolution.

5.5 Dynamics

In this section we consider two topics. The first is the possible representations of the ESs and the vibrational coordinates. The second is the ansatz for the TD propagation for spectra.

5.5.1 Possible representations

There are four possible representations for the dimer problem. The first of them is a local representation in which both the vibrational coordinates and the ESs are represented in terms of the variables associated with the local description of the monomers. The resulting representation leads to the Hamiltonian presented in Eq. 5.5. We call it as the local representation. As can be noticed, it contains two sets of non-diagonal operators, the inter-monomer interactions and the vibrational displacement terms. In this sense, this is not a convenient representation for the description of the dimer. Three other representations exist in which one of the non-diagonal terms is eliminated through linear transformations. We define these below.

5.5.1.1 Symmetrised vibrational representation

In this representation, we symmetrise the vibrational subsystem of the dimer. We define q_1 and q_2 as,

$$q_1 = \frac{{a_1}^{\dagger} + a_1}{\sqrt{2}},\tag{5.17}$$

and,

$$q_2 = \frac{{a_2}^\dagger + a_2}{\sqrt{2}}. (5.18)$$

Next, in terms of q_1 and q_2 we define two new coordinates, Q and q as shown below.

$$Q = \frac{(q_1 + q_2)}{\sqrt{2}},\tag{5.19}$$

and,

$$q = \frac{(q_1 - q_2)}{\sqrt{2}}. (5.20)$$

The ladder operators in this new coordinates system change as,

$$A^{\dagger} = \frac{a_1^{\dagger} + a_2^{\dagger}}{\sqrt{2}} \tag{5.21}$$

$$a^{\dagger} = \frac{a_1^{\dagger} - a_2^{\dagger}}{\sqrt{2}} \tag{5.22}$$

and their hermitian adjoints. The electronic subsystem is left unchanged. In terms of these new coordinates the Hamiltonian becomes,

$$H_{D} = |\phi_{1}\rangle \epsilon \langle \phi_{1}| + |\phi_{2}\rangle \epsilon \langle \phi_{2}| + |\phi_{1}\rangle J \langle \phi_{2}| + |\phi_{2}\rangle J \langle \phi_{1}| + \frac{\hbar\omega}{2} |\phi_{1}\rangle [A^{\dagger}A + A^{\dagger}a + a^{\dagger}A + a^{\dagger}a] \langle \phi_{1}| + \frac{\hbar\omega}{2} |\phi_{2}\rangle [A^{\dagger}A - A^{\dagger}a - a^{\dagger}A + a^{\dagger}a] \langle \phi_{2}| + \frac{V}{\sqrt{2}} |\phi_{1}\rangle (Q + q) \langle \phi_{1}| + \frac{V}{\sqrt{2}} |\phi_{2}\rangle (Q - q) \langle \phi_{2}|$$

$$(5.23)$$

There is no advantage in the above representation as none of the terms get cancelled. The nature of the Hamiltonian makes both the coordinates on both the surfaces as tuning.

5.5.1.2 Symmetrised electronic representation

In this representation, we transform the electronic basis, ϕ_1 and ϕ_2 to a symmetrised electronic basis. We call them ψ_1 and ψ_2 , respectively. These are defined below.

$$\psi_1 = \frac{(\phi_1 + \phi_2)}{\sqrt{2}} \tag{5.24}$$

and,

$$\psi_1 = \frac{(\phi_1 - \phi_2)}{\sqrt{2}} \tag{5.25}$$

The vibrational coordinates are left alone. In terms of these coordinates, the Hamiltonian transformation is given by,

$$H_{D} = |\psi_{1}\rangle (\epsilon + J) \langle \psi_{1}| + |\psi_{2}\rangle (\epsilon - J) \langle \psi_{2}| + (5.26)$$

$$\frac{\hbar \omega}{2} [|\psi_{1}\rangle \left(a_{1}^{\dagger} a_{1} + a_{2}^{\dagger} a_{2}\right) \langle \psi_{1}| + |\psi_{1}\rangle \left(a_{1}^{\dagger} a_{1} - a_{2}^{\dagger} a_{2}\right) \langle \psi_{2}|$$

$$+ |\psi_{2}\rangle \left(a_{1}^{\dagger} a_{1} - a_{2}^{\dagger} a_{2}\right) \langle \psi_{1}| + |\psi_{2}\rangle \left(a_{1}^{\dagger} a_{1} + a_{2}^{\dagger} a_{2}\right) \langle \psi_{2}| +$$

$$\frac{V}{2} [|\psi_{1}\rangle \left(a_{1}^{\dagger} + a_{1} + a_{2}^{\dagger} + a_{2}\right) \langle \psi_{1}| +$$

$$|\psi_{1}\rangle \left(a_{1}^{\dagger} + a_{1} - a_{2}^{\dagger} - a_{2}\right) \langle \psi_{2}| +$$

$$|\psi_{2}\rangle \left(a_{1}^{\dagger} + a_{1} - a_{2}^{\dagger} - a_{2}\right) \langle \psi_{1}| +$$

$$|\psi_{2}\rangle \left(a_{1}^{\dagger} + a_{1} + a_{2}^{\dagger} + a_{2}\right) \langle \psi_{2}|]$$

This representation gets rid of interstate electronic coupling. However, it induces the vibrational modes to become both coupling and tuning modes on both the surfaces.

5.5.1.3 Global symmetrised representation

In this representation, both vibrational coordinates and ESs are chosen as SALCs. These are symmetry coordinates, Q, q and the states, ψ_1 and ψ_2 . In these terms these symmetrised variables, the Hamiltonian is rewritten as follows,

$$H_{D} = |\psi_{1}\rangle (\epsilon + J) \langle \psi_{1}| + |\psi_{2}\rangle (\epsilon - J) \langle \psi_{2}| + (5.27)$$

$$\frac{\hbar \omega}{2} [|\psi_{1}\rangle (A^{\dagger}A + a^{\dagger}a) \langle \psi_{1}| + |\psi_{1}\rangle (A^{\dagger}a + a^{\dagger}A) \langle \psi_{2}|$$

$$+ |\psi_{2}\rangle (A^{\dagger}a + a^{\dagger}A) \langle \psi_{1}| + |\psi_{2}\rangle (A^{\dagger}A + a^{\dagger}a) \langle \psi_{2}|] +$$

$$\frac{V}{\sqrt{2}} [|\psi_{1}\rangle Q \langle \psi_{1}| + |\psi_{1}\rangle q \langle \psi_{2}| + |\psi_{2}\rangle q \langle \psi_{1}| + |\psi_{2}\rangle Q \langle \psi_{2}|]$$

It retains the advantages of both the previous representations, in the sense that the

electronic off-diagonal elements are now eliminated. One of the symmetric normal coordinate vibrations, Q, becomes independent of the ES upto the linear level. It becomes a globally displaced oscillator and hence, is a tuning mode with identical displacements on the two surfaces. The two ESs are now coupled through an energy-exchange mechanism ($A^{\dagger}a + a^{\dagger}A$ operator). Otherwise, there is no interstate coupling. The asymmetric normal coordinate,q couples the two ESs and thus, is a coupling mode. The Hamiltonian has a constant of motion ($A^{\dagger}A + a^{\dagger}a$). A configuration-interaction calculation needs to be carried out with the subset of $|k, m, n\rangle$, where, (n + m = N) for some fixed N. We shall develop the MRTDCCM within this and the local mode representation.

5.5.2 Ansatz

As we noted earlier, the dimer problem admits two limiting conditions. In the absence of vibrations, the WF can be written as,

$$\psi = C_1 |\phi_1\rangle + C_2 |\phi_2\rangle. \tag{5.28}$$

This WF propagates under the influence of the reduced Hamiltonian,

$$H = |\phi_1\rangle \,\epsilon \langle \phi_1| + |\phi_2\rangle \,\epsilon \langle \phi_2| + |\phi_1\rangle \,J \langle \phi_2|$$

+ $|\phi_2\rangle \,J \langle \phi_2|$ (5.29)

In the other limit, in the absence of interstate couplings in the Hamiltonian, the problem reduces to a pair of displaced HOs. Displaced HOs can be diagonalised by a simple exponential ansatz, $exp(Sa^{\dagger} + S_o)$, if the initial state is a HO GS. The more general ansatze involving annihilation operators can be written if a more general doorway state is required. Even for finite temperature systems, the doorway state can be reduced to a Gaussian, as we will see later. In view of this, we choose the ESs as the system HS and the vibrational space as bath. With this, just as we did in Chapter 4, we define the ansatz for the dimer as,

$$\psi = \exp(S) |\psi_0(t)\rangle \tag{5.30}$$

with,

$$|\psi_0(t)\rangle = C_1(t) |\phi_1\rangle + C_2(t) |\phi_2\rangle,$$
 (5.31)

and,

$$S = \sum_{ij} |\phi_i\rangle \left[S_{\alpha}^{ij} a_{\alpha}^{\dagger} + S_{\alpha\beta}^{ij} a_{\alpha}^{\dagger} a_{\beta}^{\dagger} + ...\right] \langle \phi_j|. \tag{5.32}$$

So, the ansatz is to be substituted in the TDSE for obtaining the dynamics. The equations are similar to those derived in Chapter 4.

5.6 Extension to finite temperatures

We now move on to the extension of this formalism to finite temperatures. As is well known, the absorption spectrum from an initial ES, $|I\rangle$ to a final ES, $|F\rangle$ is given by,

$$P = \int d\omega e^{i\omega t} \langle I, v|e^{-iH_F t}|I, v\rangle.$$
 (5.33)

The initial state, $|I, v\rangle$ is not a single vibronic state at finite temperature. Instead, one has the thermal density matrix to represent the initial thermal state. We need to extend this state to such a thermal distribution. This leads to the result,

$$P = Tr_{v} \int d\omega e^{i\omega t} \langle I, v|e^{-iH_{F}t}\rho(\beta)|I, v\rangle.$$
 (5.34)

Here, P is the vibrational TDM. Using the invariance of permutations under traces, we rewrite this equation as,

$$P = Tr_v \int d\omega e^{i\omega t} \langle I\rho(\beta/2)|e^{-iH_F t}|\rho(\beta/2)I\rangle.$$
 (5.35)

We next turn to the evaluation of ρ . We do this for a single oscillator. Extension to two oscillators is a trivial exercise. We assume that the thermal effects are carried by vibrational subsystems alone. The TDM, ρ is

$$\sum_{n} |n\rangle e^{-\beta n\hbar\omega} \langle n| \tag{5.36}$$

This in turn is equal to,

$$\rho = \sum_{n} \frac{(a^{\dagger})^n}{n!} |0\rangle e^{-\beta n\hbar\omega} \langle 0| a^n.$$
 (5.37)

That the annihilation operator acts as if it is a creation operator when acting to the left, has been used in writing this equation. Given that the vacuum state (the HO GS) is real, it is possible to define another fictitious oscillator with a creation operator, b^{\dagger} (and, obviously an associated annihilation operator, b). Thus, we rewrite the above equation as,

$$\rho = \sum_{n} \frac{(a^{\dagger})^n}{n!} |0_a\rangle e^{-\beta n\hbar\omega} (b^{\dagger})^n |0_b\rangle.$$
 (5.38)

It is possible to rewrite Eq. 5.38 as,

$$\rho = \sum \frac{(a^{\dagger}b^{\dagger})^n}{n!} (e^{-\beta H_o}) |0_a\rangle |0_b\rangle. \tag{5.39}$$

Here,

$$H_o = \hbar \omega a^{\dagger} a. \tag{5.40}$$

In this equation, $|0_a\rangle$ and $|0_b\rangle$ are the vacuum states of the original HO and the fictitious HO that we have defined to represent the bra part of the density matrix as in Eq. 5.39. Notice that the H_o term right in the beginning has replaced $n\hbar\omega$ as it acts upon the state, $(a^{\dagger})^n |0_a\rangle$. Thus, it gives the correct probability weight.

We now perform two more changes. First, we move $(e^{-\beta H_o})$ to the right. Second, we recognise that $a^{\dagger}a|0\rangle = 0$. With this,

$$\rho = \sum_{n} e^{-\beta H_o} \frac{(a^{\dagger}b^{\dagger})^n}{n!} e^{\beta H_o} |0_a\rangle |0_b\rangle, \qquad (5.41)$$

$$\rho = \sum_{n} \frac{(a^{\dagger}b^{\dagger}e^{-\beta\hbar\omega})^{n}}{n!} e^{-\beta H_{o}} |0_{a}\rangle |0_{b}\rangle, \qquad (5.42)$$

$$\rho = exp[fa^{\dagger}b^{\dagger}]|0_a\rangle|0_b\rangle, \qquad (5.43)$$

where,

$$f = e^{-\beta\hbar\omega}. (5.44)$$

Our next goal is to reduce the correlated Gaussian in Eq.5.43 to a separable form. This is trivially achieved by defining two new HOs as linear combinations of the old set

 a^{\dagger} and b^{\dagger} .

$$c^{\dagger} = \frac{(a^{\dagger} + b^{\dagger})}{\sqrt{2}},\tag{5.45}$$

and,

$$d^{\dagger} = \frac{(a^{\dagger} - b^{\dagger})}{\sqrt{2}}.\tag{5.46}$$

Replacing $a^{\dagger}b^{\dagger}$ in Eq.5.43 with the new set, we obtain,

$$\rho = e^{\frac{f(c^{\dagger})^2}{\sqrt{2}}} e^{\frac{-f(d)^2}{\sqrt{2}}} |0_a\rangle |0_b\rangle. \tag{5.47}$$

Note that this is essentially a simple coordinate rotation by 90° in the coordinate space of a and b oscillators. Since, a and b oscillators are degenerate, the 2-D Gaussian has cylindrical symmetry. Thus, the state $|0_a\rangle|0_b\rangle$ is also the vacuum state for the c-d oscillator space. So,

$$\rho = e^{fc^{\dagger}c^{\dagger}} e^{-fd^{\dagger}d^{\dagger}} |0_c\rangle |0_d\rangle. \tag{5.48}$$

In the final step of our manipulations, we eliminate the operator $(e^{fc^{\dagger}c^{\dagger}})$ from Eq. 5.48. We define yet another bosonic operator, r^{\dagger} to carry out the well known Bogoliubov transformation,

$$r^{\dagger} = xc^{\dagger} + yc, \tag{5.49}$$

where,

$$x = \frac{1}{\sqrt{(1 - 4f^2)}}\tag{5.50}$$

and,

$$y = \frac{-2f}{\sqrt{(1 - 4f^2)}}. (5.51)$$

Similarly, $(e^{-fd^{\dagger}d^{\dagger}})$ term is eliminated. The difference is in the signs of f. So, the only change is in the value of the variable y in Eq. 5.49. It now becomes,

$$y = \frac{2f}{\sqrt{1 - 4f^2}}\tag{5.52}$$

With this, we have reached our goal of transforming the TDM into a Gaussian vacuum state in terms of the last set of coordinates, r instead of c and d.

5.7 Conclusion

In summary, we had originally the TDM in terms of

$$\rho = e^{fa^{\dagger}b^{\dagger}} |0_a\rangle |0_b\rangle \tag{5.43}$$

We transformed these to new set of operators and coordinates c and d to give,

$$\rho = e^{\frac{f(c^{\dagger})^2}{\sqrt{2}}} e^{\frac{-f(d)^2}{\sqrt{2}}} |0_c\rangle |0_d\rangle \tag{5.51}$$

involving a simple coordinate rotation,

$$q_c = \frac{(q_a + q_b)}{\sqrt{2}} \tag{5.52}$$

$$q_d = \frac{(q_a - q_b)}{\sqrt{2}} \tag{5.53}$$

Next, we carried out a Bogoliubov transformation on the two oscillators c and d in terms of r and s. Using these space rotations,

$$q_r = (x+y)q_c,$$

$$= (x+y)\frac{(q_a+q_b)}{\sqrt{2}},$$

$$= \frac{\sqrt{1-2f}}{\sqrt{2(1+2f)}}(q_a+q_b).$$
(5.54)

$$q_r = (x - y)q_d$$

$$= (x - y)\frac{(q_a - q_b)}{\sqrt{2}}$$

$$= \frac{\sqrt{1 + 2f}}{\sqrt{2(1 - 2f)}}(q_a - q_b).$$
(5.55)

The TDM acts as a vacuum to the ladder operators defined in terms of q_r and q_s and their conjugate momenta. We finally have the vacuum state (albeit with double the DOF) that represents the TDM. TD calculations can be carried out at 0 K. One only has to rewrite the Hamiltonian in terms of the thermal coordinates and their conjugate momenta. This is a trivial exercise since mapping from (q_a, q_b) to (q_r, q_s) is a simple linear transformation.

A program was written to calculate the spectra of model dimer system both at 0 K and at finite temperatures. It is currently in the debugging phase.

Chapter 6

Conclusions

The focus of this thesis work was on three goals. First aim was to develop a set of criteria for classifying system and bath variables in the framework of system-bath approaches to study NAD. Second, the focus was on using two different ansatze for the bath WFs. And last, the goal was an extension of MRTDCCM to finite temperatures in the context of dimer spectra. We reviewed some essential methods available in the literature to simulate the NAD in the vicinity of a CI numerically. We were mainly focused on the system-bath approaches for the description of NAD. In these methods, the overall molecular system is divided into two subspaces. The first subspace consists of the system DOF. These vibrational DOF are crucial in dominating the dynamics in the neighbourhood of a CI. These DOF must be treated rigorously. The second subspace consists of those DOF that have very insignificant effects on the NAD. A suitable approximation is sufficient to treat these. In this way, SB methods for NAD tackle the exponential problem associated with the number of vibrational DOF in a NAS. In the adiabatic representation of the PESs, calculation of the dynamics becomes too complex. This is because the NAC terms become too large to compute. A diabatic representation is chosen to get rid of this issue. In this representation, the NAC terms disappear. Instead, the off-diagonal interstate couplings arise. We wrote a diabatic Hamiltonian at the quadratic/bilinear coupling level. We identified the types of the vibrational modes in this Hamiltonian. The tuning modes belong to the group for on-diagonal coupling, and these modes modulate the electronic energy gap. Next, the modes belonging to the off-diagonal interstate couplings are called the coupling modes. The modes that neither tune nor couple the ESs are called the spectator modes. The guiding principles of our work were taken from the work of Schneider et al. In this work, the authors analysed the dissipative features of the NAD. They presented the reduced probability densities

of the tuning modes and a coupling mode for a 2-state, 3-mode system. They showed that the reduced density matrices were the source of the monotonic increase in the statistical entropies of such active modes. These, in turn, were linked to the dephasing of the WP. However, the mechanism of the WP dephasing was not discussed in this work. Elaborating on this mechanism inspired the work presented in this thesis.

Next, a systematic discussion of the WP CC in the direction of the coupling and tuning modes was done. In the region of the SCC, the coupling modes become active. We assumed that the WP was initially located on the upper electronic surface and that $|\nu_c\rangle$ was its initial coupling mode QS. As this WP reaches the vicinity of the SCC, a part of it crosses onto the other surface. This CC initiates a change in the QS of the coupling mode. This CC repeats along the coupling mode, and the WP fragmentation continues with each crossing. The result is an increased population of the coupling mode states on both surfaces. We concluded that the increased population of the coupling mode states due to the repeated CC is the reason for a monotonic increase in the statistical entropies of the coupling modes. We also noted that the WP dephasing in the direction of the coupling modes is linked to the repeated CCs. Then, the discussions on the CC in the direction of the tuning modes were added to the discussions for the coupling modes. The structure of WP is different for the tuning modes. But, the changes induced in the WP along the two types of vibrational modes occur more or less simultaneously. After the CC along the coupling modes ends, the WP fragments move on their respective ESs in the direction of the tuning modes. This movement is seamless, and each of the WPs moves under the influence of the Hamiltonian determined by its electronic surface. There will be some tuning modes along which the WP fragments reach the SCC more frequently than in the direction of other tuning modes. Hence, such tuning modes become essential for the dephasing of the WP.

With these discussions, we identified that the extent of the WP dephasing in the direction of a given vibrational mode determines its classification as either a system mode or a bath mode. Next, the criteria for choosing the system DOF were outlined. Outlining these criteria was the primary goal of my thesis work. The first part of the criteria states that the spectator modes which do not couple or tune the ESs must be put in the BS. This is because such modes will not significantly affect the overall dynamics. The next part of the criteria states that all coupling modes must be put in the SS. The WP CC happens along the coupling modes. Hence, these modes lead to an extensive dephasing of the WP and must be classified as a system mode. The degree of WP dephasing along a tuning mode depends on whether the WP encounters the SCC before

reaching the turning point on its trajectory. At one-dimensional level we labelled the tuning modes for which the WP crosses the SCC as direct-crossing modes. The direct-crossing modes must be put in the SS. There will be some tuning modes which do not take the WP to SCC along their own trajectories but WP can dephase in its two-dimensional plane with a direct-crossing mode. We labelled these vibrational modes as mutually-assisted crossing modes. We elaborated these types of crossings in Chapter 2. It was shown that in the plane where none of the two tuning modes is a direct-crossing mode, there is no WP CC. In addition, it was shown that the extent of WP CC in the two-dimensional plane differs for different pairs of tuning modes. Whether the mutually-assisted tuning mode will be identified as a system mode or a bath mode will be determined by the degree of the WP CC.

After establishing the criteria, in the next three chapters of my thesis some numerical studies were presented to test the validity of these criteria. The first case for testing was a 24-mode pyrazine molecule. It has a single coupling mode, v_{10a} and five tuning modes. Out of the five modes, one tuning mode v_{6a} is the only direct-crossing mode. Two other tuning, v_1 and v_{9a} modes show varying degrees of mutually-assisted crossing in their respective planes with mode v_{6a} . For rest of the two tuning mode, v_{8a} and v_2 , the WP is located more or less near the FC zone and does not undergo any appreciable extent of mutually-assisted crossing. Thus, according to the guidelines in the criteria, modes v_{10a} and v_{6a} are to be kept in the SS and the modes, v_{8a} and v_2 are put in the BS. Based on the CC shown in their two-dimensional planes, we posited that a 3-mode SS with (v_{10a}, v_{6a}, v_1) is adequate to reproduce the overall NAD in pyrazine and that the fourth mode, v_{9a} , can be kept in the BS without any significant loss in the description of the NAD.

For the treatment of the bath DOF, we used the generalized MRTDCCM ansatz for the BS. It is a simple approximation where the total WF is written as the product of the WFs for the two subspaces with their averaged interactions taken into account. In this manner, the SS are treated rigorously by using a numerically converged HO basis set and the bath DOF are treated by a T-GWP. We use the harmonic potentials for the bath modes and for these, this approximation becomes exact. To this end, we tested a (3+1)-model and (4+0)-model for pyrazine. The ACFs in the two cases are near identical and thus, support our argument that a 3-mode SS is sufficient. We extended the two model by including the rest of the bath modes to give, (3+21)- and (4+20)-models. The effect of adding these additional DOF do not induce any significant change in the ACFs. For all these cases, we presented the corresponding spectra. The spectra catch

the necessary complexities in the NAD. In addition, the ACF and the spectra for the TDSCF method was compared against the numerically exact MCTDH results. The matching of the two ACFs was not appreciable and this is probably because of the huge difference in the system configurations used in the two approaches. However, the matching between our spectra (for (3+21)-model) and the MCTDH spectra was very good. We also presented the comparison of the electronic populations for the two testing models. The electronic populations for the (3+21)- and (4+20)-models are close to each other. However, the matching of our results with that of G-MCTDH was not very good. This is again attributed to the much bigger size of the configurations used in the G-MCTDH for the system and bath modes. Overall, our results agreed with our hypothesis that a 3-mode SS for pyrazine is adequate to describe its NAD near CI.

Next, in the same chapter we tested another model in support of our criteria. We used a 3-mode spin-boson model. In the spin-boson model, the two ESs are coupled by a constant and hence, there is no off-diagonal coupling term. There are only tuning modes in this model. As a consequence, the discussions presented in Chapter 2 on the WP CC are only valid for the case of tuning modes in the spin-boson model. We analysed the CC for the three tuning modes. We found that there is only one direct-crossing mode (mode 2) in this model. The other two tuning modes have different extents of CC in their two dimensional plane with mode 2. We compared the exact SS including these three modes against three cases of 2-mode SS. In the 2-mode calculations, one of the three tuning modes was dropped out one at a time and the ACF and the spectra were compared against those of the exact calculations. These results elaborated the importance of the second mode as a direct-crossing tuning mode. From comparing the results for the other two tuning modes, we suggested that a spin-boson mode with 2mode SS of mode 1 and mode 2 with the third mode in the bath will reciprocate the dynamics satisfactorily. Thus, with these we concluded that our criteria stand in good light against the meticulous numerical testing done in chapter 3. Further, these results show TDSCF method, even though being simple in nature, is sufficient for the treatment of the bath DOF.

Chapter 4 of this thesis consists of the formalism of MRTDCCM for treating the bath DOF. Within the SB framework, the goal of this chapter was to test the MRTD-CCM as an approximation for the BS. We presented the total WF in terms of the system and bath WFs. An exponential projection operator for the BS acts upon the MS which contains the system DOF. This exponential ansatz is written as a power series of the

excitation operators. We truncated the series upto the two-boson excitations. The working equations for the MS and the BS were derived and programmed. The numerical validity of this approach was tested first on the butatriene cation which has a CI between its electronic GS and the first excited state. In line with our criteria, we suggested that a (2+16)-model should be adequate for the description of the NAD in butatriene cation. We presented the numerical results for ACF and the spectra. In the first case, we separately presented the ACF for the GS and the first excited state using the MRT-DCCM method. The results were compared at three levels of calculations, (MS-only), (MS+S1) and (MS+S1+S2). The results seemed to adequately simulate the signatures of the dynamics upto two boson excitations. We also compared each of the ACFs with the corresponding results of the MCTDH method. The two ACFs for the B_{2u} state did not match very well because of the huge configuration-size difference in the two calculations. However, both ACFs showed high degree of dephasing on the upper surface. The two ACFs matched well for the case of the electronic GS. The extent of the dephasing is much less for the GS. This is explained through our criteria by the fact that none of the tuning mode lead the WP to CC on this surface. Finally, the spectra for the net population of the two ESs was presented and the MRTDCCM was able to capture all the essential features of the NAD in butatriene cation. In addition, the matching between the two spectra from the MRTDCCM and MCTDH approach was fairly good. We also tested the MRTDCCM approach on the (3+21)-model case of pyrazine but the calculation could not be run beyond the (MS+S1) level.

At last, we made an incomplete analysis of the dimer spectra in the framework of MRTDCCM. We showed that both 0 K and finite temperature situations can be dealt within the structure of MRTDCCM. The only requirement was to carry out some linear transformations of the coordinates. We have not been able to complete the computational studies so far.

Appendix A

In Fig. A.1 terms for the system subspace Hamiltonian, H_s , are drawn. It includes diagonal terms for electronic energy and vibrational energy. Linear and bilinear/quadratic diagonal terms for changes in electronic state via tuning system modes, t^s , also go into H_s . Off-diagonal linear couplings via coupling mode, c and bilinear couplings between t^s and c are included in the system Hamiltonian.

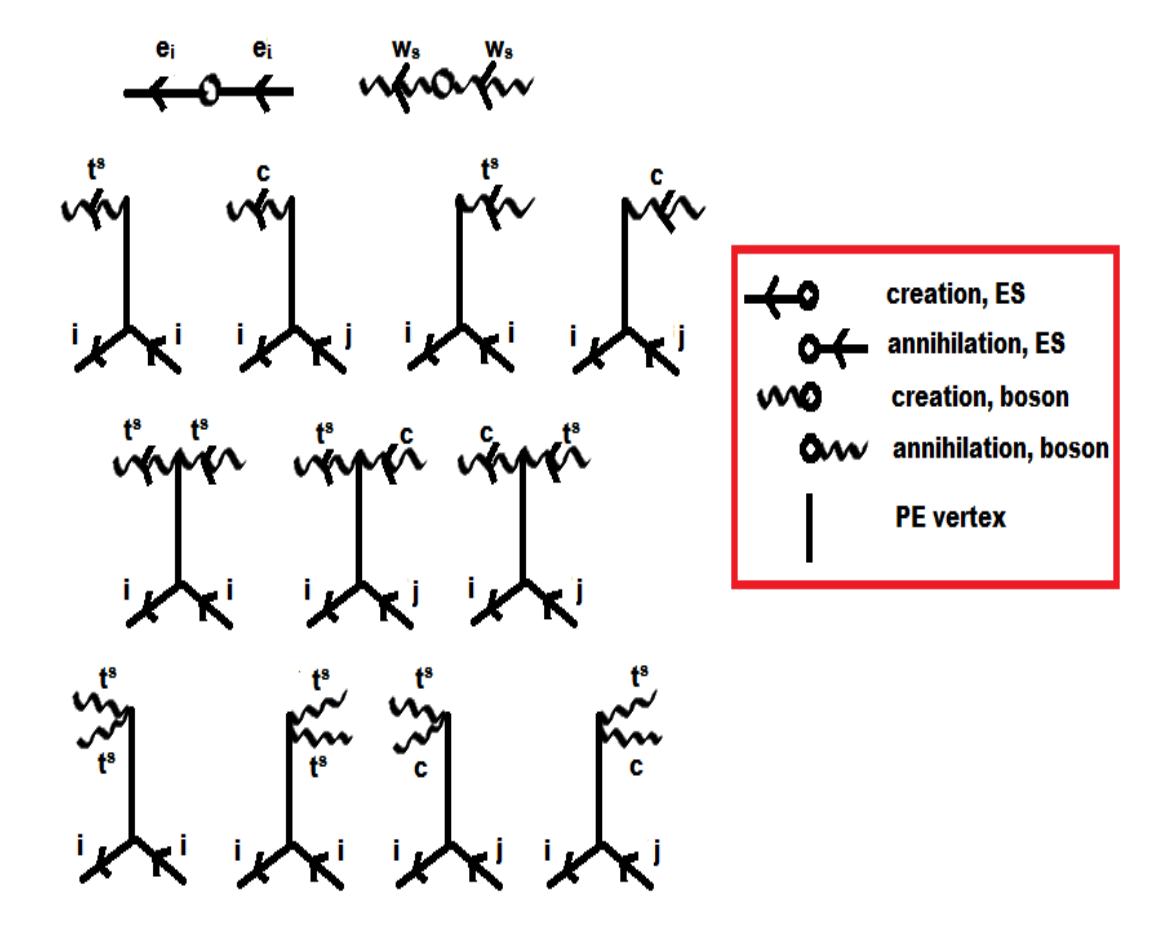


Figure A.1: Diagrammatic representation of terms included in system subspace Hamiltonian.

In Fig. A.2 terms for the effective system subspace Hamiltonian, H_{eff} , are drawn. It includes diagonal changes for electronic energy only which occur due to the contraction of a V-vertex and S-operators.

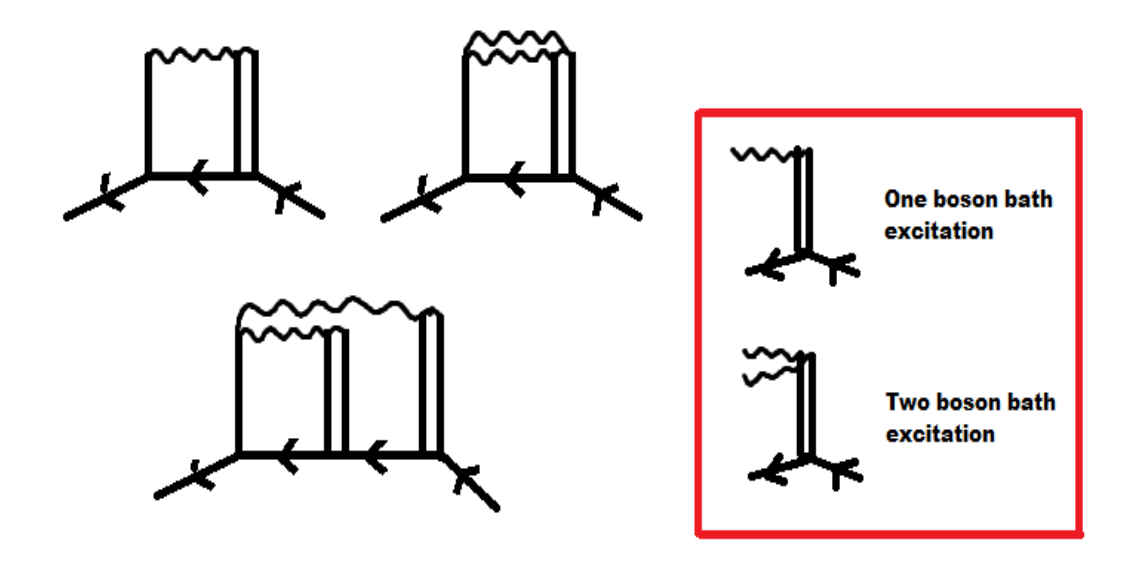


Figure A.2: Effective Hamiltonian for SS

In Fig. A.3 some representative diagrams for $i\dot{S}_1$ are drawn. Various contraction of V- and S-operators give effective one boson excitation. Thus, higher order diagrams are absorbed at lower orders. Similarly, Fig. A.4 represent some of the $i\dot{S}_2$ diagrams.

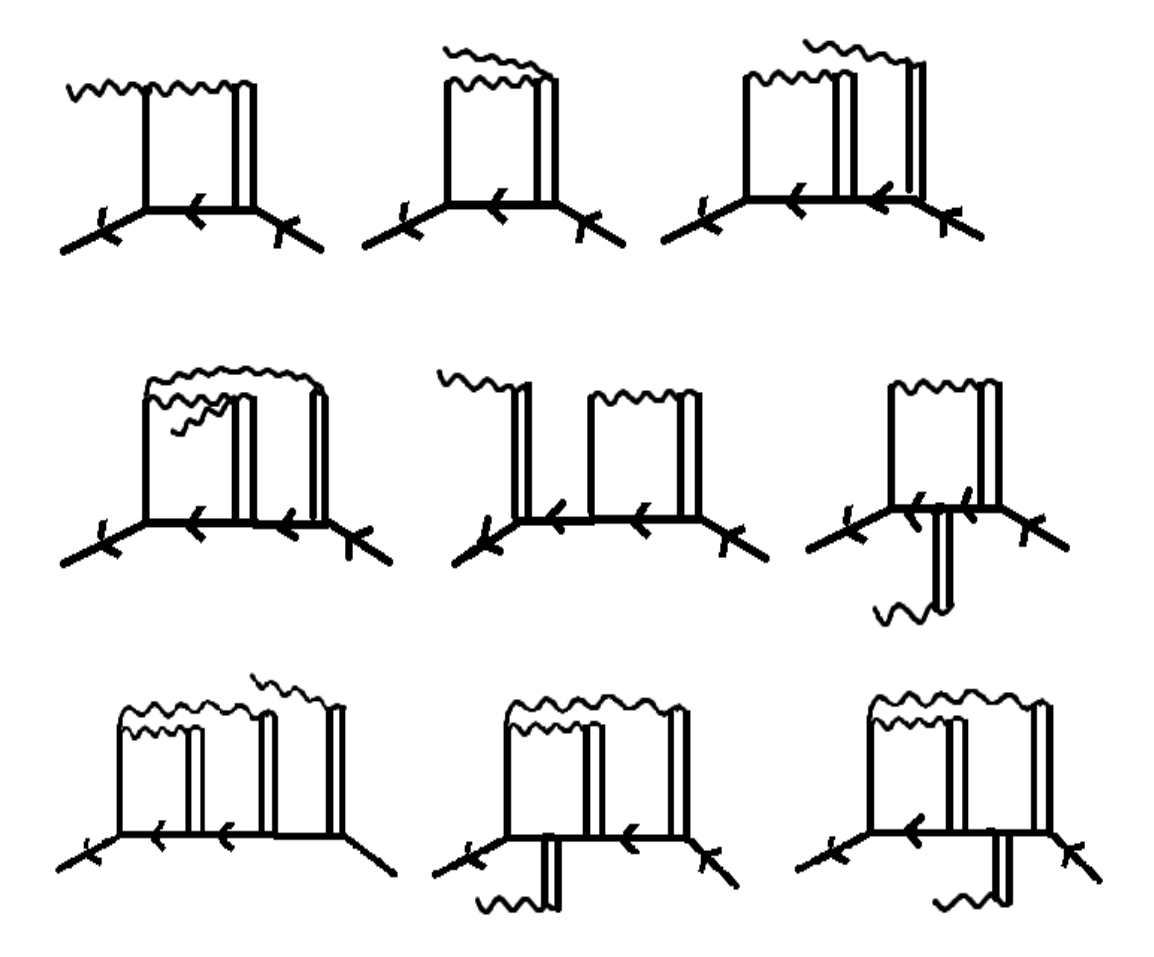


Figure A.3: Some representative diagrams for $i\vec{S}_1$

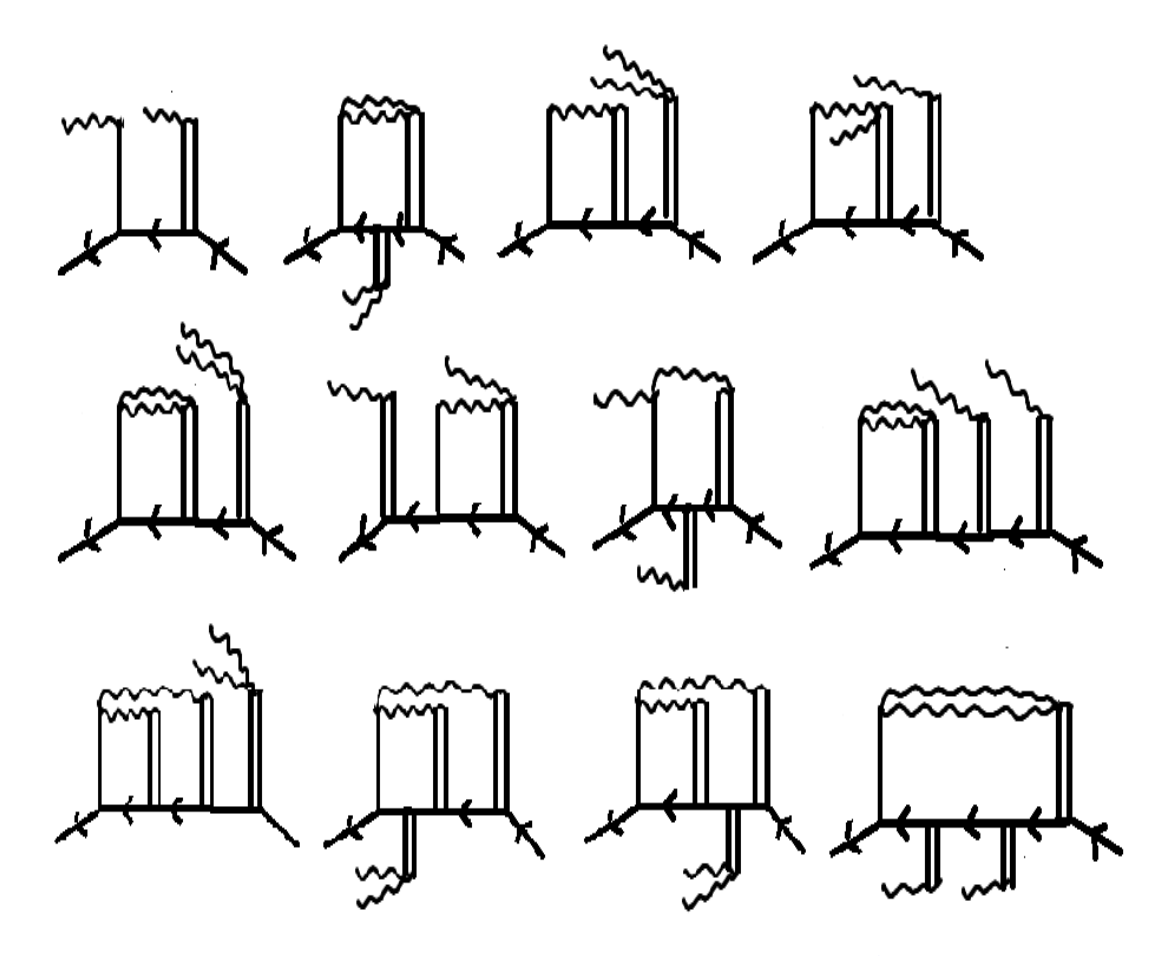


Figure A.4: Some representative diagrams for $i\dot{S_2}$

- [1] Graham A. Worth and Lorenz S. Cederbaum. Beyond born-oppenheimer: molecular dynamics through a conical intersection. *Annu. Rev. Phys. Chem.*, 55:127–158, 2004.
- [2] Horst Köppel, Wolfgang Domcke, and Lorenz S. Cederbaum. Multimode molecular dynamics beyond the born-oppenheimer approximation. *Adv. Chem. Phys.*, 57:59–246, 1984.
- [3] Wolfgang Domcke, David R. Yarkony, and Horst Köppel, editors. *Conical intersections: electronic structure, dynamics and spectroscopy*, volume 15. World Scientific, Singapore, 2004.
- [4] David R. Yarkony. Conical intersections: Diabolical and often misunderstood. *Acc. Chem. Res.*, 31:511–518, 1998.
- [5] Ralph G. Pearson. Symmetry rules for chemical reactions. *Acc. Chem. Res.*, 4: 152–160, 1971.
- [6] Karl. F. Freed. *Energy dependence of electronic relaxation processes in poly-atomic molecules*, pages 23–168. Springer Berlin Heidelberg, Berlin, Heidelberg, 1976. ISBN 978-3-540-38209-6.
- [7] Robert L. Whetten, Gregory S. Ezra, and Edward R. Grant. Molecular dynamics beyond the adiabatic approximation: New experiments and theory. *Annu. Rev. Phys. Chem.*, 36:277–320, 1985.
- [8] Isaac B. Bersuker and Victor Z. Polinger. *Vibronic Interactions and the Jahn-Teller Theoirem*, volume 49, pages 5–30. Springer Berlin Heidelberg, Berlin, Heidelberg, 1989.
- [9] Neil R. Kestner, Jean Logan, and Joshua Jortner. Thermal electron transfer reactions in polar solvents. *J. Phys. Chem.*, 78:2148–2166, 1974.

[10] M. Desouter-Lecomte, D. Dehareng, B. Leyh-Nihant, M. T. Praet, A. J. Lorquet, and J. C. Lorquet. Nonadiabatic unimolecular reactions of polyatomic molecules. *J. Phys. Chem.*, 89:214–222, 1976.

- [11] S. H. Lin. Rate of interconversion of electronic and vibrational energy. *J. Chem. Phys.*, 44:3759–3767, 1966.
- [12] K. F. Freed and J. Jortner. Multiphonon processes in the nonradiative decay of large molecules. *J. Chem. Phys.*, 52:6272–6291, 1970.
- [13] S. H. Lin, C. H. Chang, K. K. Liang, R. Chang, Y. J. Shiu, J. M. Zhang, T.-S. Yang, M. Hayashi, and F. C. Hsu. *Ultrafast Dynamics and Spectroscopy of Bacterial Photosynthetic Reaction Centers*, pages 1–88. John Wiley and Sons, Ltd, NY, 2002. ISBN 9780471264316.
- [14] Q. Peng, Y. Yi, Z. Shuai, and J. Shao. Excited state radiationless decay process with duschinsky rotation effect: Formalism and implementation. *J. Chem. Phys.*, 126:114302, 2007.
- [15] Y. Niu, Q. Peng, C. Deng, X. Gao, and Z. Shuai. Theory of excited state decays and optical spectra: Application to polyatomic molecules. *J. Phys. Chem. A*, 114: 7817–7831, 2010.
- [16] Wolfgang Domcke and David R. Yarkony. Role of conical intersections in molecular spectroscopy and photoinduced chemical dynamics. *Annu. Rev. Phys. Chem.*, 63:325–52, 2012.
- [17] J. von Neumann and E. Wigner. On the behavior of eigenvalues in adiabatic processes. *Phys Z*, 30:467–470, 1929.
- [18] Martial Boggio-Pasqua. Computational mechanistic photochemistry: The central role of conical intersections. 07 2015.
- [19] A. Raab, G. A. Worth, H.-D. Meyer, and L. S. Cederbaum. Molecular dynamics of pyrazine after excitation to the s2 electronic state using a realistic 24-mode model hamiltonian. *J. Chem. Phys.*, 110(2):936–946, 1999.
- [20] L.S.Cedebaum, W. Domcke, H. Köppel, and W. Von Niessen. Strong vibronic coupling effects in ionization spectra: The "mystery band" of butatriene. *Chem. Phys.*, 26:169–177, 1977.

[21] H. Köppel, L. S. Cederbaum, and W. Domcke. Strong nonadiabatic effects and conical intersections in molecular spectroscopy and unimolecular decay: $c_2h_4^+$. *J. Chem. Phys.*, 77:2014, 1982.

- [22] R. Schneider and W. Domcke. $s_1 s_2$ conical intersection and ultrafast $s_1 \rightarrow s_2$ internal conversion in pyrazine. *Chem. Phys. Lett.*, 150:235–242, 1988.
- [23] C. Woywod, W. Domcke, A. L. Sobolewski, and H.-J. Werner. Characterization of the s1-s2 conical intersection in pyrazine using ab initio multiconfiguration selfconsistent-field and multireference configuration-interaction methods. *J. Chem. Phys.*, 100:1400–1413, 1994.
- [24] E. J. Heller. Time-dependent approach to semiclassical dynamics. *J. Chem. Phys.*, 62:1544–1555, 1975.
- [25] W. H. Miller. Classical-Limit Quantum Mechanics and the Theory of Molecular Collisions, volume 25. John Wiley and Sons, Ltd, NY, 1974. ISBN 9780470143773.
- [26] Eric J. Heller. Time dependent variational approach to semiclassical dynamics. *J. Chem. Phys.*, 64:63, 1976.
- [27] J. Frenkel. Wave mechanics; advanced general theory. Oxford, Clarendon, 1934.
- [28] A. D. Mclachlan. A variational solution of the time-dependent schrodinger equation. *Mol. Phys.*, 8:39–44, 1964.
- [29] M. Durga Prasad. Self-consistent-field dynamics of a model non-adiabatic system. *Chem. Phys. Lett.*, 194:27–31, 1992.
- [30] S. Krempl, M. Winterstetter, H. Plöhn, and W. Domcke. Path-integral treatment of multi-mode vibronic coupling. *J. Chem. Phys.*, 100:926–937, 1994.
- [31] S. Krempl, M. Winterstetter, and W. Domcke. Path-integral treatment of multimode vibronic coupling. ii. correlation expansion of class averages. *J. Chem. Phys.*, 102:6499–6510, 1995.
- [32] S. Krempl, W. Domcke, and M. Winterstetter. Real-time path-integral approach for general two-state multi-mode vibronic- coupling models. *Chem. Phys.*, 206: 63–72, 1996.
- [33] M S Child. Molecular collision theory, volume 4. Academic Press, New York, New York, 1974.

[34] M. Thoss, W. H. Miller, and G. Stock. Semiclassical description of nonadiabatic quantum dynamics: Application to the s1–s2 conical intersection in pyrazine. *J. Chem. Phys.*, 112:10282–10292, 2000.

- [35] G. Stock and M. Thoss. Semiclassical description of nonadiabatic quantum dynamics. *Phys. Rev. Lett.*, 78:578–581, 1997.
- [36] M. Thoss and G. Stock. Mapping approach to the semiclassical description of nonadiabatic quantum dynamics. *Phys. Rev. A*, 59:64–79, 1999.
- [37] M. Ben-Nun and Todd J. Martinez. Nonadiabatic molecular dynamics: Validation of the multiple spawning method for a multidimensional problem. *J. Chem. Phys.*, 108:7244, 1998.
- [38] C. Y. Zhu, Y. Teranishi, and H. Nakamura. *Nonadiabatic transitions due to curve crossings: complete solutions of the landau-zener-stueckelberg problems and their applications*, volume 117. John Wiley and Sons, Ltd, NY, 2001.
- [39] William H. Miller. Classical s matrix: Numerical application to inelastic collisions. *J. Chem. Phys.*, 53:3578, 1970.
- [40] P. Puzari, R. S. Swathi, B. Sarkar, and S. Adhikari. A quantum-classical approach to the photoabsorption spectrum of pyrazine. *J. Chem. Phys.*, 123:134317, 2005.
- [41] D. V. Shalashilin. Nonadiabatic dynamics with the help of multiconfigurational ehrenfest method: Improved theory and fully quantum 24d simulation of pyrazine. *J. Chem. Phys.*, 132:244111(1–11), 2010.
- [42] D. V. Shalashilin. Multiconfigurational ehrenfest approach to quantum coherent dynamics in large molecular systems. *Faraday Discuss.*, 153:105–116, 2011.
- [43] D. V. Makhov, W. J. Glover, T. D. Martinez, and D. V. Shalashilin. Ab initio multiple cloning algorithm for quantum nonadiabatic molecular dynamics. *J. Chem. Phys.*, 141:054110, 2014.
- [44] J. C. Tully and Richard K. Preston. Trajectory surface hopping approach to nonadiabatic molecular collisions: The reaction of h^+ with d_2 . J. Chem. Phys., 55:562, 1971.
- [45] D. V. Shalashilin and M. S. Child. Real time quantum propagation on a monte carlo trajectory guided grids of coupled coherent states: 26d simulation of pyrazine absorption spectrum. *J. Chem. Phys.*, 121:3563–3568, 2004.

[46] N. Makri and W. H. Miller. Time-dependent self-consistent field (tdscf) approximation for a reaction coordinate coupled to a harmonic bath: Single and multiple configuration treatments. *J. Chem. Phys.*, 87:5781, 1987.

- [47] H.-D. Meyer, U. Manthe, and L. S. Cederbaum. The multi-configurational time-dependent hartree approach. *Chem. Phys. Lett.*, 165:73–78, 1990.
- [48] U. Manthe, H.-D. Meyer, and L. S. Cederbaum. Wave-packet dynamics within the multiconfiguration hartree framework: General aspects and application to nocl. *J. Chem. Phys.*, 97:3199–3213, 1992.
- [49] G. A. Worth, H.-D. Meyer, and L. S. Cederbaum. The effect of a model environment on the s2 absorption spectrum of pyrazine: A wave packet study treating all 24 vibrational modes. *J. Chem. Phys.*, 105(11):4412–4426, 1996.
- [50] M. H. Beck, A. Jäckle, G. A. Worth, and H.-D. Meyer. The multiconfiguration time-dependent hartree (mctdh) method: a highly efficient algorithm for propagating wavepackets. *Phys. Rep.*, 324:1–105, 2000.
- [51] H.-D. Meyer and G. A. Worth. Quantum molecular dynamics: propagating wavepackets and density operators using the multiconfiguration time-dependent hartree method. *Theor. Chem. Acc.*, 109:251–267, 2003.
- [52] H.-D. Meyer, F. Gatti, and G. A. Worth, editors. *Multidimensional Quantum Dynamics: MCTDH Theory and Applications*. Wiley-VCH, Weinheim, 2009. ISBN 978-3-527-32018-9.
- [53] I. Burghardt, H.-D. Meyer, and L. S. Cederbaum. Approaches to the approximate treatment of complex molecular systems by the multiconfiguration time-dependent hartree method. *J. Chem. Phys.*, 111:2927–2939, 1999.
- [54] I. Burghardt, K. Giri, and G. A. Worth. Multimode quantum dynamics using gaussian wavepackets: The gaussian-based multiconfiguration time-dependent hartree (g-mctdh) method applied to the absorption spectrum of pyrazine. *J. Chem. Phys.*, 129:174104, 2008.
- [55] I. Burghardt, M. Nest, and G. A. Worth. Multiconfigurational system-bath dynamics using gaussian wave packets: Energy relaxation and decoherence induced by a finite-dimensional bath. *J. Chem. Phys.*, 119:5364–5378, 2003.

[56] R. Schneider, W. Domcke, and H.Köppel. Aspects of dissipative electronic and vibrational dynamics of strongly vibronically coupled systems. *J. Chem. Phys.*, 92:1045–1061, 1990.

- [57] L. S. Cederbaum, E. Gindensperger, and I. Burghardt. Short-time dynamics through conical intersections in macrosystems. *Phys. Rev. Lett.*, 94:113003, 2005.
- [58] E. Gindensperger, I. Burghardt, and L. S. Cederbaum. Short-time dynamics through conical intersections in macrosystems. i. theory:effective-mode formulation. *J. Chem. Phys.*, 124:144103, 2006.
- [59] E. Gindensperger, I. Burghardt, and L. S. Cederbaum. Short-time dynamics through conical intersections in macrosystems. ii.applications. *J. Chem. Phys.*, 124:144104, 2006.
- [60] E. Gindensperger, I. Burghardt, and L. S. Cederbaum. Hierarchy of effective modes for the dynamics through conical intersections in macrosystems. *J. Chem. Phys.*, 126:034106, 2007.
- [61] R. Martinazzo, K. H. Hughes, F. Martelli, and I. Burghardt. Effective spectral densities for system-environment dynamics at conical intersections: S2–s1 conical intersection in pyrazine. *Chem. Phys.*, 377:21–29, 2010.
- [62] R. Martinazzo, B. Vacchini, K. H. Hughes, and I. Burghardt. Communication: Universal markovian reduction of brownian particle dynamics. *J. Chem. Phys.*, 134:011101, 2011.
- [63] D. Picconi, A. Lami, and F. Santoro. Hierarchical transformation of hamiltonians with linear and quadratic couplings for nonadiabatic quantum dynamics: Application to the $\pi\pi^*/n\pi^*$ internal conversion in thymine. *J. Chem. Phys.*, 136:244104, 2012.
- [64] D. Picconi, F. J. Avila Ferrer, R. Improta, A. Lami, and F. Santoro. Quantum-classical effective-modes dynamics of the $\pi\pi^*$ $n\pi^*$ decay in 9h-adenine. a quadratic vibronic coupling model. *Faraday Discuss.*, 163:223–242, 2013.
- [65] Y. Liu, J. Cerezo, N. Lin, X. Zhao, R. Improta, and F.Santoro. Comparison of the results of a mean-field mixed quantum/classical method with full quantum predictions for nonadiabatic dynamics: application to the $\pi\pi^*$ $n\pi^*$ decay of thymine. *Theor Chem Acc*, 137:40:1–11, 2018.

[66] S. Mahapatra, G. A. Worth, H.-D. Meyer, L. S. Cederbaum, and Köppel. The $\tilde{A}^2e/\tilde{B}^2b_2$ photoelectron bands of allene beyond the linear coupling scheme: An ab initio dynamical study including all fifteen vibrational modes. *J. Phys. Chem. A*, 105:5567–5576, 2001.

- [67] G. S. Latha and M. Durga Prasad. Time-dependent coupled cluster approach to multimode vibronic dynamics. *J. Chem. Phys.*, 105:2972–2977, 1996.
- [68] G S Latha and M Durga Prasad. On the development of exponential ansatze for quantum dynamics in finite dimensional vector spaces. *Theo. Chim. Acta.*, 86: 511–524, 1993.
- [69] G Madhavi Sastry and M Durga Prasad. Some aspects of the algebraic description of anharmonic dynamics. *Theo. Chim. Acta.*, 89:193–209, 1994.
- [70] James Wei and Edward Norman. Lie algebraic solution of linear differential equations. *J. Math. Phys.*, 4:575, 1963.
- [71] Chr. Cattarius, G. A. Worth, H.-D. Meyer, and L. S. Cederbaum. All mode dynamics at the conical intersection of an octa-atomic molecule: Multi-configuration time-dependent hartree (mctdh) investigation on the butatriene cation. *J. Chem. Phys.*, 115:2088, 2001.
- [72] Michael J. McIntire, Eric S. Manas, and Frank C. Spano. Spontaneous emission and absorption in model aggregates of π -conjugated oligomers. *J. Chem. Phys.*, 107:8152, 1997.
- [73] A. Eisfeld. A simple method to obtain information on the conformation of dipole-dipole coupled dimers. *Chem. Phys. Lett.*, 445:321, 2007.
- [74] F. C. Spano. Analysis of the uv/vis and cd spectral line shapes of carotenoid assemblies: Spectral signatures of chiral h-aggregates. *J. Am. Chem. Soc.*, 131: 4267, 2009.
- [75] F. C. Spano. Absorption and emission in oligo-phenylene vinylene nanoaggregates: The role of disorder and structural defects. *J. Chem. Phys.*, 116:5877, 2002.
- [76] F. C. Spano. The fundamental photophysics of conjugated oligomer herringbone aggregates. *J. Chem. Phys.*, 118:981, 2003.
- [77] F. C. Spano. Temperature dependent exciton emission from herringbone aggregates of conjugated oligomers. *J. Chem. Phys.*, 120:7643, 2004.

[78] Gerhard Ritschel et al. Non-markovian quantum state diffusion for temperature-dependent linear spectra of light harvesting aggregates. *J. Chem. Phys.*, 142: 034115, 2015.

- [79] J. S. Briggs and A. Herzenberg. The absorption bandshape of a molecular dimer. *Mol. Phys.*, 23:203–208, 1972.
- [80] R. L. Fulton and Martin Gouterman. Vibronic coupling. i. mathematical treatment for two electronic states. *J. Chem. Phys.*, 35:1059, 1961.
- [81] R. L. Fulton and M. Gouterman. Vibronic coupling. ii. spectra of dimers. *J. Chem. Phys.*, 41:2280, 1964.
- [82] Andrzej Witkowski and William Moffitt. Electronic spectra of dimers: Derivation of the fundamental vibronic equation. *J. Chem. Phys.*, 32:872, 1960.
- [83] A. Eisfeld et al. Vibronic energies and spectra of molecular dimers. *J. Chem. Phys.*, 122:134103, 2005.
- [84] Raffaele Borrelli and Maxim F. Gelin. Quantum electron-vibrational dynamics at finite temperature: Thermo field dynamics approach. *J. Chem. Phys.*, 145:224101, 2016.
- [85] Ch. Sridhar Reddy and M. Durga Prasad. Finite temperature vibronic spectra of harmonic surfaces: a time-dependent coupled cluster approach. *Mol. Phys.*, 113: 3023, 2015.
- [86] Lipeng Chen and Yang Zhao. Finite temperature dynamics of a holstein polaron: The thermo-field dynamics approach. *J. Chem. Phys.*, 147:214102, 2017.

Studies On Nonadiabatic Dynamics Within System-Bath Framework

by Prachi Pandey

Submission date: 29-Dec-2022 10:35AM (UTC+0530)

Submission ID: 1987219438

File name: tudies_On_Nonadiabatic_Dynamics_Within_System-Bath_Framework.pdf (852.16K)

Word count: 20510 Character count: 96242

Studies On Nonadiabatic Dynamics Within System-Bath

Framework					TRANSMISTER SOMEONING AND	
70			School of Chemistry Iniversity of Hyderabad			
		1%	% Hyderabad - 500046 %			
		INTERNET SOURCES	PUBLICATIONS		STUDENT PAPERS	
			•			
PRIMAR	Y SOURCES		· · · · · · · · · · · · · · · · · · ·			
1	Submitt Student Pape	ed to Universit	y of Sheffield		<1%	
2	epdf.pu Internet Sour				<1%	
3	the diss	ipative dynami tions", The Jou	Redfield descrip cs at conical rnal of Chemica		<1%	
4	Descrip		el Thoss. "Classi abatic Quantum		<1%	
5	scholars Internet Sour	share.temple.e	du		<1%	
6	zombie Internet Sour	doc.com rce			<1%	
7	Submitt Student Pape	ed to Associati	e K.U.Leuven		<1%	

